Coarse-Grained Molecular Dynamics Simulations of Silica Polystyrene Nanocomposite

Vom Fachbereich Chemie
der Technischen Universität Darmstadt

TECHNISCHE UNIVERSITÄT DARMSTADT

zur Erlangung des akademischen Grades eines
Doktor rerum naturalium (Dr. rer. nat.)

genehmigte
Dissertation

vorgelegt von

Azadeh Ghanbari, M.Sc of Physics
aus Teheran, Iran

Referent:	Prof. Dr. Florian Müller-Plathe
Korreferent:	Prof. Dr. Nico van der Vegt
Tag der Einreichung:	30 March 2012
Tag der mündliche Prüfung:	07 May 2012

Darmstadt 2012
D17

Summary

The addition of micron sized inorganic filler particles to the polymeric materials is a well known reinforcement method in composite production. Polymers reinforced with the nanoscale particles, known as nanocomposite materials (NCMs), have greater interaction with the filler particles, due to their enormous surface, and show vastly improved properties. The clear explanation of the origin of this improvement in the properties of the NCMs, compared to the conventional composites, is still missing. Polymer behaviour is modified “near” the filler particle surface, forming a so-called “interphase” region, which in turn can affect the overall properties of the NCM. The present PhD thesis is part of a large international research programme, NanoModel, in which academic and industrial partners from six different countries contributed. The ultimate aim of the project was to achieve a unified picture of the polymer behaviour in the interphase region of NCMs, considering the theoretical and experimental viewpoints and results. Such an understanding of the polymer-filler interaction and its controlling parameters and ultimate effects on the composite behaviour would improve the industrial design of the polymer NCMs. The current work, in the framework of the NanoModel, has been done by collaboration of Fribourg University, Jülich, and Epidoris for experimental investigations, and TU Darmstadt, National University of Athens, Trieste University, and BASF for computational studies.

Properties of the NCMs have been described in many experimental studies as well as in computer simulations of the molecular dynamics (MD) and Monte Carlo (MC) type. An introduction containing the main motivations, overview of the recent experimental results and theoretical and simulation investigations of the polymer chains in the presence of the nanoparticle is presented in the first chapter of this thesis. This review is focused on different aspect that are crucial for NCMs, like structural and dynamical modifications induced by filler particle in the interfacial region and the important parameters for dispersing the filler particles in the host polymer.

The long relaxation times of the systems, however, which are outcome of the large number of degrees of freedom, restrict the atomistic simulations to the composites with not too large nanoparticles, and polymer matrices formed by short chains. In the length- and time-scales accessible by atomistic simulations many interesting phenomena cannot be monitored. Larger length- and time-scales can be simulated by MD and MC variants in a so-called coarse-grained (CG) resolution. In this level of sophistication the atoms of the polymer and of the nanoparticle are

grouped together to superatoms, frequently denoted as CG beads. Coarse-graining restricts the degrees of freedom to those which are assumed to be relevant for the composite quantities of interest.

The CG simulations based on iterative Boltzmann inversion (IBI) method have been used for a model system of Silica nanoparticles (NPs) embedded in atactic polystyrene (PS) to study the structural and dynamical properties of interfacial region and its dependency to different parameters like matrix and grafted polymer chain length, grafting density and etc. To do this the existing CG program IBIsCO was changed partially to simulate nanocomposite systems. The major part of this PhD work was to optimize the required CG potentials, develop analysis tools for calculation of the interfacial structural properties as well as dynamical properties and comparing those to the experimental results.

Although many quantities of the complex polymer composites can be studied already in the CG picture, there are others where an atomistic resolution is an absolute must. The correlation between measured neutron diffraction data and MD or MC calculated ones is just one example. Thus there is a strong need to transform a CG mapping of the system back into an atomistic resolution, once the relaxation and equilibration of the CG sample have been performed. This process of introducing atomistic details into a CG simulation, denoted as backmapping (BM) or inverse mapping, is dealt with in the second chapter of the thesis by development of a novel BM method suitable for polymers with rigid side group. The development of this method is necessitated due to adopted mapping scheme for polystyrene, which had no corresponding BM method in the literature.

In the third chapter of thesis, the interphase structure of a polystyrene matrix filled with either a bare or a grafted nanometre-sized silica particle is investigated by means of MD simulations, at the CG level. The transferability of the IBI potentials, optimized for short free chains and a bare NP, to the longer chains and grafted NPs is addressed, via comparison with CG potentials optimized specifically for some test systems. This study has been a simplified way to gain experience on transferability issues of CG potentials before tackling the complex systems with multiple NPs and also potential mean-force discussed in the forth chapter. The simulations in this chapter provide the insight into how the structural properties of the polymer matrix and the grafted corona are affected by grafting density and matrix polymer length. Structural modifications in matrix chains were found to persist to one radius-of-gyration distance from surface. Wet-to-dry transition of the grafted corona was observed, in agreement with experiment, by increasing the matrix chain length.

In the fourth chapter, monomer dynamics of the free and grafted PS chains surrounding six silica nanoparticles (bare or grafted) in concentric shells around NPs center-of-mass has been investigated. The effects of the grafting density and free chain length on the dynamics of the grafted monomers and free monomers as well as NPs have been discussed. The interphase thickness defined by the spatial extension of perturbations in polymers dynamics compared to the corresponding bulk behavior, measured through self scattering function or mean square displacement, is in agreement with the structural interphase thicknesses. It is shown how the grafting density and the matrix chain length affect the monomer dynamics of the grafted chains. Since the dispersion of the nanoparticles in the polymer matrix is a vital control key in NCM development, the second and major part of this chapter is devoted to the investigation of the polymer mediated interaction between two non-interacting NPs. It is shown how the potential of mean-force between NPs is affected by changing different parameters like grafting density, matrix chain length and the grafted chain length. Also, the conformation of the chains in the inter-particle distances has been investigated.

Finally, the fifth chapter summarizes the results obtained in this PhD work, and discusses the possibilities to extend the current model to further investigate the challenging topics in the nanocomposite field.

Zusammenfassung

Die Zugabe von anorganischen Füllstoffen zu Polymeren ist eine bekannte Methode der Kunststoffindustrie, Polymere zu verstärken. Polymere, die mit Nanoteilchen verstärkt werden, i.e. sogenannte Nanokompositen (NCM), besitzen aufgrund ihrer größeren Oberfläche stärkere Wechselwirkungen mit den Füllstoffen und zeigen dadurch deutlich verbesserte Eigenschaften. Die genaue Ursache für die Verbesserung der Nanokompositen gegenüber den herkömlichen Polymeren ist noch unklar. In der Nähe der Füllstoffe ändern Polymere ihr Verhalten und es kommt zur Bildung einer sogenannten Interphase, welche wiederum die gesamten Eigenschaften der Nanokomposite beeinflusst. Die vorliegende Doktorarbeit ist Teil eines großen internationalen Forschungsprojekts, NanoModel, an dem Partner aus Industrie und Forschung aus über sechs verschiedenen Ländern zusammenarbeiten. Ziel dieses Nanomodel-Projektes war ein tieferes Verständnis über das Verhalten der Polymere im Bereich der Interphase von Nanokomposite unter Berücksichtigung der theoretischen und experimentellen Gesichtspunkte und Ergebnisse. Ein solches Wissen über die Polymer-Füllstoff Wechselwirkung und den dazugehörenden Parametern sollte die Synthese maßgeschneiderter Nanokomposite in der industriellen Herstellung ermöglichen. Die vorliegende Arbeit entstand im Rahmen des Projekts NanoModel in Zusammenarbeit mit der Universität Fribourg, dem Forschungszentrum Jülich und Epidoris SAS bei der Proben-Präparation und Charakterisierung sowie der TU Darmstadt, den Universitäten Athen und Triest und der BASF bei den Computersimulationen.

Die Eigenschaften der Nanokomposit-Materialien wurden sowohl in vielen experimentellen Studien als auch in Computer-Simulationen vom Molekulardynamik (MD)- und Monte Carlo (MC)-Typ beschrieben. Eine Einführung zur Motivation der vorliegenden Arbeit, ein Überblick über experimentelle Ergebnisse sowie theoretische und Computerstudien von Polymerketten in der Gegenwart von Nanoteilchen wird im ersten Kapitel der Arbeit gegeben. Diese Übersicht behandelt besonders die Themen, die für das Verhalten von Nanokompositen wichtig sind, z. B. Änderungen in der Struktur und Dynamik, die durch die Füllstoffe in der Interphase verursacht werden sowie wichtige Bedingungen für die Dispersion dieser Füllkörper.

Die langen Relaxationszeiten der Proben, die durch die große Anzahl von Freiheitsgraden verursacht wird, limitieren Simulationen in atomarer Auflösung auf nicht zu große Nanoteilchen und Polymermatrizen mit kürzeren Ketten. In der Längen- und Zeitskala, die atomar zugänglich sind,

lassen sich viele Phänomene nicht untersuchen. Größere Längen- und Zeitskalen lassen sich mit MD- und MC-Verfahren vom sogenannten Coarse-grained (CG)-Typ (i.e. vergröberte Modelle) analysieren. In dieser Näherung werden die Atome des Polymers und des Nanoteilchens zu „Superatomen“ zusammengefasst, die oft als CG-Perlen bezeichnet werden. Die vergröberten Modelle beschränken die System-Freiheitsgrade auf solche, die für die Eigenschaften des Komposit-Materials als relevant erachtet werden.

Im Rahmen des „NanoModel“-Projektes wurden Coarse-grained (CG)-Simulationen mit der iterativen Boltzmann-Inversion (IBI) an einem Modell-System für Silica-Nanoteilchen (NP) durchgeführt, die von ataktischem Polystyrol (PS) umgeben sind. Unser Interesse galt den strukturellen und dynamischen Eigenschaften in der Interphase und deren Abhängigkeit von verschiedenen Parametern, wie z.B. der Polymerlänge, der Pfropfungsdichte oder dem Volumenanteil an Nanoteilchen etc. Für diese Untersuchungen wurde unser CG-Programm IBIsCO so verändert, dass Nanokomposit-Materialien simuliert werden können. Den größten Teil dieser Dissertation hat die Optimierung der benötigten CG Potentiale und die Entwicklung analytischer Werkzeuge für die Berechnung von strukturellen und dynamische Eigenschaften der Interphase sowie deren Vergleich mit experimentellen Ergebnissen benötigt.

Obwohl bereits viele Eigenschaften komplexer Polymer-Mischungen in einer vergröberten (i.e. CG) Beschreibung untersucht werden können, ist eine atomare Auflösung für andere Eigenschaften eine absolute Notwendigkeit. Der Vergleich experimentell gemessener Neutronen-Beugungsdaten mit Werten aus MD- oder MC-Simulationen ist nur ein Beispiel. Deshalb ist es von großem Interesse, Ergebnisse, die im CG-Bild erhalten wurden, nach der Relaxation und Equilibrierung der CG-Probe wieder in eine atomare Auflösung zu transformieren. Dieser Prozess, atomare Details in ein CG-Bild zu implementieren, den man als Rück- oder inverse Transformation (BM) bezeichnet, wird im zweiten Kapitel dieser Doktorarbeit beschrieben. Dazu wurde eine neue BM-Methode für Polymere mit starren Seitengruppen entwickelt. Dies wurde durch das gewählte CG-Abbildungsschema für Polystyrol erzwungen. In der Literatur ist für diese Problematik noch kein BM-Verfahren beschrieben.

Im dritten Kapitel dieser Arbeit wird die Struktur der Interphase einer Polystyrol-Matrix mit nichtgepfropften und gepfropften Silica-Teilchen von einigen Nanometern durch MD-Simulationen im CG-Bild untersucht. Die Übertragbarkeit von IBI-Potentialen, die für kurze freie Ketten und ein einfaches Nanoteilchen optimiert wurden, auf längere Ketten und gepfropfte Nanoteilchen wird

mithilfe von CG-Potentialen getestet, die für einige Modellsysteme berechnet wurden. Diese Untersuchungen haben es in einfacher Weise ermöglicht, Erfahrungen über die Übertragbarkeit von Potentialen zu sammeln, bevor Rechnungen an komplizierten Systemen mit mehreren Nanoteilchen oder „potential of mean force“-Berechnungen durchgeführt wurden, die in Kapitel vier beschrieben sind. Die Simulationen in diesem Kapitel geben einen Einblick in strukturelle Veränderungen der Polymermatrix oder des gepfropften Bereiches um das Nanoteilchen als Funktion der Pfropfungsdichte und der Polymerlänge. Strukturelle Änderungen in den Ketten der Polymermatrix haben eine Ausdehnung von der Oberfläche, die einem Gyrationsradius entspricht. Mit zunehmender Kettenlänge in der Matrix beobachtet man einen „wet-to-dry“-Übergang im Kranz der gepfropften Polymere, ein Simulationsergebnis, das mit dem Experiment übereinstimmt.

Im vierten Kapitel wird die Monomer-Dynamik von freien und aufgepfropften Polystyrolketten innerhalb konzentrischer Schalen um den Massenmittelpunkt von sechs Nanoteilchen untersucht. Der Einfluss der Pfropfungsdichte und der Länge der freien Ketten auf die Dynamik der gepfropften und freien Monomereinheiten sowie der Nanoteilchen wird hier erläutert. Zwei Definitionen der Interphase führen hier zu gleichen Ergebnissen. Eine Definition korreliert die Dicke der Interphase auf Basis der Ausdehnung einer geänderten Polymerdynamik mit dem sogenannten „Bulk“-Verhalten. Relevant für diese Berechnung ist die sogenannte „self scattering“-Funktion. Die Variation dieser Größe stimmt mit der Dicke der Interphase auf Basis struktureller Parameter überein. Es wird gezeigt, wie die Pfropfungsdichte und die Länge der freien Ketten die Monomer-Dynamik der aufgepfropften Ketten beeinflusst. Da die Dispersion von Nanoteilchen in einer Polymermatrix ein wichtiger Parameter in der Entwicklung von Nanokomposit-Verbindungen ist, beschäftigt sich der zweite, größere Teil dieses Kapitels mit der polymerinduzierten Wechselwirkung von zwei wechselwirkungsfreien Nanoteilchen. Es wird gezeigt, wie das „potential of mean force“ von verschiedenen Parametern wie Pfropfungsdichte oder der Länge der freien und aufgepfropften Ketten beeinflusst wird. Auch die Konformation der Ketten wird in diesem Kapitel untersucht.

Im fünften Kapitel meiner Doktorarbeit werden die Ergebnisse zusammengefasst und Möglichkeiten diskutiert, die entwickelten Modelle zu erweitern, um herausfordernde Themen von Nanokomposit-Materialien zu behandeln.

Table of Content

1. Introduction

Polymer materials are widely used in the industry due to their unique features: including light weight, ductility, easy production and low costs. Their mechanical features are still poor compared to metals and ceramics, which are also widely used in the industry, and hence need to be improved. A common method to improve mechanical features of polymer systems is to reinforce them with inclusions or fillers, which works even with very low filler volume fraction[1]. The embedment of fillers in the host matrix gives the resulted composites properties not achieved by either of the components alone, maintaining their light weight and ductility[2]. Nanocomposite materials (NCMs) are formed by filling a polymer matrix with inorganic particles which have at least one dimension of the order of a few nanometers. The current high demand for polymer nanocomposites in the industry arises from their applications in different sections, ranging from biomedical and electronic to automotive and aerospace, each bringing up different design and functional requirements to be met by nanocomposite material[3]. For instance nanocomposites are of great interest to biomedical technologies such as bone substitute and dental applications[4] because their mechanical properties, biocompatibility and biodegradability may be tailored to suit the need. As another example, it has been observed that the addition of NPs to polymer materials can lower their viscosity[5]. Such a modification is useful in extrusion and injection molding processes. Due to their outstanding properties compared to the traditional composites, which is achieved by switching the filler size from micro- to nano-scale, NCMs have further attracted academic interests[6–9], besides the industrial applications.

1.1. Challenges in Nanocomposite Study

The main challenge in the NCM field, as in any other growing field, is to understand the fundamental parameters controlling the overall properties of the material. At the level of a single filler particle, the nano-sized inclusion induces conformational changes and deformations in the polymer chains in the interfacial region; where the filler particle and the polymer matrix meet each other. These perturbations are manifested by structural (like: layering around the filler particle depicted by multiple density peaks, or chains stretching or wrapping around the filler particle) or dynamical (slower mobility of the chains) changes of chains around the particle, compared to the

bulk polymer. The alterations induced in the interphase area, where the polymer does not yet retain bulk-like behavior, are direct outcome of the matrix-filler interaction type, size ratio, and filler size and shape. Unlike in conventional composites, the size of the filler particles is comparable to the molecular and atomistic dimensions. This enhances the role of the nanoscopic properties of the both components; matrix and filler. Due to their nano-size nature, the embedding of the filler particles to the polymer matrix introduces a large surface-area for matrix-filler interactions in the nanocomposites, compared to the conventional composites. At the level of collective behavior and organization of the inclusions within the matrix, dispersion of the filler particles throughout the NCM provides the highest specific area (and hence surface energy) at one hand, and homogeneity of the resulted NCM on the other hand. Besides the interphase, then, the physics of the dispersion of the filler particles in the matrix is another challenge in the field. Even though a large number of experiments, simulations and theoretical works have been focused to understand the impacts of the interfacial area on the entire properties of the NCM, still comprehensive results have not been achieved. This can in part be attributed to the qualitative and quantitative dependency of the interfacial perturbations on different parameters like polymer molecular weight, shape and size of the NPs and interaction between NP and matrix polymer. The current thesis as a part of larger research programme, NanoModel, is intended to shed some light on this yet unclear issue.

1.2. Experimental Achievements

The knowledge of the atomic arrangement in any given material is a prerequisite for theoretical understanding of its properties on one hand, and further modeling, manipulation and controlling of the emerging properties on the other hand. As the mere existence of the interfacial region changes the properties of the material from that of polymer to that of a NCM, enormous efforts have been done on the experimental study of this region. Besides the usual difficulties in the experimental investigation of the conventional polymer composites, including good sample preparation and the polydispersity and heterogeneity of the chains and filler particles, the small length scales associated with the nanocomposites make it even more difficult to study the structural and dynamical characteristics of the interfacial polymer chains and collective properties of the fillers[10]. Typically, the structural characterization tools include force, optical, and electron microscopy; X-ray, neutron, and light scattering; spectroscopic methods; electrical and dielectric characterization; and mechanical spectroscopy. Depending on the details of the nanoparticle (NP) and the polymer matrix,

each of these methods can provide unique information on the dispersion state and polymer and nanoparticle arrangement over size scales ranging from nanometers to millimeters. These are often used in combination to provide detailed information on the hierarchical morphology in nanocomposites[11]. Changes in the polymer dynamics is monitored as alterations in the glass transition temperature, relaxation times, or dielectric loss of the polymers when mixed by filler particles[12]. So, the experimental methods like quasi-elastic neutron scattering, nuclear magnetic resonance (NMR) and differential scanning calorimetry can be employed to investigate the dynamical properties of the NCMs. The layering structure and parallel organization of the matrix near the surface has been observed for different combinations of filler types and shapes and matrix polymers. Despite the general consensus on the existence of such layers around the filler particles, the alterations in the chains' mobility within these layers in the polymer-filler interface has been subject of ongoing debate. In the following, results of different experiments on the dynamical properties of the interfacial region are shortly reviewed.

One of the criteria for assessing the different dynamics within the interfacial region is glass transition measurement in NCMs. Various experimental studies reported a “rubber shell” around the nanoparticle. The presence of such a layer has been suggested by monitoring two distinct glass transition temperatures (T_g) one for bulk polymer and the other one for polymer chains in the rubbery shell. The reason of so-called rubber layer is that the mobility of the polymer at the interface with the particle is restricted in comparison to the bulk, either due to the strong adsorption of polymer segments to the interface due to the polymer-filler interaction, or due to the increased density of polymer near the surface which leads to increased entanglements.

1.2.1. Dynamical Bulk Properties

Measurement of the glass transition temperature using thermodynamical and bulk properties of the nanocomposites has led to different experimental observations. Differential scanning calorimetry (DSC) measures the T_g of the sample from the sudden changes in the sample heat capacity upon heating or cooling. It showed no change in T_g of Polydimethylsiloxane (*PDMS*) filled with up to 20 nm diameter silica particles, as reported by Arrighi et al.[13]. Similarly, no change in the T_g, measured by DSC, was reported for filled polyvinylacetate (PVAc)[14] and polyurethane[15], consistent with the absence of a glassy polymer interphase. DSC on the other hand revealed increase in T_g of polymethylmethacrylate (PMMA) filled with silver/carbon nanoparticles[16], silica-filled poly(2-

vinylpyridine)[17] and hyperbranched polymer molecules with suspensions of silica and glass particles[18]. Moreover, reinforcement with alumina particles was reported to reduce the T_g of PMMA by as much as 25°C[19]. The elastomers in vicinity of the filler surface was shown to experience some degree of stiffening, conducting atomic force microscopy, but it was not considerable effect on the segment dynamics of the polymer chains to be counted as glass transition[20].

1.2.2. Polymer Segment Dynamics

Monitoring the polymer segment dynamics is another method to probe the filler-induced modifications in the interphase dynamics. In an inelastic neutron scattering study on polyisoprene filled with carbon black, below its glass transition temperature, Nakatani et al[21]. found that chains bound to the carbon black particles had greater mobility than the neat polymer. In another study of PDMS and PVAc reinforced with silica particles, carried out by Gagliardi et al.[22], neutron scattering revealed the presence of an immobilized interfacial polymer phase around the silica particles. Dynamic mechanical spectroscopy (DMS) is another technique to study the effect of filler particle on polymers' T_g. While Vieweg et al.[23], carrying out a DMS study on styrene-butadiene copolymer (SBR) filled by carbon-black, didn't see any appreciable changes in of the segmental relaxation in vicinity of the carbon-black, Tsagaropoulos et al.[24,25] reported shift to higher T_g as a sign of immobilized chains near the surface, in silica filled uncross linked polymers, using the same method.

1.2.3. Sub-monomer Dynamics

The NMR method has been used as a tool for characterizing polymer motions in the presence of the filler particles measured by proton spin-spin relaxation times. Even NMR studies, which probe the polymer dynamics in sub-monomer level, have led to contrary results of polymer immobilization by filler particles. As in the case of above mentioned experimental methods, there are some NMR studies concluding the existence of the immobilized rubber shell or higher T_g phase in the interfacial region[26–28], while others reached the opposite conclusion[29–31]. Even though this shows the ambiguity concerning the existence of the immobilized layer next to filler surface, at least some of it can be attributed to the interpretation of the data. In the case of NMR approach, for example, the identification of the polymer phases according to their mobility is usually done by fitting the proton relaxation data to a sum of functions, where number of the terms in the fitted equation is equal to the number of the polymer phases. This approach, however, may lead to more than one possible fit for a

given relaxation curve, if it doesn't follow a very clear feature. This has been tested by Robertson et al.[12] for the case of polybutadiene filled with carbon black. They found that different number of terms, and hence polymer phases, are needed when different fitting functions are used. While some of the discrepancy in the experimental results mentioned above can be attributed to the different polymers and fillers, and also different sample preparation methods, still a precise explanation for such different observations with a given method is to be provided more carefully by further theoretical and experimental investigations.

1.2.4. Nanoparticles Dispersion

As mentioned above, the uniform dispersion of the filler particles within the polymer matrix is crucial for improved properties of the NCMs. At this level there is a general consensus that surface modification of the filler particles with end grafted polymers prevents aggregation of the particles and hence enhances the filler particle dispersion[32–34]. The overall structure of the system reflected by sample morphology - size, shape and the degree of dispersion of the inclusions - can be directly assessed, thanks to the advances in microscopy and spectroscopy methods. Small-angle X-ray and neutron scattering (SAXS, SANS) have made it possible to probe extremely small q-vectors, corresponding to structures above the 100nm range[35–39]. One recent experimental study on the dispersion mechanism in silica-PS nanocomposites was performed by Chevigny et al.[40], using complementary scattering (SAXS/USAXS) and imaging (TEM) techniques. The authors showed that the mass ratio between grafted and free chains, Q, is the relevant parameter of the dispersion, which controls the arrangement of the NPs in the matrix, either as large and compact aggregates ($Q < 0.24$) or as individual NPs ($Q > 0.24$). They also showed that aggregation of the fillers is associated with a significant collapse of the grafted corona. In a separate study[41], they demonstrated that the grafted chains become compressed interacting with longer matrix chains.

A direct look at the individual atoms or molecules and their contribution to the structural and dynamical characteristics of the matrix-filler and filler-filler interactions can not be provided by the existing experimental methods. In this regime, however, theoretical and (especially) computer models based on the precise empirical observations can provide the perfect tools to study the system in question down to single atom level, without the complications and limits encountered in the experimental methods. It should be noted, however, that the computer models have their own limitations. For example, depending on the scale at which a system is modeled, some of the

information is ignored. Moreover, the observed behavior of the atoms or molecules is not exactly the same as reality, depending on how close the employed interaction potentials are to the real ones. Following brief review of some experimental results which highlighted by number of open question and hinted, now we will comment on the simulation studies of NCM.

1.3. Computer Modeling Insight

In parallel to experimental investigations, computer modeling can also be employed to study the behavior of the polymer chains confronting the filler surface. Given a suitable force field, the atomistic and coarse-grained (CG) molecular dynamics (MD) as well as Monte Carlo (MC) simulations provide access to the matrix-filler interactions at single atom or single monomer level for evaluating the properties of interest. Structural features of the interfacial chains can be monitored by examining the polymer density, bond, segment and chain orientation and chain radius of gyration versus distance from filler surface. Their dynamical properties can be further analyzed by investigating the monomer and chain mean square displacement (MSD) or the relaxation times computed by self-intermediate scattering function or segment or chain orientations. In addition to these fine details of information, computer modeling has the advantage of investigating the structural and dynamical properties of a NCM model at the same time, which is difficult, if not impossible, in the experiment.

1.3.1. Interfacial Structure

The filler particles induce a structuring influence on the polymer in their vicinity. This is easily visible in all structural quantities analyzed, via computer simulations, in the literature[42–51]. Embedded particles of all diameters, surface decorations and interaction strengths induce: (i) layering of chain monomers around the filler particle, demonstrated by oscillations in the radial monomer density; (ii) chain elongation, shown by an increase in the chain radius-of-gyration; and (iii) segment and chain orientation, being tangential to the filler surface in the vicinity of the particle. The layer structure of polymers around filler particle is consistent with the monomer density profile observed near a smooth wall[52–54], manifested by an enhanced density peak at surface proximity and the following oscillations which damp by distance from surface, until a bulk-like value is reached. The shape and spatial extension of the density peaks, which cause the formation of an interphase, have been shown to be very weakly dependent on polymer chain length, for a given composite[42,51].

The density amplitudes around a bare particle, however, are shown to increase with the diameter of the nanoparticle. The reason is that the monomers near a surface of smaller curvature have less freedom for lateral motions, compared to the surface with higher curvature, and this induces stronger ordering effect near the flatter surface.[49].

At the level of single chain properties, the local packing of the polymer chains, as measured with radius-of-gyration (R_g), is shown to be perturbed in the interfacial region. Starr et al. showed that the R_g of 20-mer chains increases accompanied by decrease in its radial component near the bare surface, indicating that the matrix chains become increasingly elongated and ‘‘flattened’’ as they approach the filler surface[42,55], an effect reported by other studies too[49,51,56], including MC bead-spring and material-based atomistic simulation studies. This stretched chain structure, however, was found to be independent of polymer-filler interaction strength, as also confirmed by Liu et al.[51], suggesting that the altered shape of the polymers is primarily due to geometric constraints of packing the chains close ($d \leq R_g$) to the surface[43,46,48,51,57]. In addition to their stretched geometry, polymer chains tend to be aligned tangential to the filler surface for attractive polymer-filler interaction, or perpendicular to the surface (in radial direction) for purely repulsive polymer-filler interaction. When R_g of polymer chains is larger than filler size, this preferred orientation angle happens mainly in bond and segment scales (i.e. chain bonds and segments which are near surface). The increase of the polymer-filler attraction strength is shown to enhance the preferred tangent-to-the-filler-surface orientations on the bond, segment, and chain length scales[51], even though R_g remains insensitive as mentioned above. The local orientation of chain segments near the filler particle surface was found to be weakly affected by the polymer chain length, within the framework of a MC study carried out by Vogiatzis[48] on a silica-polystyrene NCM model. The chain length dependence of the thickness of the layer at which the whole chain conformation is perturbed, however, has not been examined for a given filler size and polymer-filler interaction. Such a measurement, as a sign of interphase thickness in the presence of short and long chains, would be interesting especially when performed for a material-based model of NCM, and therefore is discussed in the current study.

The grafting state of the nanoparticle surface is known to induce further alterations in the interfacial region, making the access of the matrix chains to the surface more difficult. For example, Milano et al.[50], employing a MD study of the interface between polystyrene and gold nanoparticles, showed that the ordering of the polymer chains near the surface is stronger for bare particles than for

particles grafted with alkyl compatibilisers. This happens due to the screening effect of the grafted corona, which inhibit the approach of the matrix chains to the NP[49] and restricts the orientation of the penetrated ones. Despite the theoretical and experimental studies on the wetting and drying of the grafted corona of a flat surface[41,58–67] and spherical filler particle[41,68,69] with different matrix chain lengths, still few theoretical[70] and computer simulation studies have addressed the structural modifications in the grafted corona of a nanoparticle confronting different matrix chains. Such structural modifications of the grafted corona of a nanoparticle by matrix chains, which are expected to be different from that of a flat surface considering its strong curvature, can influence the overall properties of the NCMs through controlling the filler dispersion, as observed experimentally[40,41]. Furthermore, any structural perturbations induced by matrix chain length are likely to be accompanied by dynamical modifications too, because of the structure-dynamics inter-relation. Investigation of this phenomenon, called "wet-to-dry" transition is one of the subjects of the third chapter of the current PhD thesis.

1.3.2. Interfacial Dynamics

Several polymer-surface parameters including the surface curvature, roughness, and repulsion / attraction nature of the interaction influence the interfacial polymer dynamics which in turn determine the overall material properties. The fact that polymer dynamics is measured directly by monomer mobility in the computer simulations, and the easy distinction between chain monomers at different distances from surface, has led to much less contradictory results, unlike experiments. Starr et al.[55,71] studied the single monomer dynamics through the self scattering function, which is the Fourier transform of the real-space time-dependent spatial-correlation function, within well-defined layers surrounding a bare filler particle. They found that the relaxation of the monomers become slower approaching the nanoparticle surface, if the interaction of the monomers and nanoparticle is attractive. In contrast, the relaxation of the closer monomers was significantly enhanced compared to the bulk, for non-attractive interaction of the monomers and the nanoparticle. Performing a coarse-grained model-based MD simulation, Liu et al.[51] examined the MSD of monomers as a function of distances from the nanoparticle, tuning the polymer-filler interaction from strongly attractive to weakly attractive and purely repulsive. They found reduced chain mobility in vicinity of the filler surface for strongly attractive polymer-filler interaction, and increased mobility for the purely repulsive interaction. However, they found no obvious change in the chain mobility, when the

interaction was weak. Both groups reported that the behavior of the bulk mobility recovers after some distance from surface, suggesting that the restricted region of polymer mobility is confined within a distance given by chain size R_g[51,55,71], as in the case of structural modifications. This shows how the different polymer-filler interaction types can lead to different mobility gradient of the monomers in the interface region. Such a decreased monomer mobility in vicinity of an attractive filler particle has been reported by other groups[43,51,72]. The decreased interfacial monomers dynamics observed in the computer simulations is reported to be different from that of a glassy layer, in which polymer chains are almost completely immobilized and the MSD is almost zero. The interfacial polymer chains here still retain some mobility, manifested by their MSD or self scattering function. When the polymer-filler interaction is strongly attractive (equivalent to the hydrogen bond), some polymer segments become adsorbed to the surface, and still experience desorption / adsorption process as a function of time. The interfacial polymer chains do not exhibit the glassy behavior, hence. This has led to the conclusion that the polymer glassy layers do not exist around the filler particles[51,71], contrary to the experimental reports[18,25,28,73]. One of the important questions which have not been answered so far in the computer simulation and experimental studies, however, is the chain length dependence of the hindrance effect of the grafted filler surface on the dynamics of the matrix and grafted monomers. It can be more interesting noting that increasing the chain length leads, in the structural level, to the well-known wet-to-dry transition of the grafted corona, which opens another possibility to relate the structure and the dynamics of the system. Investigating such a chain length dependence of the matrix and grafted monomers dynamics is a part of the current thesis.

The interphase thickness, defined by distance after which the surface induced alterations in the polymer properties disappear, can be measured considering different criteria; including structural modifications such as chain or segment orientation, chain radius-of-gyration and density profile, or dynamical features like monomer or segment relaxation. There are several reports that structural and dynamical modifications last to distances of one or two single chain size[46,49,72,74–77] from the surface of the nanoparticle. The interphase thickness in the generic atomistic and coarse-grained models was found to be insensitive to the polymer-filler interaction strength and filler size, as reported by Brown et al.[46] and Liu et al.[51]. Ndoro et al.[49] showed the same filler size independence by atomistic MD simulation of silica-filled polystyrene, while grafting density of the filler particle was found to extended this layer. In order to predict and control the properties of NCMs, it is essential to further

characterize the structure and properties of this interfacial region in quantitative level. Since the thickness of the grafted corona, defined by brush height, is sensitive to the matrix chain length via wet-to-dry transition effect, the matrix chain length seems to further control the interphase thickness around grafted nanoparticles. The length of the matrix and grafted chains, however, was only 20 monomers in the atomistic work of Ndoro et al.[49], restricted in part by the accessible length-scales in a typical atomistic simulation. Tuning the matrix chain length from smaller than to larger than filler size and grafted chain length, in the framework of coarse-grained MD simulation, to further investigate the chain length dependence of the interphase thickness around a grafted filler particle will be studied in the current thesis.

1.3.3. Nanoparticle Dispersion

Aggregation of the particles obviously results in less surface accessible for the matrix polymer (interfacial area) and therefore particle aggregation is detrimental to the NCMs. One of the most fundamental parameters affecting the tendency of NPs to aggregate or disperse are the interactions between the particles, and the interactions between particles and the surrounding polymer matrix. It has been shown that when polymer-filler interaction is only slightly (~ 30-40 %) stronger than filler-filler interaction, filler particles become dispersed in the host polymer[42,78]. Recently Liu et al.[79] have shown that while increasing the polymer-filler interaction strength from weak to intermediate level results in uniform dispersion of fillers into the polymer matrix, further increase of the interaction strength would result in particles forming aggregates because a single polymer chain tends to adsorb several NPs at the same time. This means that a good dispersion of the NPs can be obtained at a moderate polymer-filler interaction, which is in agreement with theoretical prediction[79]. Correspondingly, the spatial organization of the filler particles as a function of the polymer-filler interaction can be categorized in three states: (i) phase separation of the filler and polymer, (ii) homogeneous dispersion of the filler, and (iii) local bridging of the filler via the polymer chains, when polymer-filler interaction strength is changed from weak to intermediate and then strong[79]. Another known approach to disperse the NPs in the polymer matrices is to functionalize the surface of the NPs[80], resulting in a polymer “brush” that will repel brushes of other particles, as applied to large colloidal particles for many years.

The simulation results from work of Smith et al.[81] indicate that, in addition to the theoretical prediction[79] of larger repulsion of the colloidal particles by utilization of longer grafted chains, a

good dispersion of the nano-sized filler particles can be obtained by relatively dense and very short brush[81]. The structural details of the adjacent fillers in the latter case, however, have not been studied in the literature. The investigation of the grafted chain length effect, among the other parameters including matrix chain length and grafting density, on the NPs interaction will be considered in the current study. In order to answer these questions with minimum computational cost, however, the polymer mediated interaction of only two fixed NPs - called potential of mean force - will be examined versus inter-particle distance.

1.4. Thesis Structure

After highlighting the achievements in the NCM studies and the unresolved issues in the state-of-the-art knowledge in this field, the structure of the current thesis, tackled problems, achieved results and further issues remaining to be resolved are provided here.

In the second chapter a new backmapping (BM) method is developed for polymers with rigid side group. In addition to the fact that such a BM method was needed for the next steps of the current work, this new method, combined with the preceding CG scheme[82], opens the possibility to consider CG models as coarse as "one monomer, one bead", which is computationally faster than "one monomer, several beads" schemes[83,84], and easily switch back to the atomistic resolution.

The third chapter starts with optimizing CG potentials against atomistic simulation, of a silica NP and free polystyrene chains, which are transferable to grafted NP and longer matrix chains cases. Employing the CG potentials the chain length dependence of the interphase layer is examined, which shows that on whole chain level interphase thickness around a bare particle is scaled by R_g. The tangential orientation of chain segments near the surface is found to be accompanied by stretching of short matrix chains (R_g < NP radius) and contraction of the longer ones (R_g > NP radius). In the case of grafted NP, the influence of the matrix chain length on the grafted brush is examined. The grafted brush is wetted by matrix chains shorter than grafted ones, and becomes dried facing with longer free chains. This helps to better understand the experimentally observed aggregation of the grafted NPs in the presence of longer matrix chains[40,41]. The dynamical modifications of the grafted corona which happen in parallel to the structural changes during the above mentioned "wet-to-dry" transition are further investigated in the fourth chapter.

The mere presence of NP is shown, in chapter four, to slow down the monomer dynamics near the surface, for all chain lengths and surface decorations, but does not lead to an immobile or glassy

region which experiments refer to[18,25,28,73]. The shorter matrix chains induce relatively faster dynamics (than longer ones) in the grafted corona, in addition to their relatively more favorable presence in this region. Therefore the dynamical deceleration in NP proximity can be controlled by matrix chain length. The last part of the fourth chapter deals with polymer-induced interaction of NPs of different surface decorations and with different matrix chain lengths. Whereas surface grafted repel approaching NPs, in agreement with experiment, the long grafted chains are found to increase the chances of particles aggregation due to the adsorption of the long enough grafted chains to the surface of other NPs.

1.5. References

(1) Chang, J.-H.; An, Y. U. *Journal of Polymer Science Part B: Polymer Physics* **2002**, *40*, 670-677.

(2) Akita, H.; Hattori, T. *Journal of Polymer Science Part B: Polymer Physics* **1999**, *37*, 189-197.

(3) Green, P. F. *Soft Matter* **2011**, *7*, 7914-7926.

(4) Hule, R. A.; Pochan, D. J. *MRS Bulletin* **2007**, *32*, 354–358.

(5) Mackay, M. E.; Dao, T. T.; Tuteja, A.; Ho, D. L.; Horn, B. van; Kim, H.-C.; Hawker, C. J. *Nature Materials* **2003**, *2*, 762-6.

(6) Moniruzzaman, M.; Winey, K. I. *Macromolecules* **2006**, *39*, 5194-5205.

(7) Winey, K. I.; Vaia, R. A. *MRS Bulletin* **2007**, *32*, 314-322.

(8) Schadler, L. *Nature Materials* **2007**, *6*, 257-8.

(9) Kumar, S. K.; Krishnamoorti, R. *Annual Review of Chemical and Biomolecular Engineering* **2010**, *1*, 37-58.

(10) Jadzinsky, P. D.; Calero, G.; Ackerson, C. J.; Bushnell, D. A; Kornberg, R. D. *Science (New York, N.Y.)* **2007**, *318*, 430-3.

(11) Krishnamoorti, R. *MRS Bulletin* **2007**, *32*, 341-347.

(12) Robertson, C.; Roland, C. *Rub. Chem. Technol* **2008**, *81*, 506–522.

(13) Arrighi, V.; Higgins, J. S.; Burgess, A. N.; Floudas, G. *Polymer* **1998**, *39*, 6369–6376.

(14) Bogoslovov, R. B.; Roland, C. M.; Ellis, A. R.; Randall, A. M.; Robertson, C. G. *Macromolecules* **2008**, *41*, 1289-1296.

(15) González-Irún Rodríguez, J.; Carreira, P.; García-Diez, A.; Hui, D.; Artiaga, R.; Liz-Marzán, L. M. *Journal of Thermal Analysis and Calorimetry* **2007**, *87*, 45-47.

(16) López-Martínez, E. I.; Márquez-Lucero, A.; Hernández-Escobar, C. A.; Flores-Gallardo, S. G.; Ibarra-Gómez, R.; Yacamán, M. J.; Zaragoza-Contreras, E. A. *Journal of Polymer Science*

Part B: Polymer Physics **2007**, *45*, 511-518.

(17) Harton, S. E.; Kumar, S. K.; Yang, H.; Koga, T.; Hicks, K.; Lee, H.; Mijovic, J.; Liu, M.; Vallery, R. S.; Gidley, D. W. *Macromolecules* **2010**, *43*, 3415-3421.

(18) Ruggerone, R.; Geiser, V.; Dalle Vacche, S.; Leterrier, Y.; Månson, J.-A. E. *Macromolecules* **2010**, *43*, 10490-10497.

(19) Ash, B. J.; Schadler, L. S.; Siegel, R. W. *Materials Letters* **2002**, *55*, 83-87.

(20) Robertson, C. G.; Lin, C. J.; Rackaitis, M.; Roland, C. M. *Macromolecules* **2008**, *41*, 2727-2731.

(21) Nakatani, A. I.; Ivkov, R.; Papanek, P.; Yang, H.; Gerspacher, M. *Rubber Chemistry and Technology* **2000**, *73*, 847-863.

(22) Gagliardi, S.; Arrighia, V.; Ferguson, R.; Telling, M. T. . *Physica B: Condensed Matter* **2001**, *301*, 110-114.

(23) Vieweg, S.; Unger, R.; Heinrich, G.; Donth, E. *Journal of Applied Polymer Science* **1999**, *73*, 495-503.

(24) Tsagaropoulos, G.; Eisenberg, A. *Macromolecules* **1995**, *28*, 6067-6077.

(25) Tsagaropoulos, G.; Eisenberg, A. *Macromolecules* **1995**, *28*, 396-398.

(26) Kaufman, S.; Slichter, W. P.; Davis, D. D. *Journal of Polymer Science Part A-2: Polymer Physics* **1971**, *9*, 829-839.

(27) Litvinov, V. M.; Steeman, P. A. M. *Macromolecules* **1999**, *32*, 8476-8490.

(28) Berriot, J.; Lequeux, F.; Monnerie, L.; Montes, H.; Long, D.; Sotta, P. *Journal of Non-Crystalline Solids* **2002**, *307-310*, 719-724.

(29) O'Brien, J.; Cashell, E.; Wardell, G. E.; McBrierty, V. J. *Macromolecules* **1976**, *9*, 653-660.

(30) Dutta, N. ; Choudhury, N. R.; Haidar, B.; Vidal, A.; Donnet, J. ; Delmotte, L.; Chezeau, J. *Polymer* **1994**, *35*, 4293-4299.

(31) Cohen Addad, J. P.; Frébourg, P. *Polymer* **1996**, *37*, 4235-4242.

(32) Mitchell, C. A.; Bahr, J. L.; Arepalli, S.; Tour, J. M.; Krishnamoorti, R. *Macromolecules* **2002**, *35*, 8825-8830.

(33) Zhu, J.; Kim, J.; Peng, H.; Margrave, J. L.; Khabashesku, V. N.; Barrera, E. V. *Nano Letters* **2003**, *3*, 1107-1113.

(34) Putz, K.; Krishnamoorti, R.; Green, P. *Polymer* **2007**, *48*, 3540-3545.

(35) Allegra, G.; Raos, G.; Vacatello, M. *Progress in Polymer Science* **2008**, *33*, 683-731.

(36) Rharbi, Y.; Cabane, B.; Vacher, A.; Joanicot, M.; Boué, F. *Europhysics Letters (EPL)* **1999**, *46*, 472-478.

(37) Ehrburger-Dolle, F.; Hindermann-Bischoff, M.; Livet, F.; Bley, F.; Rochas, C.; Geissler, E. *Langmuir* **2001**, *17*, 329-334.

(38) Oberdisse, J. *Soft Matter* **2006**, *2*, 29-36.

(39) Schaefer, D. W.; Justice, R. S. *Macromolecules* **2007**, *40*, 8501-8517.

(40) Chevigny, C.; Dalmas, F.; Cola, E. Di; Gigmes, D.; Bertin, D.; Boué, F.; Jestin, J. *Macromolecules* **2010**, *44*, 122-133.

(41) Chevigny, C.; Jestin, J.; Gigmes, D.; Schweins, R.; Di-Cola, E.; Dalmas, F.; Bertin, D.; Boué, F. *Macromolecules* **2010**, *43*, 4833-4837.

(42) Starr, F. W.; Glotzer, S. C. In *Soft Materials: Structure and Dynamics*; Dutcher, J. R.; Marangoni, A. G., Eds.; Marcel Dekker: New York, 2004; pp. 107-124.

(43) Barbier, D.; Brown, D.; Grillet, A.-C.; Neyertz, S. *Macromolecules* **2004**, *37*, 4695-4710.

(44) Doxastakis, M.; Chen, Y.-L.; Guzmán, O.; de Pablo, J. J. *The Journal of chemical physics* **2004**, *120*, 9335-42.

(45) Ozmusul, M. S.; Picu, C. R.; Sternstein, S. S.; Kumar, S. K. *Macromolecules* **2005**, *38*, 4495-4500.

(46) Brown, D.; Marcadon, V.; Mélé, P.; Albérola, N. D. *Macromolecules* **2008**, *41*, 1499-1511.

(47) Nair, N.; Jayaraman, A. *Macromolecules* **2010**, *43*, 8251-8263.

(48) Vogiatzis, G. G.; Voyiatzis, E.; Theodorou, D. N. *European Polymer Journal* **2011**, *47*, 699-712.

(49) Ndoro, T.; Voyiatzis, E.; Ghanbari, A.; Theodorou, D. N.; Böhm, M. C.; Müller-Plathe, F. *Macromolecules* **2011**, *44*, 2316-2327.

(50) Milano, G.; Santangelo, G.; Ragone, F.; Cavallo, L.; Di Matteo, A. *The Journal of Physical Chemistry C* **2011**, *115*, 15154–15163.

(51) Liu, J.; Wu, Y.; Shen, J.; Gao, Y.; Zhang, L.; Cao, D. *Physical Chemistry Chemical Physics* **2011**, *13*, 13058-13069.

(52) Léger, L.; Raphaël, E.; Hervet, H. *Polymers in Confined Environments*; Granick, S.; Binder, K.; Gennes, P.-G.; Giannelis, E. P.; Grest, G. S.; Hervet, H.; Krishnamoorti, R.; Léger, L.; Manias, E.; Raphaël, E.; Wang, S.-Q., Eds.; Springer Berlin Heidelberg: Berlin, Heidelberg, 1999; Vol. 138, pp. 185-225.

(53) Léger, L. *Macromolecular Symposia* **1997**, *121*, 263-267.

(54) Bitsanis, I.; Hadziioannou, G. *The Journal of Chemical Physics* **1990**, *92*, 3827.

(55) Starr, F.; Schrøder, T.; Glotzer, S. *Physical Review E* **2001**, *64*, 021802.

(56) Harton, S. E.; Kumar, S. K.; Yang, H.; Koga, T.; Hicks, K.; Lee, H.; Mijovic, J.; Liu, M.; Vallery, R. S.; Gidley, D. W. *Macromolecules* **2010**, *43*, 3415-3421.

(57) Eslami, H.; Karimi-Varzaneh, H.; Müller-Plathe, F. *Macromolecules* **2011**, *44*, 3117–3128.

(58) Zhulina, E. B.; Borisov, O. V.; Brombacher, L. *Macromolecules* **1991**, *24*, 4679-4690.

(59) Aubouy, M.; Fredrickson, G. H.; Pincus, P.; Raphaeel, E. *Macromolecules* **1995**, *28*, 2979-2981.

(60) Ball, R. C.; Marko, J. F.; Milner, S. T.; Witten, T. A. *Macromolecules* **1991**, *24*, 693-703.

(61) Lent, B. V.; Israels, R.; Scheutjens, J. M. H. ; Fleer, G. . *Journal of Colloid and Interface Science* **1990**, *137*, 380-394.

(62) Wijmans, C. M.; Zhulina, E. B.; Fleer, G. J. *Macromolecules* **1994**, *27*, 3238-3248.

(63) Shull, K. R. *Faraday Discussions* **1994**, *98*, 203-217.

(64) Martin, J. I.; Wang, Z.-G. *The Journal of Physical Chemistry* **1995**, *99*, 2833-2844.

(65) Ferreira, P. G.; Ajdari, A.; Leibler, L. *Macromolecules* **1998**, *31*, 3994-4003.

(66) Macdowell, L. G.; Müller, M. *The Journal of Chemical Physics* **2006**, *124*, 084907.

(67) Reiter, G.; Auroy, P.; Auvray, L. *Macromolecules* **1996**, *29*, 2150-2157.

(68) Borukhov, I.; Leibler, L. *Physical Review E* **2000**, *62*, R41-R44.

(69) Borukhov, I.; Leibler, L. *Macromolecules* **2002**, *35*, 5171-5182.

(70) Trombly, D. M.; Ganesan, V. *The Journal of Chemical Physics* **2010**, *133*, 154904.

(71) Starr, F. W.; Schrøder, T. B.; Glotzer, S. C. *Macromolecules* **2002**, *35*, 4481-4492.

(72) Ndoro, T. V. M.; Böhm, M. C.; Müller-Plathe, F. *Macromolecules* **2012**, *45*, 171-179.

(73) Berriot, J.; Montes, H.; Lequeux, F.; Long, D.; Sotta, P. *Macromolecules* **2002**, *35*, 9756-9762.

(74) Brown, D.; Mélé, P.; Marceau, S.; Albérola, N. D. *Macromolecules* **2003**, *36*, 1395-1406.

(75) Goswami, M.; Sumpter, B. G. *Physical Review E* **2010**, *81*, 1-8.

(76) Borodin, O.; Smith, G. D.; Bandyopadhyaya, R.; Byutner, O. *Macromolecules* **2003**, *36*, 7873-7883.

(77) Yelash, L.; Virnau, P.; Binder, K.; Paul, W. *Physical Review E* **2010**, *82*, 2-5.

(78) Starr, F. W.; Douglas, J. F.; Glotzer, S. C. *The Journal of Chemical Physics* **2003**, *119*, 1777.

(79) Liu, J.; Gao, Y.; Cao, D.; Zhang, L.; Guo, Z. *Langmuir: the ACS journal of surfaces and colloids* **2011**, *27*, 7926-33.

(80) Hooper, J. B.; Schweizer, K. S. *Macromolecules* **2006**, *39*, 5133-5142.

(81) Smith, G. D.; Bedrov, D. *Langmuir: the ACS journal of surfaces and colloids* **2009**, *25*, 11239-43.

(82) Qian, H.-J.; Carbone, P.; Chen, X.; Karimi-Varzaneh, H. A.; Liew, C. C.; Müller-Plathe, F. *Macromolecules* **2008**, *41*, 9919-9929.

(83) Harmandaris, V. A.; Adhikari, N. P.; van der Vegt, N. F. A. ; Kremer, K. *Society* **2006**, 6708-6719.

(84) Harmandaris, V. A.; Reith, D.; van der Vegt, N. F. A. ; Kremer, K. *Macromolecular Chemistry and Physics* **2007**, *208*, 2109-2120.

Macromolecules

ARTICLE

pubs.acs.org/Macromolecules

A Simple Reverse Mapping Procedure for Coarse-Grained Polymer Models with Rigid Side Groups

Azadeh Ghanbari,* Michael C. Böhm, and Florian Müller-Plathe

Eduard-Zintl-Institut für Anorganische und Physikalische Chemie and Center of Smart Interfaces, Technische Universität Darmstadt, Petersenstrasse 20, D-64287 Darmstadt, Germany

ABSTRACT: This article introduces a simple and fast method to reinsert atomistic details into mesoscale models of polymers with rigid side groups. We describe our backmapping scheme from a coarse-grained (CG) resolution to an atomistic picture in the framework of molecular dynamics (MD) simulations of a silica−atactic polystyrene (PS) composite. The CG model of Qian et al. [Macromolecules 2008, 41, 9919] has been used in the coarse-graining; it combines the atoms of one repeat unit of PS to a CG bead. In the reverse mapping only the centers of mass of these units and their chiralities are known. We show that this information is sufficient for the reverse mapping which requires simple geometrical and mechanical considerations. The capability of the suggested method is demonstrated by comparing MD results from the original atomistic model with those emerging from the reverse mapping. Because of its simplicity, the suggested technique offers the opportunity to study relaxed structures of melt chains with large molecular weights.

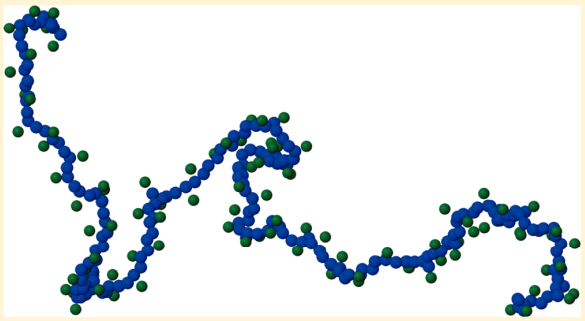

INTRODUCTION

The investigation of structure−property relations of polymeric materials by computer simulations requires the preparation of well-equilibrated melts. Large length and time scales of polymer melts can be reached by molecular dynamics (MD) and Monte Carlo (MC) variants in a so-called coarse-grained (CG) resolution, where groups of atoms are lumped together into superatoms or beads. Coarse-graining reduces the degrees of freedom to those which are assumed to be relevant for the quantities of interest.[1,2] During recent years different CG mapping schemes for polystyrene (PS) have been developed.[3−7] The CG procedures described for PS differ in the number of atoms considered in the definition of the beads as well as in the chosen bead center (the center-of-mass of the monomers or a certain atom are possible choices).[3−9] Although many quantities of complex polymer materials can be analyzed already in the CG picture, there are others where an atomistic resolution is necessary. The correlation between measured neutron diffraction data and calculated MD or MC ones is one important example.[10,11] Structural implications of absolute configurations of atoms or the determination of the orientation of ring fragments are other examples requiring atomistic simulation results. Thus, there is a need to transform CG representations of a given system back into an atomistic resolution once the relaxation and equilibration of the CG sample have been performed. This process of introducing atomistic details into a CG simulation is denoted as backmapping (BM) or reverse mapping. The variety of CG mappings implies of course the same variety in the reverse mapping schemes. Depending on the degree of coarse-graining, information on more or fewer atomic positions is lost. Hence, the demands on BM are predetermined by the type of coarse-graining. It is the purpose of the present contribution to introduce—in the framework of molecular dynamics simulations—a backmapping scheme for coarse-grained atactic polystyrene that is in contact with silica surface. This research has been motivated by our present computer simulations of silica−PS nanocomposites, where the mapping scheme of Qian et al.[3] has been used for the PS. A convenient BM procedure for the adopted CG scheme is the prerequisite to correlate CG simulations results with both atomistic data and various experimental results. Detailed studies of these samples are left for a forthcoming publication.

SYSTEM AND COMPUTATIONAL CONDITIONS

In the present article we have employed the scheme of Qian et al.[3] for coarse-graining atactic PS, the polymer component of a silica−PS nanocomposite. In this mapping scheme each repeat unit of PS is represented by one CG bead, located at the repeat unit's center-of-mass, and is called a (1:1) mapping. This CG model has two different beads (R and S) for repeat units of different chirality in order to describe tacticity. Milano et al.[4] proposed another (1:1) mapping scheme for PS which still conserves the underlying atomistic backbone, as the centers of the beads coincide with backbone-atom position. Santangelo et al.[10]

Received: March 15, 2011
Revised: May 27, 2011
Published: June 15, 2011

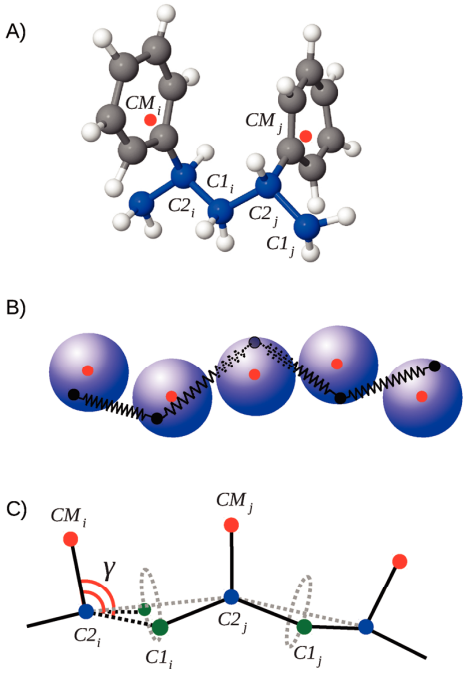

Figure 1. (A) Schematic representation of two adjacent PS monomers. CM denotes the center-of-mass of the monomer, C1 a methylene carbon in the backbone, and C2 an asymmetric backbone carbon. (B) Schematic view of a sphere−spring representation of the PS polymer. (C) Essential geometrical elements required for the insertion of the atomistic position of the methylene (C1) and chiral (C2) carbons of PS in the present backmapping scheme. γ denotes the angle between the center-of-mass CM and the backbone carbons C1 and C2.

proposed a BM procedure for the above-mentioned CG model. A simple backmapping strategy for the (1:1) CG model of Qian et al.,[3] which does not carry information about the backbone structure, has not been reported until now. A description of this type of backmapping is the heart of the present work.

In the (2:1) schemes reported by others,[6,8] where each repeat unit is coarsened to two CG beads, the coordinates of the PS backbone atoms (see Figure 1) can be conserved in the CG representation. Hence, the CG structure is quite close to the atomistic one, and reverse mappings of coarse-grained PS are simpler than in the (1:1) case. The advantage of the adopted (1:1) CG scheme compared to (2:1) ones, besides the smaller number of interactions, is that all CG beads have the same mass, which is important for facilitating long time steps in CG simulations.[3]

The silica−PS composite studied in the present work is defined by one SiO_2 nanoparticle with a diameter of 4 nm and 202 identical polystyrene chains of 20 monomers ($N_L = 20$).[2,12] Each CG bead of the nanoparticle is formed by a single SiO_2 unit, located at the Si position. The chosen diameter leads to 873 of these beads. The PS superatoms in the adopted (1:1) coarse-graining are defined by one molecular repeat unit. Thus, we arrive at 4040 CG beads for the polymer. To derive the CG potential of the studied composite, we have adopted the in-house MD code IBIsCO.[13] The iterative Boltzmann inversion (IBI)[2] has been chosen to optimize the CG potential on the basis of bonded and nonbonded radial distribution functions (RDFs) of the atomistic reference, which have been generated from atomistic trajectory files. Detailed information on the IBI can be found elsewhere.[2,14,15] Most of the present calculations have been performed at a temperature (T) of 590 K, while an ambient pressure (P) of 101.3 kPa has been assumed throughout. The choice $T = 590$ K has been a result of the atomistic precursor simulations. In this resolution equilibrations at lower T would be too time-consuming.[12] The program code IBIsCO,[13] which works with tabulated numerical potentials, has been adopted for the CG part of our study. The Berendsen thermostat[16] (coupling time (τ) of 0.2 ps) and barostat ($\tau = 5.0$ ps, isothermal compressibility of 1.0×10^{-6} kPa^{-1}) have been used. The nonbonded interactions were truncated beyond 1.5 nm; the neighbor list cutoff amounts to 1.6 nm. The time step is set up to 4 fs.

The atomistic MD simulations of the backmapped system have been performed with the YASP code.[17] The necessary force-field parameters for the polymer and the inorganic nanoparticle have been taken from our recent MD study of silica−PS composites.[12] In the final step of the backmapping we have allowed relaxation of the sample under isothermal−isobaric (NPT) conditions at $P = 101.3$ kPa and $T = 590$ K. These simulations have been executed with coupling times of 0.2 and 2.0 ps for the Berendsen thermostat and barostat. The time step now chosen amounts to 1 fs. A cutoff of 1.0 nm has been used for the nonbonded interactions. The MD results have been analyzed after relaxing the system for 2.0 ns.

BACKMAPPING STRATEGY

Backmapping of the studied silica−PS composite has been performed in two different steps in order to profit from the fixed atomic positions of the solid SiO_2 fragment. Here the BM step is straightforward and thus not commented on in the present work. The backmapping of the polymer consists of separate steps: First, atomistic fragments are threaded onto the coarse-grained backbone by geometrical operations. Second, the resulting atomistic structure is relaxed by a protocol of several very short molecular dynamics runs. The procedure is described in this section.

In an atomistic picture, each PS monomer has two backbone carbons, i.e., the methylene and chiral carbons C1 and C2 (see Figure 1A). The symbol CM in this diagram denotes the center-of-mass of a PS monomer. In the CG representation only the centers-of-mass and the chiralities of the beads are known. With the help of these data, our first BM step is the determination of the coordinates of the chiral −CHPh− carbon atom (C2 in Figure 1) of each monomer by a simple but rigorous approach. Ph states for a phenyl group. Then we locate the $-CH_2-$ methylene carbons (C1 in Figure 1) in the backbone of each monomer in a way that the desired chirality of all chain monomers is conserved. Knowledge of the coordinates of these two backbone carbons and the center-of-mass of the repeat unit is sufficient for a unique insertion of an atomistic template monomer with the help of simple rigid rotations and translations. Subsequently, we perform short MD runs to remove any overlap in the sample by gradually increasing nonbonded interactions.

Reduction of the Problem to a Sphere−Spring Model, Insertion of the C2 Atoms. For placing the chiral carbon atoms (C2) of the polymer, the average distance $R_s = \langle[(\vec{X}_{CM} - \vec{X}_{C2})^2]^{1/2}\rangle$ between CM and C2 positions in a monomer of atactic PS together with the average distance $L = \langle[(\vec{X}_{C2_i} - \vec{X}_{C2_j})^2]^{1/2}\rangle$ between C2 atoms of neighboring units are needed, where $\vec{X}_P$ symbolizes the Cartesian coordinates of point P. The indices i (from 1 to $N_L - 1$) and $j = i + 1$ denote chain monomers.

Table 1. Average Values and Associated Standard Deviations for the Bond $C2_i-C1_i$ and Angles $C2_i-C1_i-C2_j$ and $CM_i-C2_i-C1_i$ in the Considered Nanocomposite Sample[a]

$C2_i-C1_i$ (nm)	0.156 ± 0.003
$C2_i-C1_i-C2_j$ (deg)	114.89 ± 3.31
$CM_i-C2_i-C1_i$ (deg)	111.63 ± 3.51

[a] The data have been derived in the initial atomistic MD run at T = 590 K and P = 101.3 kPa.

They have been determined from the atomistic reference calculations,[12] which are the basis of the CG model: $R_s = 0.212 \pm 0.005$ nm and $L = 0.263 \pm 0.008$ nm (T = 590 K and P = 101.3 kPa).

To find the position of the C2 carbon atoms in the framework of the sphere−spring model, consider a single chain of N_L monomers. Around the center-of-mass CM of each bead, we define a sphere of radius R_s and moment of inertia I. These spheres are fixed in their position but are allowed to rotate around their center. Then we choose one random point $\vec{X}'_{C2}$ on each sphere as an initial guess for the C2 position. The points $\vec{X}'_{C2}$ of two neighboring beads are connected by a harmonic spring potential $V(l) = k(L - l)^2/2$, where L is the average equilibrium distance between two neighboring C2 atoms, l is their actual distance, or length of the spring, and k = 1 N/m is the force constant (see Figure 1B). Since most springs will not be in their equilibrium position in the initial configuration, each C2 carbon atom experience a net force from its two neighbors. Sphere i will rotate under the influence of the torque $\vec{\tau}_i = \vec{R}_{s,i} \times \vec{F}_i$, where $\vec{R}_{s,i}$ is the vector connecting $\vec{X}'_{C2}$ of the ith sphere with $\vec{X}_{CM_i}$ and $\vec{F}_i$ is net force on it. The equation of motion governing the rotation of sphere i is $\vec{\tau} = I\vec{\alpha}_i$, where $\vec{\alpha}_i$ is angular acceleration.

Defining ω_i as the angular velocity, $\Delta\theta_i = {}^1/_2\alpha_i\Delta t^2 + \omega_i\Delta t$ is the angular displacement of the ith sphere within the step Δt. To avoid uncontrolled rotations and hence divergence problem, we have chosen Δt, I, and k in a way that each sphere will rotate only a few degrees per time step. This criterion is fulfilled by setting I = 1 kg m^2, k = 1 N/m, and Δt = 0.1 s. At each time step the initial angular velocity is reset to zero, hence each sphere rotates around its rotational axis which is in the direction of $\vec{\tau}_i$. Thus, each sphere rotates so as to reduce the net force on it, which is equivalent to a steepest-descent energy minimization (SDEM) in orientation space. Thereby the potential energy of the system decreases until its minimum is reached. The SDEM procedure continues up to a point where the potential energy of the sphere−spring model cannot be reduced further. This threshold is reached when the largest residual torque falls below 0.001 N m. At this point the lengths of all the springs are within 0.015 nm of their equilibrium length L. According to our experience, the final chain configuration does not depend sizably on the initial random configuration. As a quantitative example, we applied the sphere−spring model for a CG chain with 100 monomers. These tests have been performed for 10 different initial configurations. The mean distance of predicted positions for each C2 atoms from the corresponding average position was 0.11 nm.

Up to now we have determined the position of the C2 carbon atoms in each fragment only with the knowledge of the centers of mass and the distances R_s and L. Thereby, we have localized half of the backbone atoms.

Insertion of the C1 Atoms. The next step in our backmapping procedure is the insertion of the methylene carbon $C1_i$ of each fragment i which is bonded to $C2_i$ and $C2_j$. This triplet of atoms defines the bond angle $C2_i-C1_i-C2_j$. Insertion of C1 requires

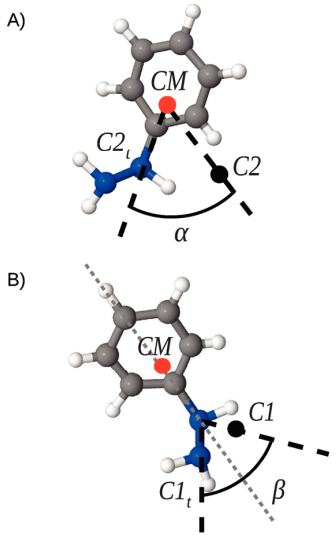

Figure 2. (A) Rotation of a molecular fragment under consideration of CM to shift the atomistic template carbon $C2_t$ to the backmapped position C2. (B) Rotation around the CM−C2 axis to shift the methylene carbon $C1_t$ to position C1.

knowledge of the chirality of the monomers. We use the average values of the bond length $C2_i-C1_i$ and bond angle $C2_i-C1_i-C2_j$ which are known from the atomistic reference trajectory (Table 1). With these geometrical parameters a circle can be generated which defines the possible location of $C1_i$ (see Figure 1C). With the help of the angle γ defined by the triplet $CM_i-C2_i-C1_i$ also available from the atomistic trajectory (Table 1), the $C1_i$ position on the ring becomes constrained to two possibilities. The chirality (R or S) of the PS monomer determines on which side of the plane spanned by $CM_i-C2_i-C2_j$ the $C1_i$ carbon atom has to be placed. At this stage, the backbone has been fully constructed.

Insertion of the Whole Fragment. For the next BM step we need two coordinate triplets $\vec{X}_{C1_t}$, $\vec{X}_{C2_t}$, $\vec{X}_{CM_t}$, and $\vec{X}_{C1}$, $\vec{X}_{C2}$, $\vec{X}_{CM}$. The index t symbolizes that these coordinates refer to an atomistic template fragment extracted for example from the original atomistic reference trajectory (as the styrene repeat unit is very stiff, the template can also be taken from other sources). The other coordinate triplet is derived in the reverse mapping steps described above. First we shift the center-of-mass of the atomistic template $\vec{X}_{CM_t}$ to the backmapped coordinate $\vec{X}_{CM}$ leading to $\vec{X}_{CM_t} = \vec{X}_{CM}$. Next we match the $\vec{X}_{C2_t}$, $\vec{X}_{C1_t}$ coordinates to the $\vec{X}_{C2}$, $\vec{X}_{C1}$ set estimated in the reverse mapping (Figure 2). The set $\vec{X}_{C2_t}$, $\vec{X}_{CM}$, $\vec{X}_{C2}$ defines a plane, $\vec{n}$ being the normal vector. By a rotation of the molecular fragment around $\vec{n}$ by an angle α (Figure 2A), we move $\vec{X}_{C2_t}$ to its correct position $\vec{X}_{C2}$. Finally, we rotate the whole fragment around the C2−CM axis by an angle β and move $\vec{X}_{C1_t}$ to $\vec{X}_{C1}$ (Figure 2B). At this point, we have a complete atomistic structure of the chain. Very recently, Ensing and Nielsen have adopted similar operations in their reverse mapping algorithm.[18] Note that the outlined procedure is applicable to all vinyl polymers whose repeat units can be considered as rigid. For flexible side chains, the procedure has to be modified. Some inter- and intrachain overlaps of the PS atoms are still possible at this stage. Also, some of the estimated bond lengths will not be in the desired range. The atomistic

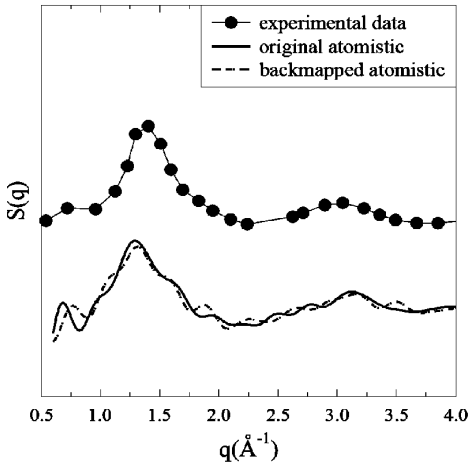

Figure 3. X-ray structure factor $S(q)$ of backmapped bulk atactic PS chains of 20-mers (continuous line) and of the original atomistic system (dashed line), both at $T = 300$ K and $P = 101.3$ kPa. Above the simulation results is shown experimental[21] X-ray scattering pattern (filled circles) of atactic PS (16 monomer per chain, $T = 323$ K).

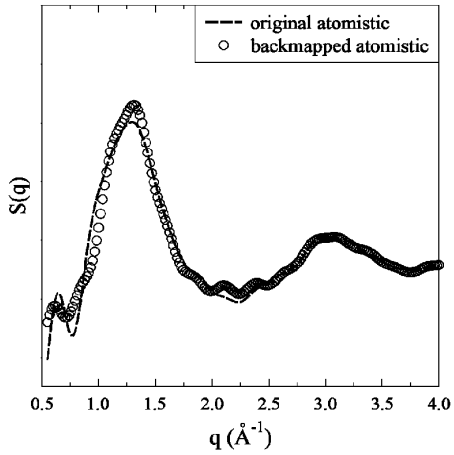

Figure 4. X-ray structure factor of the PS component of the silica−PS nanocomposite in backmapped (continuous line) and the original atomistic[12] (dashed line) resolutions. The simulations have been performed for 20-mer chains at $T = 590$ K and $P = 101.3$ kPa.

simulation protocol to further relax the system is described in the next subsections.

NVT Simulations at Zero Temperature. Initially, zero-temperature MD simulations at constant volume and using the Berendsen thermostat (coupling time (τ) of 0.5 fs and bath temperature 0 K, the average temperature is 18.78 K) are performed with a time step $\Delta t = 0.005$ fs. The number of time steps Δt is 500 000, leading to a time for this stage of 2.5 ps. To optimize the bonded part of the potential, all nonbonded interactions in the atomistic force field are switched off during this simulation. In the course of this zero-temperature run all bond lengths and angles reach their equilibrium values. The average displacement of the monomers (centers-of-mass) from their initial positions does not exceed 0.01 nm during the whole zero-temperature run so the overall chain conformation as produced by the CG simulation is preserved.

Soft-Core Simulations for the Nonbonded Interactions. In the next stage of relaxation, the nonbonded interactions are reintroduced. However, a soft-core potential is applied to them to remove possible overlaps, concatenation, and spearing between different PS chains. As this method has been commented on in detail in recent backmapping studies of the group,[19,20] only a short overview will be given here. The soft-core potential is implemented into the YASP package[17] by replacing the short-range part (<0.32 nm) of the nonbonded Lennard-Jones potential by a cubic spline. The spline coefficients have been determined to reproduce the original potential energy and its derivative at the crossover distance as well as to have a finite value V_0 and a zero derivative at a distance of zero. With this choice atoms can pass through each other, thereby allowing a relaxation of high-energy configurations. The value of V_0 is increased in four steps (50, 100, 500, and 1000 kJ/mol). For each value, an MD simulation of 50 000 time steps $\Delta t = 0.005$ fs (i.e., 0.25 ps) is performed at a bath temperature of 590 K, with a temperature coupling time of 0.5 fs. Finally, the full nonbonded potential without soft core is restored. In these runs, the time step is gradually brought from its initial value 0.005 fs to the regular value of 1 fs. For every new value of Δt (typically an order of magnitude larger than the last) we run an NVT simulation over 50 000 time steps.

These runs amount to ∼75 ps of simulation time. The last step of relaxation is a standard constant-volume simulation of 1 ns. For the subsequent data analysis, another 1 ns simulation is used.

■ VALIDATION OF THE BACKMAPPING PROCEDURE

To test the ability of the present BM method to generate structural features of polymer chains, the structure factor $S(q)$ obtained through the Fourier transform of the atomistic radial distribution functions (RDF) of the reverse mapped PS model (without a nanoparticle) was compared with the measured X-ray diffraction pattern in Figure 3. In contrast to the 590 K simulations performed for the nanocomposite, we now have chosen $T = 300$ K to allow a better comparison with experiment with has been performed at 328 K. The measured intensity pattern[21] is well reproduced by the simulated one. The so-called polymerization peak, which is mainly due to intermolecular correlations between backbone atoms, appears at the same wavenumber ($q = 0.75$ Å^{-1}) as in experiment. The main peak, known as amorphous peak, which arises primarily from phenyl−phenyl correlations and appears at 1.4 Å^{-1} in the experimental data, is centered at a bit lower wavenumber in the calculated $S(q)$, around 1.35 Å^{-1}. There is a third calculated peak at $q = 3.1$ Å^{-1} that is also found in experiment. In Figure 3, the calculated structure factor for the reference atomistic simulation is shown, too. Its good agreement with the reverse mapped X-ray pattern shows that the difference between calculated and experimental structure factors, namely the amplitude and relative position of the peaks, is due to the adopted force field. These results confirm the ability of the reverse mapping procedure to reproduce realistic structural features of polymers.

Then we applied the BM method to the PS component of the silica−PS composite, where the necessity of a fast and simple reverse mapping scheme comes from. The structure factor of the reverse mapped PS component of the nanocomposite calculated by a Fourier transform of RDFs of coarsened monomers is shown in Figure 4. The excellent agreement with calculated X-ray

Table 2. Total Mass Density (ρ) of the Silica−PS Composite, Radius of Gyration (R_g), and End-to-End Distance (R_0) of the Atactic PS Component of the Studied Nanocomposite As Derived in the Atomistic Reference Simulation, the CG Simulation, and the Atomistic Simulation after Backmapping[a]

	original atomistic	coarse-grained	backmapped atomistic
density (kg/m^3)	980.91 ± 0.08	978.24 ± 0.03	978.95 ± 0.03
radius of gyration, $\langle R_g^2\rangle^{1/2}$ (nm)	0.95 ± 0.01	1.01 ± 0.01	0.99 ± 0.01
end-to-end distance, R_0 (nm)	2.25 ± 0.05	2.43 ± 0.06	2.43 ± 0.05

[a] For each quantity we have given the MD inherent error bars, calculated as standard deviation of the quantity around corresponding average value over 1000 frames.

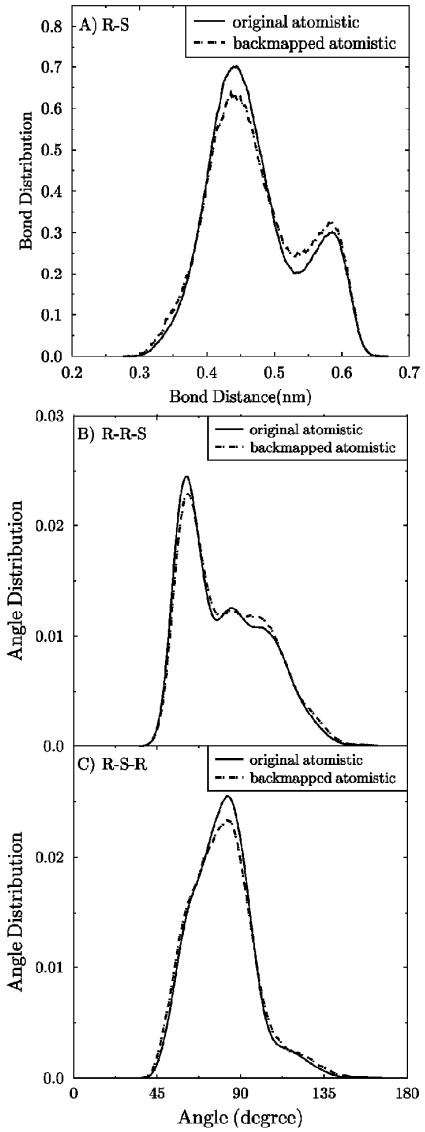

Figure 5. Distribution function of the R−S (A) bond and R−R−S (B) and R−S−R angles (C) of atactic PS according to the original atomistic target simulation[12] and the backmapping approach.

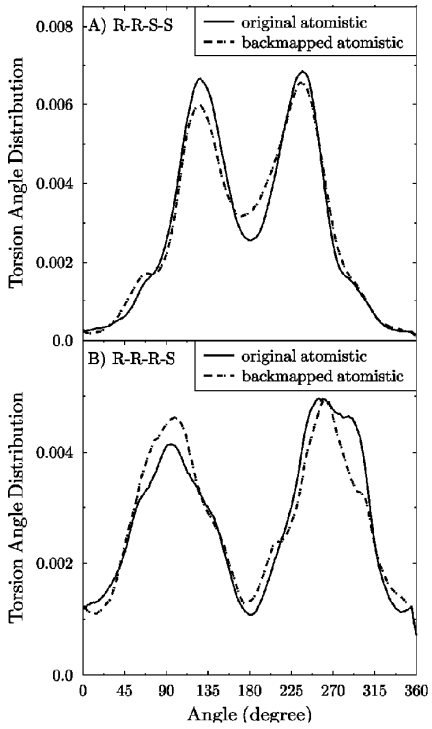

Figure 6. Distribution function of the intrachain torsional angles R−R−S−S (A) and R−R−R−S (B) of atactic PS according to the reference atomistic MD[12] and after backmapping.

pattern of the original atomistic simulation (after about 2 ns of equilibration) indicates that structural properties of the PS chains are successfully retrieved upon backmapping the CG structure also in the presence of the nanoparticle. There is a small prepeak at q = 0.7 Å^{-1}, close to the wavenumber where the polymerization peak appears in the experimental data of pure PS. The main peak at q = 1.25 Å^{-1} is followed by a third peak at approximately q = 3 Å^{-1}.

NPT simulation of the backmapped silica−PS composite at the same pressure and temperature as adopted in the CG simulations results in an overall density (ρ) of 979.0 kg/m^3, which is in good agreement with atomistic simulation data (ρ = 980.9).[12] In Table 2 we relate the two atomistic ρ (i.e., original atomistic simulation,[12] after backmapping) to the CG value. In addition to the density other structural parameters (i.e., radius of gyration $\langle R_g^2\rangle^{1/2}$ and end-to-end distance (R_0)) as derived by the three MD variants are compared. We see that the backmapped R_g and R_0 are close to the reference atomistic values as well as to the CG values.

In Figure 5, we have plotted the distribution functions of the R−S bond as well as the R−R−S and R−S−S angles of

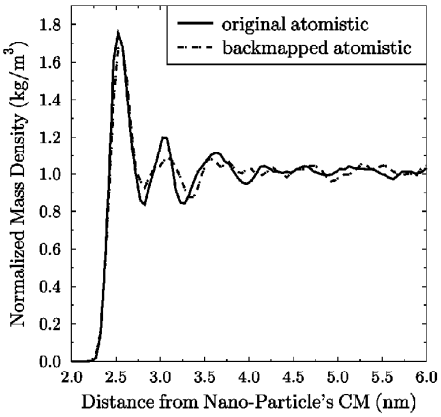

Figure 7. Radial profile of the normalized mass density $\rho(r)/\rho(\text{bulk})$ of the polymer component of the silica−PS composite from the refrence atomistic MD[12] simulation and after backmapping.

polystyrene in the nanocomposite calculated in the reference atomistic simulation (used to develop the CG model)[12] and after backmapping (T = 590 K). R and S refer to monomers of the two possible chiralities. The BM distribution functions are of the same widths as derived in the atomistic reference simulation. Even the height of the atomistic curves is reproduced with sufficient accuracy by the present reverse mapping. The same good agreement is also observed for the other bond and angle distribution functions not shown here. Figure 6 gives the distribution functions for the torsional angles R−R−S−S (top diagram) and R−R−R−S (bottom diagram) derived in the reference atomistic run and the backmapped simulations. The good agreement between the two profiles indicates that the reverse mapping retains the correct tacticity of the chains. As this must be the case by construction of the BM procedure, the agreement is evidence for a correct implementation and execution of it.

As last example, the normalized radial mass density ($\rho(r)_n$ = $\rho(r)/\rho(\text{bulk})$) of the polymer around the nanoparticle in the silica−PS nanocomposite is compared (Figure 7) for the original atomistic simulation[12] and after backmapping, where $\rho(\text{bulk})$ stands for the bulk density of a neat polymer sample. The positions of the $\rho(r)_n$ maxima and minima are reproduced with good accuracy. The strong first maximum followed by at least one second peak is characteristic for attractive nanoparticle−polymer interactions.[12] It reflects an increased ordering of the surface near polymer chains and thus the formation of an interlayer. This calculated interlayer region for the silica−PS composite is in agreement with other studies.[22−24] The observed difference in the amplitude of maxima and minima in the density profile of original atomistic and the backmapped simulations can be attributed to atomistic data not fully equilibrated. The fast CG simulations now allow further relaxation.

CONCLUSIONS

A new simple backmapping procedure has been proposed for vinyl polymers whose repeat units can be considered rigid. As a test, it has been applied for the polymer part of a silica−polystyrene nanocomposite. The present backmapping scheme makes use of elementary geometrical and classical mechanics considerations. It requires neither expensive evaluations of the potential energy nor force determinations at individual atoms. Global structural properties of the backmapped PS, such as the gyration radius and end-to-end distance, reproduce atomistic reference simulations. The structure factor of bulk PS after backmapping is in good agreement with experimental measurements as well as with that calculated in reference atomistic simulations. The same good agreement is also observed for the polymer part of the nanocomposite. Comparison with experiment is here not possible due to the lack of data.

Most of the published backmapping procedures have been designed for CG schemes in which the atomistic backbone information is preserved by the chosen bead locations.[5,10,19,25−27] In our BM procedure, this information is not needed in the coarse-graining scheme. The main advantage of our BM method compared to existing schemes is that it requires less structural information. The sphere−spring model allows the reinsertion of atomistic templates via rigid rotations.

The backmapped atomistic system prepared at this step does not have strong overlaps between the atoms. This is achieved by the energy minimization step in the sphere−spring model. Moreover, it correctly takes into account the tacticity of the chain. Santangelo et al.[10] proposed a BM scheme for PS where the concept of quaternions is used to correctly orient atomistic diads into the CG structure. They used position restraints and additional repulsive particles at the centers of phenyl rings together with scaled Lennard-Jones potentials to further relax the chains and to remove catenation of phenyl rings. The present scheme is somewhat simpler. It requires the insertion of rigid atomistic fragments (from a library) into the CG configuration. The fragments are taken from a short atomistic trajectory and have minimum-energy structure. Catenation of phenyl rings rarely happens in the proposed method because the backmapping scheme places the centers of mass of the monomers, which are close to the phenyl-ring centers, away from each other. Therefore, the probability of catenation is much reduced already in the stage of geometrical reconstruction. The main source of possible overlap in the backmapped configuration is due to the end groups, which have only one neighboring monomer. This widens the range of space where C1 and C2 carbons of the end groups can be found, increasing the chance to overlap with nearby atoms. The relative orientation of the phenyl rings, however, is not optimized in the insertion algorithm. Any possible overlap originating from this is efficiently relaxed in the ensuing molecular dynamics protocol.

Spyriouni et al.[5] proposed yet another backmapping method for atactic polystyrene. Compared to this scheme, our technique requires fewer parameters to be matched during the reverse mapping procedure. To sum up, with respect to the relaxation as well as the removal of intra- and interchain overlaps the present reverse mapping follows the lines of well established backmapping tools. In contrast to other schemes, we make explicit use of simplifications that are caused by rigid side groups. This allowed us to work with a minimum of structural information.

A comparison of the structural properties of the backmapped system with the reference simulations of the same atomistic model and also with experimental data, where available, indicates the ability of the outlined BM procedure to reproduce realistic chain configurations.

AUTHOR INFORMATION

Corresponding Author

*E-mail: a.ghanbari@theo.chemie.tu-darmstadt.de.

■ ACKNOWLEDGMENT

The authors are grateful to Tinashe Ndoro for providing the atomistic trajectory as well as to Mohammad Rahimi and Frédéric Leroy for their useful comments. Special thanks from A.G. to Jaber Dehghany for many informative discussions and his encouragement. Finally, we thank Sabine Philipp for critically reading the manuscript. This work has been funded by the EU project NanoModel (211778) as well as by the Deutsche Forschungsgemeinschaft through the Priority Programme 1369 Polymer-Solid Contacts: Interfaces and Interphases.

■ REFERENCES

(1) Müller-Plathe, F. *Soft Matter* **2003**, *1*, 1.
(2) Reith, D.; Pütz, M.; Müller-Plathe, F. *J. Comput. Chem.* **2003**, *24*, 1624.
(3) Qian, H.-J.; Carbone, P.; Chen, X.; Karimi-Varzaneh, H. A.; Liew, C. C.; Müller-Plathe, F. *Macromolecules* **2008**, *41*, 9919.
(4) Milano, G.; Müller-Plathe, F. *J. Phys. Chem. B* **2005**, *109*, 18609.
(5) Spyriouni, T.; Tzoumanekas, C.; Theodorou., D. N.; Müller-Plathe, F.; Milano, G. *Macromolecules* **2007**, *40*, 3876.
(6) Harmandaris, V. A.; Reith, D.; van der Vegt, N. F. A.; Kremer, K. *Macromol. Chem. Phys.* **2007**, *208*, 2109.
(7) Sun, Q.; Faller, R. *Macromolecules* **2006**, *39*, 812.
(8) Harmandaris, V. A.; Adhikari, N. P.; van der Vegt, N. F. A.; Kremer, K. *Macromolecules* **2006**, *39*, 6708.
(9) Sun, Q.; Faller, R. *Comput. Chem. Eng.* **2005**, *29*, 2380.
(10) Santangelo, G.; Di Matteo, A.; Müller-Plathe, F.; Milano, G. *J. Phys. Chem. B* **2007**, *111*, 2765.
(11) Tschöp, W.; Kremer, K.; Hahn, O.; Batoulis, J.; Burger, T. *Acta Polym.* **1998**, *49*, 75.
(12) Ndoro, T. V. M.; Voyiatzis, E.; Ghanbari, A.; Theodorou, D. N.; Böhm, M. C.; Müller-Plathe, F. *Macromolecules* **2011**, *44*, 2316.
(13) Karimi-Varzaneh, H. A.; Qian, H. J.; Chen, X.; Carbone, P.; Müller-Plathe, F. *J. Comput. Chem.* **2010**10.1002/jcc.21717.
(14) Carbone, P.; Karimi-Varzaneh, H. A.; Chen, X.; Müller-Plathe, F. *J. Chem. Phys.* **2008**, *128*, 064904.
(15) Reith, D.; Meyer, H.; Müller-Plathe, F. *Macromolecules* **2001**, *34*, 2335.
(16) Berendsen, H. J. C.; Postma, J. P. M.; Van Gunsteren, W. F.; Dinola, A.; Haak, J. R. *J. Chem. Phys.* **1984**, *81*, 3684.
(17) Müller-Plathe, F. *Comput. Phys. Commun.* **1993**, *78*, 77.
(18) Ensing, B.; Nielsen, S. O. In *Trends in Computational Nanomechanics Transcending Length and Time Scales*; Dumitrica, T., Ed.; Springer: Berlin, 2010; Vol. 9, p 25.
(19) Karimi-Varzaneh, H. A.; Carbone, P.; Müller-Plathe, F. *J. Chem. Phys.* **2008**, *129*, 154904.
(20) Carbone, P.; Karimi-Varzaneh, H. A.; Müller-Plathe, F. *Faraday Discuss.* **2010**, *144*, 25.
(21) Londono, J. D.; Habenschuss, A.; Curro, J. G.; Rajasekaran, J. J. *J. Polym. Sci., Part B: Polym. Phys.* **1996**, *34*, 3055–3061.
(22) Vogiatzis, G.; Voyiatzis, E.; Theodorou, D. N. *Eur. Polym. J.* **2010**10.1016/j.eurpolymj.2010.09.017.
(23) Barbier, D.; Brown, D.; Grillet, A. C.; Neyertz, S. *Macromolecules* **2004**, *37*, 4695.
(24) Brown, D.; Mele, P.; Marceau, S.; Alberola, N. D. *Macromolecules* **2003**, *36*, 1395.
(25) Queyroy, S.; Neyertz, S.; Brown, D.; Müller-Plathe, F. *Macromolecules* **2004**, *37*, 7338.
(26) Mulder, T.; Harmandaris, V. A.; Lyulin, A. V.; van der Vegt, N. F. A.; Michels, M. A. J. *Macromol. Theory Simul.* **2008**, *17*, 393.
(27) Hess, B.; Leon, S.; van der Vegt, N. F. A.; Kremer, K. *Soft Matter* **2006**, *2*, 409.

Macromolecules

Article

pubs.acs.org/Macromolecules

Interphase Structure in Silica–Polystyrene Nanocomposites: A Coarse-Grained Molecular Dynamics Study

Azadeh Ghanbari,* Tinashe V. M. Ndoro, Frédéric Leroy, Mohammad Rahimi, Michael C. Böhm, and Florian Müller-Plathe

Eduard-Zintl-Institut für Anorganische und Physikalische Chemie and Center of Smart Interfaces, Technische Universität Darmstadt, Petersenstrasse 20, D-64287 Darmstadt, Germany

ABSTRACT: Silica nanoparticles (NPs) embedded in atactic polystyrene (PS) are simulated using coarse-grained (CG) potentials obtained via iterative Boltzmann inversion (IBI). The potentials are parametrized and validated on polystyrene of 2 kDa (i.e., chains containing 20 monomers). It is shown that the CG potentials are transferable between different systems. The structure of the polymer chains is strongly influenced by the NP. Layering, chain expansion, and preferential orientation of segments as well as of entire chains are found. The extent of the structural perturbation depends on the details of the system: bare NPs vs NPs grafted with PS chains, grafting density (0, 0.5, and 1 chains/nm^2), length of the grafted chains (2 and 8 kDa), and the matrix chains (2–20 kDa). For example, there is a change in the swelling state for the grafted corona (8 kDa, 1 chains/nm^2), when the matrix polymer is changed from 2 to > 8 kDa. This phenomenon, sometimes called "wet brush to dry brush transition", is in good agreement with neutron scattering investigations. Another example is the behavior of the radius of gyration of free polymer chains close to the NP. Short chains expand compared to the bulk, whereas chains whose unperturbed radius of gyration is larger than that of the NP contract.

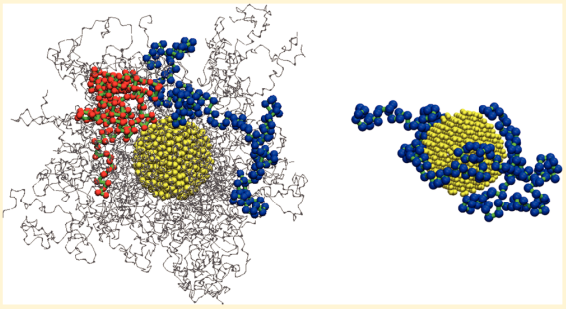

1. INTRODUCTION

Nanocomposite materials (NCMs) are formed by filling a polymer matrix with inorganic particles whose typical dimensions are of the order of a few nanometers. The nanosized fillers induce improvements in the material's macroscopic properties,[1−5] which makes them attractive for industrial applications. For instance, it has been reported by Mackay et al.[6] that the addition of nanoparticles (NPs) to polymer materials can lower their viscosity. Such a modification is useful in extrusion and injection molding processes. The presence of NPs introduces an enormous amount of interfacial area in which polymer chains undergo conformational changes and deformations at the nanoscale.[4] The interfacial contact in NCMs manifests itself as perturbation of the structure (e.g., density, chain orientation, arrangement, and stretching or wrapping around the NP)[7−9] and the dynamics (slower dynamics of the chains in the vicinity of the NP and formation of glassy polymer layers around the NP[10−13]) of the polymer. This region of altered polymer properties is commonly termed as interphase in the literature. Tuning of the interfacial interaction between the nanocomposite components is often the critical step in controlling the ultimate structural,[3,9,14,15] dynamic,[16] mechanical,[2,17] and thermodynamic[16] properties of the NCMs. A well-defined manipulation of these interactions needs a comprehensive understanding of structure–property relationships in NCMs. This includes knowledge of the structure and properties of the interphase at a quantitative level. Despite numerous experimental,[18−20] theoretical,[21−24] and computer simulation studies,[2,8,9,14,15,25] a detailed understanding of these relationships is still missing.

A possible explanation for this deficit might be the inconsistency between certain experimental results. For example, Bogoslovov et al.[26] studied the effect of reinforcement of poly(vinyl acetate) via silica NPs by modulated differential scanning calorimetry (MDSC) and dielectric relaxation measurements. They reported that the segmental relaxation dispersion and relaxation times did not show any evidence of immobilization of polymer chains residing at the silica interface. Although there may be some stiffening of the elastomer in the proximity of the fillers, Robertson et al. reported that this process does not translate into a significant suppression of the segmental dynamics in filled rubbers.[27] Tsagaropoulos and Eisenberg,[28,29] on the other hand, reported two dynamic processes within polymers filled with very fine silica particles (of 7 nm diameter), using dynamical mechanical analysis (DMA). They related one of the processes to the glass transition of the polymer matrix, while the other one has been attributed to the glass transition of immobilized chains near the

Received: September 8, 2011
Revised: November 21, 2011
Published: December 6, 2011

Table 1. Studied Nanocomposites with a Fixed Nanoparticle Radius of 2 nm (T = 590 K, P = 101.3 kPa)

grafting density (chains/nm^2)	no. of grafted chains	grafted chains length (monomers)	no. of free chains	free chains length (monomers)	NP vol fraction (%)	simulation time (ns)	mass density (kg/m^3)	box length (nm)
0.0			202	20	5.26	20	978.24 ± 2.62	9.30
0.0			202	40	2.15	12	958.41 ± 0.90	11.59
0.0			101	80	2.17	12	966.36 ± 1.32	11.55
0.0			500	100	0.35	24	938.02 ± 3.84	21.05
0.0			404	200	0.22	32	939.24 ± 0.15	24.58
0.5	25	80	808	20	0.95	16	924.45 ± 0.66	15.20
0.5	25	80	404	40	0.97	16	940.40 ± 1.20	12.12
0.5	25	80	202	80	0.98	20	948.41 ± 0.75	15.07
0.5	25	80	135	120	0.98	36	950.96 ± 1.00	15.06
0.5	25	80	101	160	0.98	40	952.09 ± 1.00	15.04
1.0	50	20	177	20	3.66	14	981.80 ± 1.06	9.70
1.0	50	80	708	20	0.96	20	929.54 ± 1.37	15.18
1.0	50	80	354	40	0.97	20	943.56 ± 0.90	15.11
1.0	50	80	177	80	0.98	20	950.24 ± 0.83	15.07
1.0	50	80	118	120	0.98	40	953.01 ± 0.87	15.06
1.0	50	80	88	160	0.98	50	953.69 ± 0.97	15.04

fillers. Similarly, Chen et al. have recently confirmed the existence of two dynamic processes, performing DMA on poly(vinyl alcohol)/silica NCMs.[30]

This discrepancy in the experimental results emphasizes the care which must be taken for further accurate and well-designed studies. Computer simulations provide the most detailed look at the nature of nanometer-sized events in the interface and interphase regions and can possibly lead to the design of more accurate experiments and/or better data interpretation. In the present molecular dynamics (MD) study, we investigate how the structure of the polymer is affected by the presence of a bare or grafted NP by simulating a coarse-grained (CG) model of silica−polystyrene (PS) nanocomposites. The dependence of interface-induced effects on the chain length, the grafting density, and the length ratio between grafted and free chains is also addressed. We have chosen a CG model[31−33] which has one superatom per chemical repeat unit of PS. The structure-based potentials of this CG model are generated by so-called iterative Boltzmann inversion (IBI).[34] For dense polymer systems, they give a typical speed-up of 3−4 orders of magnitude over atomistic calculations.[35] At the same time, they are realistic in the sense that they preserve the structural distributions of the atomistic models and can easily be backmapped if atom-based properties are to be evaluated. We use them here to investigate the polymer structure near the NP. The first major aim of the current study is to develop accurate CG potentials for silica−PS nanocomposites, which successfully reproduce the structural properties of the interphase area, and to test them. In addition to the structural investigation of this contribution, the CG potentials developed are also meant to bridge the time- and length-scale gaps between previous atomistic[8] and continuum simulations[39] of this system. Moreover, the existence of such a CG model is a prerequisite to investigate the dynamics in the interfacial region, which will be addressed in a separate publication.

To achieve maximal property enhancements in the filled polymer, a stable and uniform dispersion of the NPs is vital. Agglomeration of the particles would be detrimental to the NCMs, like for instance rendering a plastic material more brittle. Yet, adjusting the NP dispersion is still a challenge due to the difficulty of controlling both the thermodynamic and kinetic factors which play a significant role in such complex systems.[36] In a recent review article, Kumar and Krishnamoorti[37] surveyed the relevant literature about controlling NP dispersion and its ultimate role in the properties of NCMs and how these two issues depend on the particle shape. One recent experimental study on the dispersion mechanism in silica−PS nanocomposites was performed by Chevigny et al.,[38] using complementary scattering (SAXS/USAXS) and imaging (TEM) techniques. The authors showed that the relevant parameter of the dispersion, i.e., the mass ratio between grafted and free chains, Q, controls the arrangement of the NPs in the matrix, either as large and compact aggregates ($Q < 0.24$) or as individual NPs ($Q > 0.24$). They also showed that particle aggregation is associated with a significant collapse of the corona of grafted chains. In a separate study,[18] they demonstrated that interactions with longer free chains induce a compression of the grafted chains, which minimizes the free energy. The investigation of free-chain infiltration in the grafted corona and its dependence on the chain length and Q in the framework of a CG computer simulation is the second major aim of the current MD study.

In recent years, polymer nanocomposites have been simulated at different resolutions[32] including generic bead−spring[40] and lattice models.[41,42] Studying polymer NCMs by MD simulations at different levels of resolution is an ongoing effort in our group, too. Eslami and Müller-Plathe have examined the structure and dynamics of polyamide-6,6−graphene nanocomposites using different resolutions.[43−45] It was shown that polymer chains, which are layered between graphene sheets, adopt a flattened conformation parallel to the surface. Ndoro et al.[8] used atomistic MD simulations to study the structural behavior of PS chains in the vicinity of a single grafted and bare silica NP. The NP induces ordering near its surface where polymer chains form layers. The magnitude of the effect depends strongly on the particle radius and grafting density. The present contribution is an extension of that work.

2. CONSIDERED SYSTEMS AND METHODS

2.1. Systems and Mapping Scheme. A collection of all silica−PS nanocomposites studied in the present work can be found in Table 1. In addition to the number of free and grafted chains, we have given their monomer numbers as well as the NP volume fraction. Different mapping schemes for atactic PS

have been suggested in the literature.[46−50] In the present study, we have employed the method of Qian et al.[50] where each repeat unit of PS is represented by one CG bead whose interaction center is located at the repeat unit's center-of-mass. Two different beads (R and S) are necessary to account for the chirality of atactic PS. The CG interaction potentials describe the nonbonded intermolecular interactions, the bonded interactions between two neighboring beads, and that between three neighboring beads forming an angle. No torsion potential was used in our CG simulations since it was shown that the distribution of dihedral angles between beads are flat enough to be neglected.[46] Intramolecular nonbonded interactions were also employed in our calculations, except for first and second neighbors.

In addition to composites with free PS chains, we also studied systems where some of the PS chains were grafted to the NP surface. They are attached by a linker unit $(-[H_2C(H(C_2H_3)C)]_3(CH_3)_2Si-)$ as used in experiments (see Supporting Information of ref 8 for its structure). The linker has been divided into four CG beads of two kinds having approximately the same mass. The first is formed by the $-CH_2CHCHCH_2-$ group and the second by $-(CH_3)_2Si$. In both cases the CG interaction centers are located at the center of mass of the group of atoms. The mapping scheme used to define the grafted PS chains is identical to the one used for the free polymer chains.

As for the NP, the silicon and oxygen atoms of the SiO_2 units are gathered into a CG bead whose interaction center corresponds to the silicon atom's position. In order to take into account the existence of hydrogen atoms of hydroxyl groups on the NP surface, the total mass of the hydrogen atoms was uniformly distributed over all the CG beads that form the NP. In all simulations the NP is a sphere with diameter of ∼4 nm, which yields 873 CG beads. Three different approaches were followed to model the NP at the CG level. In a first attempt, only the surface layer of the NP beads was taken into account, while the inner beads were ignored. This model yielded an unphysical situation where polymer beads were also found inside the NP. In a second attempt, the entire NP was modeled with CG beads which all had the same interaction potential with the polymer beads. We have observed that such an approach yielded a too attractive interaction between the polymer chains and the NP. We finally adopted a third approach by distinguishing between the surface (shell) beads (SH) and core beads (CR). Their interaction with the polymer beads were then described by two different potentials because the SH beads of the NP have the main contribution to its interaction with the polymer matrix.

2.2. Parameterization of the Coarse-Grained Model.

The CG interaction potentials between the beads described above were obtained by means of the IBI procedure. This method has been applied to generate the CG potentials of various polymer systems; details can be found elsewhere in the literature.[34,51] In IBI a reference atomistic force field including all bonded and nonbonded interactions as well as atomic charges as employed in the preceding atomistic simulation (in the following denoted as original atomistic simulation) is used to compute the target distribution functions that should be reproduced by the CG model. The details of the atomistic simulations can be found in a recent contribution of our group.[8] The radial distribution functions (RDFs) describing the CG models at each step of the IBI procedure were computed from 0.2 ns long trajectories which were generated at a constant particle number, constant volume, and constant temperature (NVT conditions). In each IBI step all CG potentials have been optimized simultaneously. The derivation of the potentials was carried out on a system whose polymer chains contained 20 monomers. The nonbonded potentials between the SH and CR beads of the NP and the polymer beads were identical for the R or S conformation of the polymer beads. There are therefore only two different nonbonded potentials describing those interactions. The RDFs between the polymer beads (PS) and the SH beads in both atomistic and CG simulations are compared in Figure 1A. The CG results presented are those of

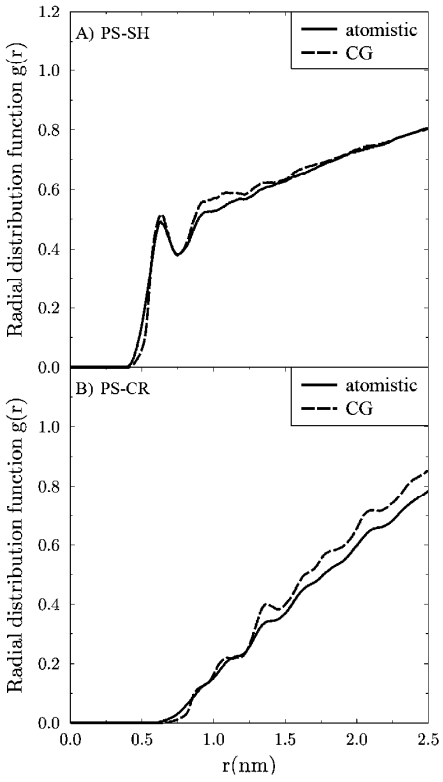

Figure 1. Calculated nonbonded radial distribution functions between SH beads of the nanoparticle and PS beads (A) as well as between CR and PS beads at 590 K and P = 101.3 kPa, as derived from atomistic and CG simulations of the bare silica−PS system.

the last iteration of the Boltzmann inversion procedure. The agreement between the CG and the atomistic data is very satisfactory. The sharp maximum observed around 0.65 nm in the atomistic simulations is reproduced. Although the RDFs are presented only for short distances for clarity, it was verified that they converged to a value of 1. The RDFs between the PS and CR beads in both atomistic and CG simulations are shown in Figure 1B. The repulsive PS−CR interaction implies that the maximum around 0.65 nm disappeared. We have mentioned above that this repulsion prevents the polymer beads from penetrating the NP and partly offsets the attraction by the shell beads. The overall attractive nature of the interaction between the NP and the PS chains leads to modifications in the local structure properties of the polymer chains in the vicinity of the NP (see section 3).

dx.doi.org/10.1021/ma202044e | *Macromolecules* 2012, 45, 572−584

For the grafted polymer chains, we have developed CG potentials using two different schemes. One is based on an original atomistic simulation followed by IBI of all nonbonded interactions (including PS−PS and NP−PS) in the same way as for the ungrafted system (see above). We call it type 1 CG potential. The second one (type 2 CG potential) uses the potentials developed for the ungrafted system also for the grafted system and augments them only by the additional interactions with the linker units. This has been done to test the transferability of these potentials to grafted systems. In this scheme, we have fixed the NP−PS and PS−PS potentials known from the ungrafted system. The interaction potentials linker−NP, linker−PS, and linker−linker have been developed using IBI. Structural properties of a given NCM system obtained with these two CG models have been compared with atomistic results to find the advantages and disadvantages of each one. See section 3.3 for the detailed comparison. The discrimination between NP beads of the SH and CR types is conserved for both CG schemes.

2.3. Generation of Initial Configuration for Composites with Long Chains. We now describe the procedure to generate the initial configuration of systems with longer chains. First one NP was inserted into the box, as done in the 20-mer nanocomposite. The chains were built using a self-avoiding random walk (SARW) along which the CG polystyrene beads were distributed, conserving the periodic boundary conditions for the simulation box. The initial density of the simulation box was chosen at 80% of the known composite density, such that SARW could easily be built without encountering configurations in which no more beads could be added. The distance between two consecutive beads on a given chain corresponded to the average distance between two bonded CG beads (∼0.5 nm), while the minimum allowed distance between two nonbonded beads (PS−PS or PS−NP) was half this length ($d_{nb} \approx 0.25$ nm). This choice has led to some close contacts which needed to be relaxed during equilibration. The alternative choice, however, a larger value of d_{nb}, resulted in configurations where no new beads could be added to some chains because of the overlap with other nonbonded monomers around.

To build a nanocomposite system of a single NP and N free chains, we started with N initial monomers randomly distributed around one NP. Then we started one SARW per chain, adding one by one only one new bead to each chain. For a given chain of i CG beads, the position of each new bead (bead number $i + 1$) was randomly chosen on the surface of a sphere of radius 0.5 nm around the last (ith) bead of the parent chain. If the new bead did not overlap with any other bead in the system (including NP beads), we put bead number $i + 1$ at the chosen position. Otherwise, another random point was chosen on the surface of the same sphere. If the new bead could not be placed, due to the overlap with other beads in the system, after 1000 attempts, an abortion of the algorithm should occur. Such a process, however, was circumvented choosing the box size large enough as mentioned above. At the end of a step each chain has gained one additional bead. Repeating this step until all chains have their desired chain length, all polymer chains were grown simultaneously. In this scheme, bond angles were not considered. Because of the absence of strong overlaps between beads, however, bond angles regained the distribution determined by the angle potentials, during the equilibration. After preparing the initial configuration, NPT simulations (of 4−10 ns duration, depending on the chain length) were carried out to relax the systems to their equilibrium densities. The ensuing production runs took 16 ns.

2.4. Simulation Details. The obtained potentials were used to perform simulations of systems with 20−200 monomers per chain. Depending on the polymer chain length, trajectories of different lengths were used to produce the structural data which will be discussed later. For the 20 monomer chains, the system was equilibrated first at NVT condition for 2 ns. A subsequent run of 2 ns at NPT was performed where the last 0.4 ns were used to accumulate the data. For the 40−200 monomer chains the systems were first equilibrated at constant pressure for 4−8 ns. The systems were then simulated in NVT/NPT ensemble for 8−50 ns. The last 4−20 ns was used to accumulate the production data depending on the chain length. All MD runs were carried out at a pressure of 101.3 kPa and a temperature of 590 K, while a time step of 4 fs was employed. The CG simulations in this study were performed with the code IBIsCO developed in our group.[52] Berendsen's thermostat (with a coupling time of 0.2 ps) and barostat (with a coupling time of 5 ps and isothermal compressibility of 1.0×10^{-6} kPa) were used to control temperature and pressure. The cutoff for the nonbonded interactions was 1.5 nm, and the neighbor list cutoff was 1.6 nm. Configurations were sampled every 1000 time steps (4 ps). The error bars provided in some of the figures and tables denote the standard deviations calculated over all polymer molecules and all their frames.

3. RESULTS AND DISCUSSION

3.1. Ungrafted Nanoparticle: 20-mer Systems. The polymer monomer number density profile as a function of the distance from the NP surface in both atomistic and CG simulations is shown in Figure 2A. In all that follows, the NP surface is defined by the average radial distance of the outermost beads from NP center of mass. The NP radius is therefore taken as 2 nm. Oscillations in the density profile show a layered structure of the polymer chains around the NP, which has also been reported in experiment[12,13] and atomistic simulations.[8,14,25,53,54] The CG simulation successfully reproduces the atomistic structure of the polymer matrix around the NP, although the intensity of the first peak is larger. The structuring effect results in three distinguishable density peaks, after which the density profile approaches the bulk value (∼2 nm from NP surface). The first peak in the density profile appears at a distance of 0.6 nm from the NP surface. This first layer is characterized by a density which is almost twice the bulk density. A second layer is observed at about 1 nm from the surface, followed by a third one at 1.6 nm whose amplitude is similar to the second one. Position and amplitude of the density peaks are independent of the chain lengths considered. The first two peaks of the CG density profile are slightly displaced from the positions derived in the atomistic simulation, although in opposite directions. These shifts mainly arise because of the orientation properties of the PS phenyl rings close to the surface (see below), which are captured by the atomistic model but not by the spherical CG superatoms. Another reason for the larger excess of monomers in the first CG peak might be the geometrical smoothness of the NP surface induced by coarsening. In the surface layer of silica monomers the oxygen atoms are included in their parent bead, which is at the position of the silicon atom. This results in a withdrawal of the oxygen atoms, which stick out of the surface in the atomistic

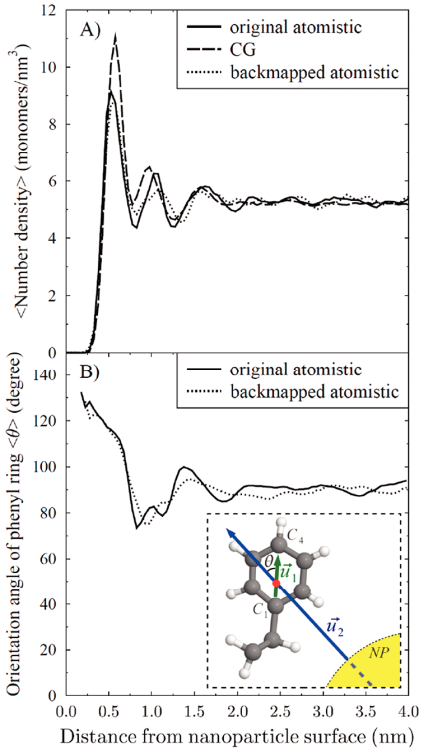

Figure 2. Radial profile of the monomer number density (A) of the polymer component of the bare silica–PS composite, as derived from the original atomistic MD simulation, coarse-grained, and backmapped atomistic simulations. Orientation angle of the phenyl rings with respect to the radial distance form the nanoparticle surface (B) from original and backmapped atomistic simulations. The inset shows the definition of the phenyl orientation angle θ: angle between center-of-mass vector ($\vec{u}_2$) of the monomer and a unit vector ($\vec{u}_1$) connecting C_1 and C_4 carbon atoms of the phenyl ring.

simulation. The larger corrugation in the atomistic simulation forces the first layer of PS monomers into further distances.

The atoms were reinserted into the equilibrated CG configuration model by a backmapping procedure, which has been described in detail.[55] The backmapped atomistic configuration was used as a starting configuration to produce a second atomistic trajectory of 2 ns duration. The two atomistic PS densities agree better with each other than with the CG results. This is another indication that the density deviations are due to fundamental differences between an atomistic and a CG description rather than to insufficient equilibration. The fact that successive coarse-graining and backmapping recreates a realistic structure opens the possibility to study systems with many more NPs and polymers as well as longer chains in the future. As shown below, the CG potentials developed here can be transferred to systems with longer chains.

The orientation of the PS monomers is influenced by the NP. In the atomistic resolution, the orientation of a single monomer can be characterized by the angle between a particular monomer-fixed vector and a vector connecting the center of mass of the NP to that of the monomer, i.e., the surface normal u_2. We take as unit vector, u_1, the in-plane vector from the phenyl carbon atom C_1 in the direction of C_4 (Figure 2B). The orientation angle of the phenyl rings in immediate contact with the NP surface is above 90° in both the original and the backmapped atomistic simulations. As a matter of fact, the PS chains in the interface expose mainly their phenyl rings to the NP (Figure 2B), as already reported by Milano et al.[15] We assume that the observed orientation of the surface near phenyl rings is caused by both excluded volume effects and surface–phenyl attraction. This region (~0.6 nm from the surface) corresponds to the position of the first monomer layer (Figure 2A). The second monomer layer (density peak ~1.0 nm in Figure 2A) shows a small preference for orienting the phenyl groups away from the NP (Figure 2B). Beyond that layer, the orientation quickly converges to the random average of 90°.

Also, the global conformation and orientation of PS chains are affected by their distance from the NP (Figure 3). In order

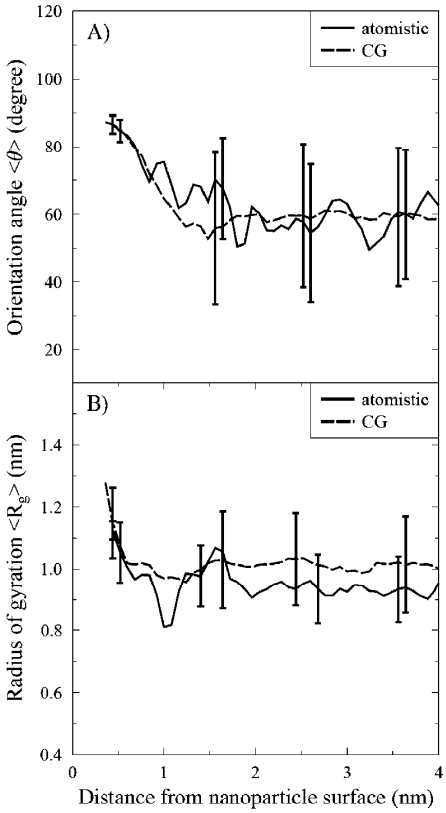

Figure 3. Average orientation angle $\langle\theta\rangle$ (A) and radius of gyration $\langle R_g\rangle$ (B) of free chains of 20 monomers as a function of the distance from the surface of the bare nanoparticle in atomistic and coarse-grained resolution. The orientation angle is taken between the chains' longest principal axis and the surface normal.

to probe whether the CG model can reproduce this dependence, the chains' radius of gyration and their orientation angle are shown. The chain orientation angle θ is defined as the angle between the longest principal axis of the gyration tensor of the individual chains and the surface normal, defined as the vector connecting the centers of mass of the NP and the polymer chain (Figure 3A). Note that the principal axis has no sign; therefore, θ varies between 0° (radial orientation) and 90°

dx.doi.org/10.1021/ma202044e | *Macromolecules* 2012, 45, 572–584

(tangential orientation), with an average of 57.3° for random orientation. This definition differs from the above one of the orientation vector (Figure 2B). Free chains in the vicinity of the NP tend to align tangential to the surface in both atomistic and CG models, in agreement with previous observations.[8,14,15] At distances larger than ∼1.5 nm from the NP surface, the PS chains show a random orientation. This convergence thus happens before that of the density (2 nm, Figure 2A). One should note that the unperturbed radius of gyration of the polymer is around 1.0 nm (Figure 3B). Vogiatzis et al.[14] and Brown et al.[3] reported the same behavior for chain segments around NP surfaces.

To better understand the conformational changes of the polymers in the vicinity of the NP, we computed the radius of gyration of the chains as a function of their distance from the NP surface (Figure 3B). It indicates that free chains become elongated near the surface compared to the bulk. The increase of the radius of gyration is up to 30% above the bulk value and, together with the orientation angle profile in Figure 3A, indicates that the polymers elongate and flatten significantly, orienting with the NP surface. The convergence to the bulk value happens at about 1.0 nm from the surface, i.e., when the chain is about one (unperturbed) radius of gyration away. Other structural properties like average radius of gyration and average end-to-end distance as well as the nanocomposite density computed with CG and atomistic models are compared in Table 2. They show sufficient agreement between these computational methods.

Table 2. Total Mass Density of the Silica−PS Composites as Well as Radius of Gyration $\langle R_g \rangle$ and End-to-End Distance $\langle R_0 \rangle$ of the Atactic Polystyrene Component (Chain Length 20) as Derived in Original Atomistic, Backmapped Atomistic and Coarse-Grained Simulations[a]

	coarse-grained	backmapped atomistic	original atomistic
density (kg/m^3)	978.24 ± 2.62	978.95 ± 0.97	978.10 ± 0.87
$\langle R_g \rangle$ (nm)	1.01 ± 0.16	0.99 ± 0.12	0.95 ± 0.12
$\langle R_0 \rangle$ (nm)	2.43 ± 0.85	2.44 ± 0.71	2.25 ± 0.76

[a]For each quantity we have given the MD inherent error bars, calculated as standard deviation of the quantity around the corresponding mean value over 1000 frames.

3.2. Ungrafted Nanoparticle: Chain Length Dependence. Coarse-grained calculations of bare silica−PS nanocomposites with longer polymer chains have been performed for the following reasons. First, the simulations were carried out without reoptimization of the CG interaction potentials. They therefore represent a test of the transferability of a potential which was developed at a given chain length (here 20 monomers) to longer chains. For pure bulk PS without NPs the transferability of model parameters to different chain lengths has already been demonstrated;[50] this was confirmed in this work (not shown) before examining the transferability in the presence of NPs (see below). Second, we have been able at the same time to study the influence of the polymer chain length on the structure and properties of the nanocomposite. Polymer chains containing 40, 80, 100, and 200 monomers together with one NP were simulated.

To investigate how the NP influences the behavior of longer chains in the interphase, the monomer number density of the chains (with 20−200 monomers per chain) was examined. Interestingly, the chain length has no effect on the layer structure around a bare NP, neither qualitatively nor quantitatively. Even the thickness of the shell in which the density deviates from the bulk value (< 2 nm) does not change with the polymer length. Only the limiting bulk density for longer chains is slightly higher, as expected. For the long chains we analyzed first the local polymer structure by dividing the chains into segments of 10 monomers instead of carrying out an analysis of the whole chain. We have accepted this choice as the distance between the NP and the chain center of mass is no longer a characteristic distance parameter for the monomers of a chain. The segment orientation was investigated as a function of their distance to the surface. The definition of the orientation angle is the same as before, only that the longest principal axis of the gyration tensor is calculated for each chain segment (Figure 4A). Systems with short and long chains show the same

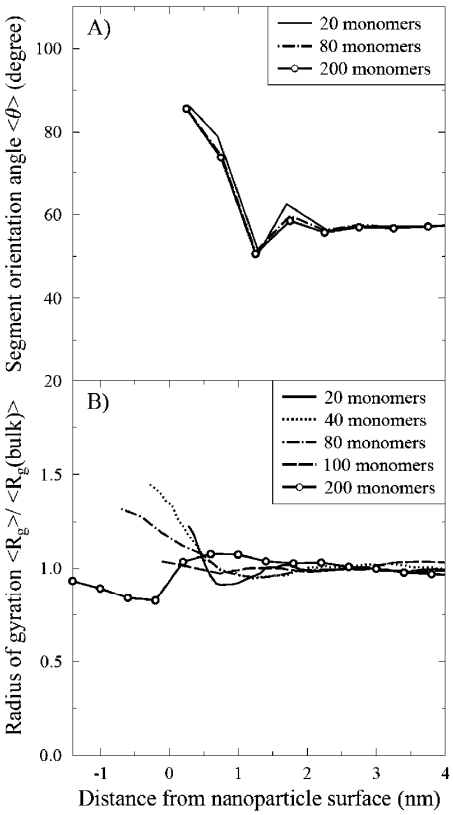

Figure 4. Segment orientation angle (A) of chains with 20, 80, and 200 monomers in the bare silica−PS composite at T = 590 K. Each segment contains 10 monomers. Since data points for different chain lengths coincide, data for chains of 40 and 100 monomers are not shown. Radius of gyration (B), normalized by the corresponding bulk value, of polymers with 20−200 monomers per chain in the bare silica−PS composite at 590 K. Negative distances mean that the center of mass of a chain is located inside the particle but not its individual monomers.

behavior. At close distances, the segments are tangential to the NP; at ∼1 nm they have a small preference for radial orientation before converging at ∼2.2 nm to the random orientation (57.3°) characteristic for the bulk. The origin of the

dx.doi.org/10.1021/ma202044e | Macromolecules 2012, 45, 572−584

minimum can possibly be attributed to those segments which are leading their parent chains from the first layer around the NP to the second and hence leave the NP neighborhood in radial direction. From the foregoing, it is clear that the local structure of the polymer near the interface (monomer density and orientation of segments of 10 monomers) is independent of the chain length for chains between 20 and 200 monomers. This spans radii of gyration between 1.01 and 3.39 nm, i.e., from below to above the NP radius (~2 nm). The local structure of the polymer at the interface is thus unaffected by its length.

The global polymer structure near the NP is better reflected by the radius of gyration of the entire chain (Figure 4B). For the different chain lengths, the radii of gyration have been normalized by the corresponding bulk values. The behavior of the radius of gyration as a function of the center-of-mass distance from the NP surface changes qualitatively with the polymer length. For shorter chains ($N \leq 80$), the radius of gyration increases near the NP, as close chains squeeze against the particle surface. However, this effect decreases with chain length, so that chains of length $N = 100$ have an almost uniform distribution of $R_g \sim R_g(\text{bulk}) \sim 2.2$ nm. The longest chain ($N = 200$) actually shows a reduced R_g near the NP. The reason is also visible in Figure 4B: long chains are also squeezed against the NP surface, but due to their size, they engulf at least part of the curved surface, as is shown by their centers of mass which fall inside the NP. As attraction causes them to follow the surface (NP radius: 2 nm), their radius of gyration is smaller than in the bulk (3.4 nm). An example of a chain wrapped around the NP is shown in the abstract figure (right).

3.3. Grafted Nanoparticle: Short 20-mer System. The grafted systems contain a NP of radius 2 nm, this time grafted with 50 PS chains of 20 monomers (corresponding to a grafting density of 1 chains/nm^2), unless noted otherwise, and 177 free PS chains of 20 monomers. The simulations are run again at 590 K. In Figure 5, the overall monomer number density

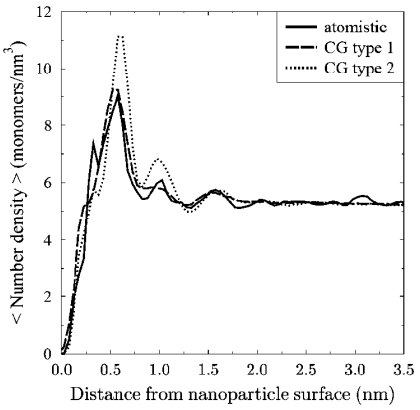

Figure 5. Overall monomer number density of the grafted system (1 chains/nm^2 grafting densities) as a function of the radial distance from the nanoparticle surface in an atomistic simulation as well as coarse-grained simulations using potentials of type 1 and type 2.

obtained from the CG models of type 1 (all potentials of the grafted system are evaluated by IBI) and type 2 (all potentials already available from the ungrafted system are transferred and only the additional potential terms involving the linker beads are determined by IBI) is compared with the corresponding original atomistic system. Similar to the bare system, the monomers form a layered structure in the vicinity of the NP surface, regardless of the CG potential type used. The layering of the polymers causes three separated density peaks, which appear at the same distances as the atomistic ones. For the type 1 CG potential, the amplitudes of all three peaks agree well with the atomistic profile. As the minimum between the first and second peaks is not as deep as in atomistic resolution, the second peak now appears more like a shoulder. For the type 2 CG potential, the amplitudes of the first and second peaks are higher than in the atomistic and the type 1 CG model. This shortcoming is probably carried over transferring the potentials from the ungrafted system, where this density excess is also found (cf. Figure 2A). The overall density profiles of Figure 5 are further decomposed into contributions of the free and grafted chains (Figure 6). Both grafted and free chains

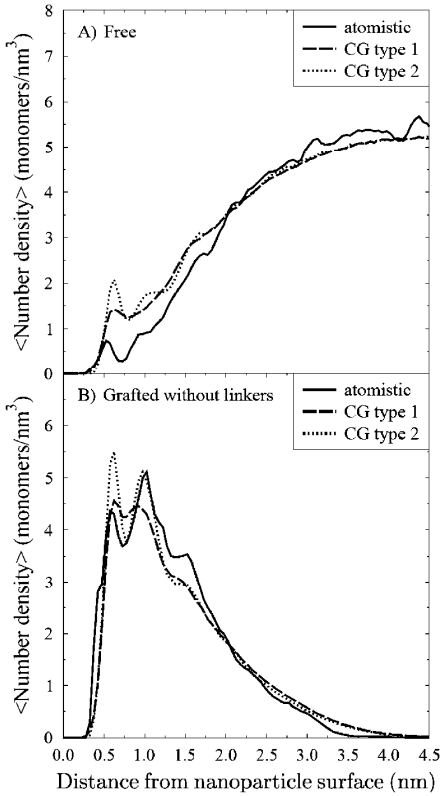

Figure 6. Monomer number density for free (A) and grafted (B) chains in atomistic as well as CG simulations using potentials of type 1 and type 2. The linker beads are excluded from the grafted-chain profiles (B).

contribute to the enhancement of the first peak in the density profile of the type 2 CG potential. In general, type 2 CG potentials have sharper features than type 1 potentials. Both coarse-grained potentials lead to a slight excess of free chains in the near-surface region (<2 nm) and a corresponding depletion of grafted chains, compared with the atomistic simulations.

Table 3 shows larger radii of gyration and brush heights for the grafted chains for both CG models compared to the atomistic results. The brush height is a measure for the

Table 3. End-to-End Distance $\langle R_0 \rangle$ and Radius of Gyration $\langle R_g \rangle$ of Free (Average over All Free Chains) and Grafted Chains as Well as Brush Height $\langle h \rangle$ for a Grafted Silica–Polystyrene System Using Atomistic and Coarse-Grained Simulations[a]

	atomistic	CG type 1	CG type 2
$\langle R_0 \rangle$ free chains (nm)	2.29 ± 0.79	2.41 ± 0.82	2.42 ± 0.82
$\langle R_0 \rangle$ grafted chains (nm)	2.31 ± 0.61	2.62 ± 0.80	2.54 ± 0.81
$\langle R_g \rangle$ free chains (nm)	0.96 ± 0.13	1.01 ± 0.16	1.02 ± 0.16
$\langle R_g \rangle$ grafted chains (nm)	0.93 ± 0.09	1.04 ± 0.16	1.02 ± 0.16
$\langle h \rangle$ (nm)	1.20 ± 0.35	1.34 ± 0.41	1.27 ± 0.41

[a]The system contains one nanoparticle and PS chains of length 20 (both free and grafted). The grafting density is 1 chains/nm^2 and the temperature amounts to 590 K, while a pressure of 101.3 kPa has been used. Type 1 and type 2 potentials are used in the CG simulations.

extension of the grafted chains from the NP surface. It is calculated as the average radial distance of the grafted monomers from the surface. Since the NP is not an ideal sphere, this distance has been defined with respect to the radius at which the first linker superatom (connecting the chain to the NP) of the chosen chain is located. Figure 6B shows a small excess of grafted monomers density at distances beyond 2 nm from the NP surface for both CG potentials. Together with the depletion of grafted chains at closer distances, this can be interpreted as grafted chains which are more stretched in the CG than the atomistic model.

Figure 7B shows the radius of gyration of the free chains as a function of distance from the NP. In contrast to the bare NP, here there is no strong distance dependence except for the CG curves at the smallest distance (0.5 nm). This increase is due to the small number of free chains which actually penetrate into this region (Figure 6A). In the case of the type 1 CG potential, for example, there was only one time-frame in which a single chain had its center of mass at that distance from the NP. Beyond this first data point (0.5 nm < r < 1 nm), the free chains show an increase of up to 10% in their radius of gyration near the surface. The reason is not that the free chains are prevented from a close approach to the NP. Comparison of Figures 3 and 7B shows that at least some of the free chain monomers can approach the NP in the presence of grafted chains, almost as close as a bare NP. Therefore, in CG resolution the presence of grafted chains must attenuate the strong ordering influence of the NP surface. A second result is that all curves are within each other's error bars; there is no difference between CG and atomistic or between the two CG models. While not being particularly stretched in the vicinity of the NP, the free chains are still oriented tangentially to the surface, also in the presence of grafted chains (Figure 7A). The orientation angle profile is relatively noisy in the atomistic calculation; it becomes much smoother in both CG models. However, the overall shapes of the curves are similar.

To investigate the local chain orientation, we examined the bond orientation angle (Figure 8). The orientation of each bond with respect to the surface normal is defined by a vector connecting neighboring monomers (their centers of mass), while the midpoint of the vector defines the position of the bond. Both CG models reproduce reasonably well the atomistic structure, although there is some inconsistency for the free chains (Figure 8B). We believe that this is due to the atomistic system not having fully relaxed. This idea is confirmed because atomistic and CG data agree better when the atomistic

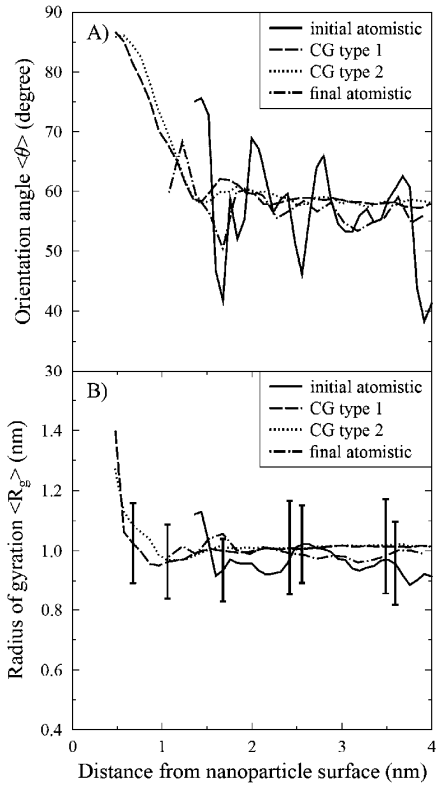

Figure 7. Average orientation angle $\langle \theta \rangle$ (A) and radius of gyration $\langle R_g \rangle$ (B) of the free chains as a function of the distance from the nanoparticle surface for a grafting density of 1 chains/nm^2 at T = 590 K. Grafted and free chains are made up of 20 monomers. "Initial atomistic" is the atomistic system from which we developed the CG potentials, while curve "final atomistic" belongs to exactly the same system when it has been run for an additional 59.55 ns. The sampling was done over 2 ns. Only representative error bars are shown for clarity in panel B. Error bars of all the curves were of the same order at each distance from nanoparticle.

simulation is taken to much longer times (curve "final atomistic" in Figure 8B).

Both CG potentials capture the essential structure of the polymer near the NP. Both have their advantages and disadvantages. The type 1 CG potential (full optimization) reproduces correctly the amplitude and position of the monomer density peaks. The second peak, however, is not as sharp as in the atomistic scheme, and the preceding minimum is suppressed. Moreover, the layering of the grafted chains around the NP is missing when CG type 1 potential is used. The type 2 CG potential (transferred from the ungrafted systems and supplemented by the additional interaction types) reproduces a clear layer structure of monomers with three different peaks. They appear at the same position as in the atomistic simulation, albeit that the amplitudes of the first two peaks are enhanced. Since this potential reproduces acceptably the expected structure of the polymer near the NP (number of distinguished layers, density peak position, radius of gyration, and chain and bond orientation angles), the type 2 CG potentials originally developed for a bare system seem to be transferable to the grafted systems, too.

dx.doi.org/10.1021/ma202044e | *Macromolecules* 2012, 45, 572–584

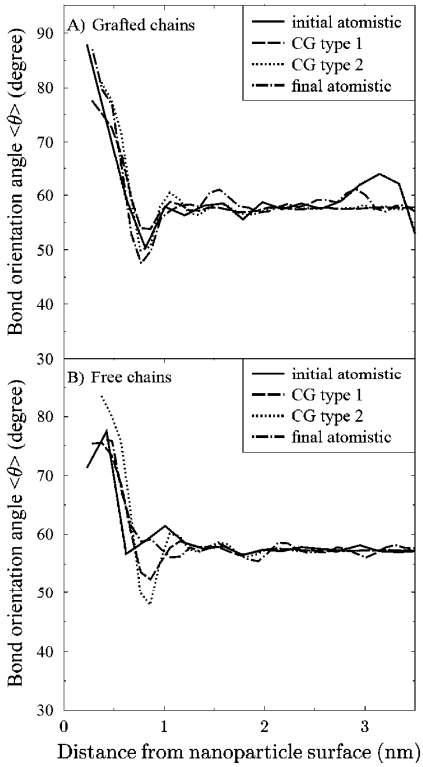

Figure 8. Angle between the bond vectors connecting nearest-neighbor monomers and the surface normal of the grafted chains (A) and free chains (B) in a grafted system of 1 chains/nm^2 grafting density at 590 K. Grafted and free chains are made up of 20 monomers. "Initial atomistic" is the atomistic system from which we developed the CG potentials, while the curve "final atomistic" belongs to exactly the same system when it has been run for an additional runtime of 59.55 ns. The sampling was done over 2 ns.

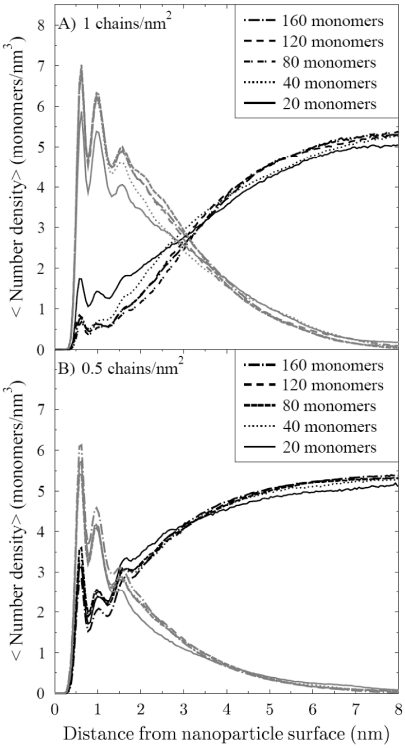

Figure 9. Monomer number density of free (black) and grafted chains (gray) in grafted systems as a function of distance from nanoparticle surface. Linker monomers are not included in the density of grafted chains. The grafted chains are made up of 80 monomers while the length of the free chains varies (20, 40, 80, 120, and 160 monomers per chain). We have studied grafting densities of 1 (A) and 0.5 (B) chains/nm^2. In the insets we have given the length of the free chains for each simulation. The volume fraction of the nanoparticle in all the systems is ∼1%.

3.4. Grafted Nanoparticle: Long Chains Regime. For the sake of comparison with existing atomistic simulations, we have so far considered only polymers of 20 monomers, which is much shorter than typical polymer lengths in technical NCMs. Here, we investigate the polymer structure near the NP, when the length of the free and grafted chains is changed. We adopt the potentials developed for the 20-mer system for larger silica−PS systems without reoptimization. We have fixed the length of the grafted chains at 80 monomers and varied the length of the free chains: N = 20, 40, 80, 120, and 160, corresponding to grafted-to-free chain ratios Q = 4, 2, 1, 0.67, and 0.5, respectively. We kept the volume fraction of the NP constant (∼1%) by adapting the number of free chains in each simulation. All systems had only one NP and their number of grafted chains was 50 (1 chains/nm^2).

Monomer number densities of the free and grafted chains are shown in Figure 9A for all systems. Note that beads corresponding to the linker molecules are not included in these graphs. For the higher grafted system, there is a marked change between N = 20 and N = 40 monomers, as the free chains are repelled from the grafted chains corona. The depletion of the free chains in the interfacial region is accompanied by a pull back of the grafted chains toward the NP surface. This is visible as a shift of the monomer number density profile of the grafted chains (Figure 9A) and a decrease in the average brush height (Table 4). Increasing the free chains length to 80 monomers results in further expulsion of polymer matrix chains from the grafted corona; the effect then stays constant for longer free chains. Such a transition from deeply penetrating free chains and a swollen grafted corona, called wet brush, to a less mixed structure, where grafted chains are less stretched and the free chains retreat from them, called dry brush, has been reported both in theoretical[22] and experimental studies.[18] From a theoretical point of view, the free energy of the polymer brush governs the emerging structure. It has two terms: an entropy term arising from mixing the grafted brush with free chains and an elastic term from stretching the grafted brush's conformation. Interpenetration of the chains is driven by entropic effects, and hence it is favorable for short free chains (larger Q) to mix with the grafted corona and swell it by stretching the individual grafted chains. On the other hand, increasing the length of the free chains makes it easier to be expelled from the grafted corona because of their reduced translational entropy.

Controlling the interpenetration of the polymer matrix and grafted corona is important for tuning the properties of the corresponding NCM. Borukhov and Leibler[22] showed theoretically that there can be an attractive interaction between two

Table 4. Radius of Gyration, Brush Height, and Density Crossover Distance for Grafted Systems at Different Grafting Densities[a]

	pure PS	1 chains/nm^2			0.5 chains/nm^2		
free chains length (monomers)	$\langle R_g \rangle$, free (nm)	$\langle R_g \rangle$, grafted (nm)	$\langle h \rangle$ (nm)	r_{co} (nm)	$\langle R_g \rangle$, grafted (nm)	$\langle h \rangle$ (nm)	r_{co} (nm)
160	3.15 ± 0.73	2.27 ± 0.44	3.07 ± 0.87	5.08	2.18 ± 0.41	2.56 ± 0.89	3.70
120	2.75 ± 0.61	2.23 ± 0.46	2.99 ± 0.86	4.94	2.39 ± 0.53	2.69 ± 0.95	3.41
80	2.20 ± 0.47	2.34 ± 0.47	2.93 ± 0.83	5.04	2.31 ± 0.54	2.71 ± 0.85	3.51
40	1.51 ± 0.28	2.33 ± 0.45	3.03 ± 0.74	4.95	2.29 ± 0.45	2.71 ± 0.89	3.50
20	1.03 ± 0.16	2.44 ± 0.51	3.23 ± 0.94	4.66	2.38 ± 0.47	2.96 ± 1.00	3.35

[a]The grafted chains have a length of 80 monomers. Brush height $\langle h \rangle$, radius of gyration $\langle R_g \rangle$ of grafted chains, density crossover distance (r_{co}). The radius of gyration of free polymer chains in pure PS (no nanoparticle) is included for reference. The volume fraction occupied by the nanoparticle (~1%) is kept constant for all systems. Errors are calculated as standard deviation of the quantity around the corresponding average value over configurations and chains. Errors of the crossover distance r_{co} are equal to one-half of the bin width used for the density profile (0.025 nm).

dry brushes immersed in a polymer melt. Existence of such an attraction between grafted brushes of different NPs can lead to aggregation of the NPs and to a destabilization of the NCM. When the length of the free chains is changed from 20 to 40, the inner layers of grafted chains (closer than 1.2 nm from surface) are packed more densely to fill the space vacated by the monomers of free chains (Figure 1A). Further drying of the brush, by going to free chains of 80 monomers, causes an extension of the region of densified grafted chains to beyond 1.2 nm from the surface without any more disturbances at closer distances. Longer free chains of 120 and 160 monomers cause no further change in the free or grafted density profiles. We should emphasize that the total number density profile does not depend on the length of the free chains. Conducting an experimental study, Chevigny et al. have recently reported a similar wet-to-dry transition induced by compression of the grafted chains in the interaction with longer free chains of the same polymer.[18]

To investigate if and how this behavior depends on the grafting density, we have repeated the above simulations with a grafting density of 0.5 chains/nm^2, keeping the grafted chain length of 80 monomers. The distance dependence of the number changes (Figure 9). Lengthening the free chains does not deform the grafted chains as much as for the higher grafting density if the distances are smaller than 1.2 nm. Only a partial collapse of the grafted chains from farthest distances is observed, which saturates for free chains longer than 40 monomers. This can be attributed to the availability of space for free chains near the NP, thanks to the low grafting density. This shows that mixing of the polymer matrix with a grafted corona is critically dependent on the grafting density as was already found in atomistic simulations of these systems.[8] The brush height value in this case decreased going from free chains of 20 to those of 40 monomers, and it did not further change for longer free chains, as shown in Table 4. We also note that the crossover distance, i.e., the distance at which the monomer density of the free chains is equal to that of the grafted chains increases with the grafting density, which agrees with our earlier atomistic results.[8] It is, however, nearly independent of the length of the free chains, which is a new result obtained only with the CG model, as atomistic simulations for chains with $N > 20$ were computationally unaffordable.

To investigate the global conformational state of the free chains in the vicinity of the NP, their normalized radius of gyration is shown in Figure 10A for a grafting density of 1 chains/nm^2. Note that the distance from the surface is plotted in units of the respective unperturbed radius of gyration R_g(bulk). All chains show bulklike behavior at distances far

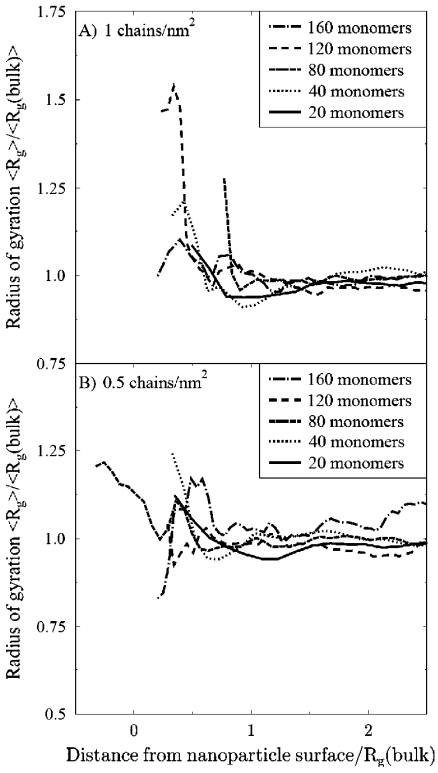

Figure 10. Radius of gyration (normalized by the respective bulk value) of free chains of different length as a function of the distance of the chain center of mass from the nanoparticle surface (also normalized by the respective bulk radius of gyration) in grafted systems of 1 chains/nm^2 (A) and 0.5 chains/nm^2 (B) grafting density. The grafted chains are made up of 80 monomers.

from the NP, while getting disturbed when approaching the particle surface to distances below their respective bulk radius of gyration. Chains at close distance (< 0.7 R_g(bulk)) are mostly stretched, except very few of the longest chains (N = 120, 160), which compact at extremely close distances (< 0.4 R_g(bulk)), as they follow the NP surface with its smaller R_g. This behavior is carried over from the composites with a bare NP (section 3.2). The stretching is a consequence of the close chains being pressed against the NP in a way very similar to the situation found in the case of bare NPs. Examples of such chains are visualized in Figure 11. For some chains there is a

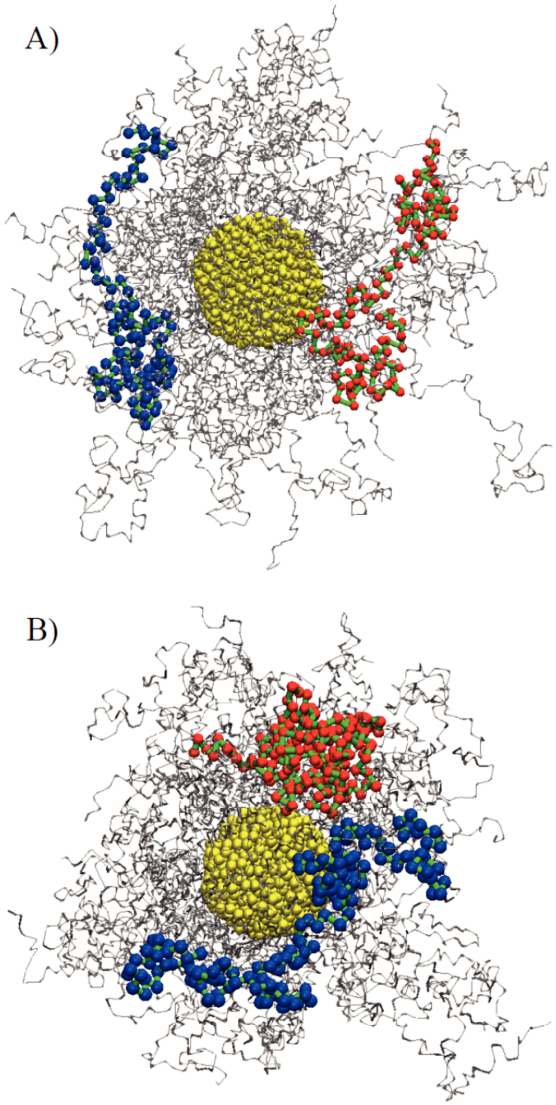

Figure 11. Examples of conformations of free chains of 120 (A) and 160 (B) monomers near a grafted nanoparticle (yellow) of 1 chains/nm^2 grafting density and its corona (gray). Blue and red colors show two different free chains, whereas the green color represents the bonds between monomers. The grafted chains monomers are resized for better visibility of the free chains. Free chains that are pressed against the grafted nanoparticle become deformed, partially engulfing the nanoparticle and its corona.

hint of a shallow minimum of their R_g when they are about 1 R_g(bulk) away from the surface. It is not yet clear whether this is more than a statistical artifact and, if yes, where it comes from. Comparison of Figures 10A and 10B shows that the structuring effects are of similar magnitude for both grafting densities.

Despite the difference in the global structure of free chains of different length, there is little difference in the local packing of their segments. In Figure 12, the radius of gyration of segments of M = 10 monomers of free chains is split into the tangential ($R_{g\parallel}$) and radial ($R_{g\perp}$) components, relative to the NP; they are

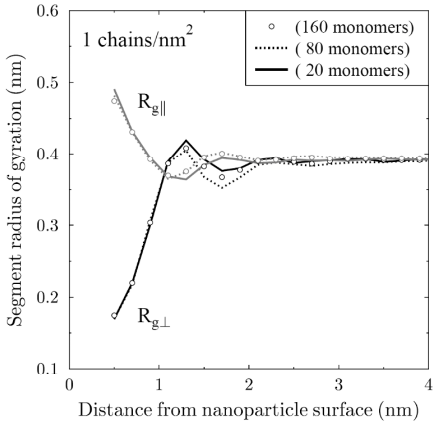

Figure 12. Radius of gyration of segments of 10 monomers of free chains with lengths of 20, 80, and 160 monomers as a function of the distance from the nanoparticle surface, in grafted systems of 1 chains/nm^2 grafting density. The grafted chains have 80 monomers. The volume fraction of the nanoparticle is the same for all systems (~1%). Black symbols show the normal (radial) component of the radius of gyration, $R_{g\perp}$, and the gray ones show the tangential component, $R_{g\parallel}$, multiplied by a factor of 0.5, because there are two tangential directions contributing to this component.

shown as a function of the distance form the NP surface. Since the NP is approximately spherical, the radial direction is the surface normal. The squared radius of gyration of a segment is defined as $R_g^2 = (1/2M^2)\langle\sum_{i,j=1}^{M}(\vec{r}_i - \vec{r}_j)^2\rangle$, where M is the number of monomers that make up the segment, $\vec{r}_i$ is the position of the ith monomer (conveniently measured from the center of the NP), and $\langle ... \rangle$ denotes the average over chains and configurations. The normal component, $R_{g\perp}^2$, is then found by substituting the vector $\vec{r}_i - \vec{r}_j$ by its projection on the surface normal, which can be calculated as its normalized bisector[54] $[(\vec{r}_i - \vec{r}_j)(\vec{r}_i + \vec{r}_j)]/|\vec{r}_i + \vec{r}_j|$. In the orthogonal coordinates there remain two directions perpendicular to the radial direction, for which we calculated the average tangential component of the radius of gyration, $R_{g\parallel}^2$. It is nicely shown in Figure 12 that segments of free chains, independent of their length, become tangential to the surface at close distances (<1 nm). The tangential orientation of the chain segments, however, happens in 0.5 and 1.6 nm from the NP surface, which coincides with the positions of the first and third layers in the monomer number density profile (cf. Figure 5). Moreover, there is a narrow layer at about 1 nm from the surface, where the segments show a small preference for a normal orientation.

4. SUMMARY AND CONCLUSIONS

The interphase structure of PS matrices filled with either a bare or grafted nanometer-sized silica NP has been investigated by means of MD simulations at the CG level. These simulations provide insight into how the structural properties of the polymer matrix and the grafted corona are affected by the presence of the NP and how these effects are dependent on the polymer length (both grafted and matrix chains) and the grafting density of the NP.

A CG model for silica−PS nanocomposites has been developed using the IBI method. While the CG potentials have reproduced the correct structure for bulk PS, the capability for describing the molecular structure in the polymer interphase

around bare and grafted MPs had to be assessed here. To this end, the polymer structure predicted by the CG model has been compared with atomistic simulations of the same system. The results of both agree in general and only show small quantitative differences, such as density peak amplitudes. It was also found that the CG potentials, which were originally developed for a bare system, can be transferred to the grafted NP systems by augmenting them with the additional terms involving the linker units. Except minor differences in the results (mainly the amplitude of the density peaks), this transfer of potentials results in acceptable values of all investigated quantities when compared with the original atomistic data. The CG potentials can also be transferred from the 20-monomer chains they were developed for to much longer chains, grafted as well as matrix ones. The transferability holds for pure PS as well as for systems containing a silica NP. The local structure of the interphase of polymers is not length dependent. The wet-to-dry brush transition observed for grafted particles as a function of the length of the free chains of different lengths, which is a less local property, is in agreement with the experimental data.

Polymer chains around the NP show structure at different levels. The effective width of the zone in which the polymer structure is disturbed, i.e., the interphase, varies according to the structural element being monitored. On the lengths scale of monomer diameters, density fluctuations and preferential orientation of the monomers are observed for about 3 shells (< 2 nm). This is approximately the same for all chain lengths and grafting states (cf. Figures 2 and 5). The contributions of the free and grafted chains to the overall density (Figure 9), however, change with the mass ratio between grafted and free chains. Matrix chains shorter than the grafted chains penetrate the grafted corona, swelling the brush much like a solvent, whereas longer matrix chains are expelled from the NP's vicinity by the grafted brushes (Figure 9A). Not surprisingly, this wet-to-dry brush transition becomes less visible for lower grafting densities (Figure 9B). The relative independence from the chain length and grafting states is not only found for monomer fragments but extends to polymer segments which are significantly shorter than the chains: Segments of 10 monomers show the same orientation distribution near the NP, which becomes random also after 2 nm.

In contrast, all structure exhibited by entire polymer chains (radius of gyration and orientation with respect to the surface) depends strongly on the chain length. Consequently, the interphase thickness defined via these properties varies with the chain length and the grafting state of the NP. The radius of gyration of the polymer is here the governing length scale, as these long-scale structural features reproduce bulklike behavior only at a distance of at least one coil radius away from the NP, which can be as much as 3 nm in our simulations (Figure 10). At close distances, polymer chains tend to be both extended (R_g goes up) and oriented parallel to the surface. This points to polymer conformations where the chains are squashed against the surface. Figure 3 shows how chain stretching and orientation around a NP are correlated for free chains of 20 monomers; Figure 7 shows the same for a grafted NP. There is, however, a qualitative change of this picture for longer chains. While free chains with R_g less than that of the NP become stretched in the interphase area and hence show an increase in R_g, longer free chains show a smaller R_g with respect to its bulk value (Figures 4 and 10). This behavior can be explained by a picture of long chains engulfing the NP. As they are adsorbed on its surface, their radius of gyration is reduced to that of the NP. This picture is supported by the fact that the R_g reduction for chains at close distances is the strongest for the bare NP (Figure 4) and the weakest for the highest grafting density (Figure 10).

■ ACKNOWLEDGMENTS

Special thanks from A.G. to Jaber Dehghany for many informative discussions and his encouragement. This work has been funded by the EU project NanoModel (211778) as well as by the Deutsche Forschungsgemeinschaft through the Priority Programme 1369 "Polymer-Solid Contacts: Interfaces and Interphases".

■ REFERENCES

(1) Balazs, A. C.; Emrick, T.; Russell, T. P. *Science (New York, N.Y.)* **2006**, *314*, 1107−1110.
(2) Adnan, A.; Sun, C. T.; Mahfuz, H. *Compos. Sci. Technol.* **2007**, *67*, 348−356.
(3) Brown, D.; Marcadon, V.; Mélé, P.; Albérola, N. D. *Macromolecules* **2008**, *41*, 1499−1511.
(4) Roy, M.; Nelson, J. K.; MacCrone, R. K.; Schadler, L. S.; Reed, C. W.; Keefe, R.; Zenger, W. *IEEE Trans. Dielectr. Electr. Insul.* **2005**, *12*, 629−643.
(5) Putz, K.; Krishnamoorti, R.; Green, P. *Polymer* **2007**, *48*, 3540−3545.
(6) Mackay, M. E.; Dao, T. T.; Tuteja, A.; Ho, D. L.; Van Horn, B.; Kim, H. C.; Hawker, C. J. *Nature Mater.* **2003**, *2*, 762−766.
(7) Starr, F. W.; Glotzer, S. C. *Soft Matter* **2004**, 107−124.
(8) Ndoro, T. V. M.; Voyiatzis, E.; Ghanbari, A.; Theodorou, D. N.; Böhm, M. C.; Müller-Plathe, F. *Macromolecules* **2011**, *44*, 2316−2327.
(9) Liu, J.; Wu, Y.; Shen, J.; Gao, Y.; Zhang, L.; Cao, D. *Phys. Chem. Chem. Phys.* **2011**, 13.
(10) Montes, H.; Lequeux, F.; Berriot, J. *Macromolecules* **2003**, *36*, 8107−8118.
(11) Merabia, S.; Sotta, P.; Long, D. R. *Macromolecules* **2008**, *41*, 8252−8266.
(12) Harton, S. E.; Kumar, S. K.; Yang, H. C.; Koga, T.; Hicks, K.; Lee, E.; Mijovic, J.; Liu, M.; Vallery, R. S.; Gidley, D. W. *Macromolecules* **2010**, *43*, 3415−3421.
(13) Ruggerone, R.; Geiser, V.; Vacche, S. D.; Leterrier, Y.; Manson, J. A. E. *Macromolecules* **2010**, *43*, 10490−10497.
(14) Vogiatzis, G. G.; Voyiatzis, E.; Theodorou, D. N. *Eur. Polym. J.* **2011**, *47*, 699−712.
(15) Milano, G.; Santangelo, G.; Ragone, F.; Cavallo, L.; Di Matteo, A. *J. Phys. Chem. C* **2011**, *115*, 15154−15163.
(16) Zeng, Q. H.; Yu, A. B.; Lu, G. Q. *Prog. Polym. Sci.* **2008**, *33*, 191−269.
(17) Jordan, J.; Jacob, K. I.; Tannenbaum, R.; Sharaf, M. A.; Jasiuk, I. *Mater. Sci. Eng., A* **2005**, *393*, 1−11.
(18) Chevigny, C.; Jestin, J.; Gigmes, D.; Schweins, R.; Di-Cola, E.; Dalmas, F. *Macromolecules* **2010**, *43*, 48833−44837.
(19) Chevigny, C.; Gigmes, D.; Bertin, D.; Jestin, J.; Boue, F. *Soft Matter* **2009**, *5*, 3741−3753.
(20) Dukes, D.; Li, Y.; Lewis, S.; Benicewicz, B.; Schadler, L.; Kumar, S. K. *Macromolecules* **2010**, *43*, 1564−1570.
(21) Gast, A. P.; Leibler, L. *Macromolecules* **1986**, *19*, 686−691.
(22) Borukhov, I.; Leibler, L. *Macromolecules* **2002**, *35*, 5171−5182.
(23) Hooper, J. B.; Schweizer, K. S. *Macromolecules* **2006**, *39*, 5133−5142.
(24) Trombly, D. M.; Ganesan, V. *J. Chem. Phys.* **2010**, *133*, 184901−184910.
(25) Barbier, D.; Brown, D.; Grillet, A. C.; Neyertz, S. *Macromolecules* **2004**, *37*, 4695−4710.
(26) Bogoslovov, R. B.; Roland, C. M.; Ellis, A. R.; Randall, A. M.; Robertson, C. G. *Macromolecules* **2008**, *41*, 1289−1296.

(27) Robertson, C. G.; Lin, C. J.; Rackaitis, M.; Roland, C. M. *Macromolecules* **2008**, *41*, 2727−2731.
(28) Tsagaropoulos, G.; Eisenberg, A. *Macromolecules* **1995**, *28*, 396−398.
(29) Tsagaropoulos, G.; Eisenberg, A. *Macromolecules* **1995**, *28*, 6067−6077.
(30) Chen, L.; Zheng, K.; Tian, X. Y.; Hu, K.; Wang, R. X.; Liu, C.; Li, Y.; Cui, P. *Macromolecules* **2010**, *43*, 1076−1082.
(31) Müller-Plathe, F. *ChemPhysChem* **2002**, *3*, 755−769.
(32) Müller-Plathe, F. *Soft Matter* **2003**, *1*, 1−31.
(33) Karimi-Varzaneh, H. A.; Müller-Plathe, F. In *Multiscale Molecular Methods in Applied Chemistry*; Krichner, B., Verabec, J., Eds.; Springer-Verlag: Berlin Heidelberg, 2011; Vol. 307, pp 295−321.
(34) Reith, D.; Putz, M.; Müller-Plathe, F. *J. Comput. Chem.* **2003**, *24*, 1624−1636.
(35) Harmandaris, V. A.; Kremer, K. *Macromolecules* **2009**, *42*, 791−802.
(36) Mackay, M. E.; Tuteja, A.; Duxbury, P. M.; Hawker, C. J.; Van Horn, B.; Guan, Z. B.; Chen, G. H.; Krishnan, R. S. *Science* **2006**, *311*, 1740−1743.
(37) Kumar, S. K.; Krishnamoorti, R. *Annu. Rev. Chem. Biomol. Eng.* **2010**, *1*.
(38) Chevigny, C.; Dalmas, F.; Di Cola, E.; Gigmes, D.; Bertin, D.; Boue, F.; Jestin, J. *Macromolecules* **2010**, *44*, 122−133.
(39) Rahimi, M.; Karimi-Varzaneh, H. A.; Böhm, M. C.; Müller-Plathe, F.; Pfaller, S.; Possart, G.; Steinmann, P. *J. Chem. Phys.* **2011**, *134*, 154108.
(40) Smith, G. D.; Bedrov, D. *Langmuir* **2009**, *25*, 11239−11243.
(41) Ozmusul, M. S.; Picu, C. R.; Sternstein, S. S.; Kumar, S. K. *Macromolecules* **2005**, *38*, 4495−4500.
(42) Wang, Q.; Nealey, P. F.; de Pablo, J. J. *J. Chem. Phys.* **2003**, *118*, 11278−11285.
(43) Eslami, H.; Karimi-Varzaneh, H. A.; Müller-Plathe, F. *Macromolecules* **2011**, *44*, 3117−3128.
(44) Eslami, H.; Müller-Plathe, F. *J. Phys. Chem. B* **2009**, *113*, 5568−5581.
(45) Eslami, H.; Müller-Plathe, F. *J. Phys. Chem. B* **2010**, *114*, 387−395.
(46) Milano, G.; Müller-Plathe, F. *J. Phys. Chem. B* **2005**, *109*, 18609−18619.
(47) Spyriouni, T.; Tzoumanekas, C.; Theodorou., D.; Müller-Plathe, F.; Milano, G. *Macromolecules* **2007**, *40*, 3876−3885.
(48) Sun, Q.; Faller, R. *Macromolecules* **2006**, *39*, 812−820.
(49) Harmandaris, V. A.; Reith, D.; van der Vegt, N. F. A.; Kremer, K. *Macromol. Chem. Phys.* **2007**, *208*, 2109−2120.
(50) Qian, H. J.; Carbone, P.; Chen, X. Y.; Karimi-Varzaneh, H. A.; Liew, C. C.; Müller-Plathe, F. *Macromolecules* **2008**, *41*, 9919−9929.
(51) Carbone, P.; Varzaneh, H. A. K.; Chen, X. Y.; Müller-Plathe, F. *J. Chem. Phys.* **2008**, *128*, 064904.
(52) Karimi-Varzaneh, H. A.; Qian, H. J.; Chen, X. Y.; Carbone, P.; Müller-Plathe, F. *J. Comput. Chem.* **2011**, *32*, 1475−1487.
(53) Brown, D.; Mele, P.; Marceau, S.; Alberola, N. D. *Macromolecules* **2003**, *36*, 1395−1406.
(54) Starr, F. W.; Schroder, T. B.; Glotzer, S. C. *Macromolecules* **2002**, *35*, 4481−4492.
(55) Ghanbari, A.; Böhm, M. C.; Müller-Plathe, F. *Macromolecules* **2011**, *44*, 5520−5526.

4. A Coarse-Grained Molecular Dynamics Simulation of Polystyrene-Silica Nanocomposite: Dynamics in the Interphase and Polymer-Mediated Interactions of Nanoparticles

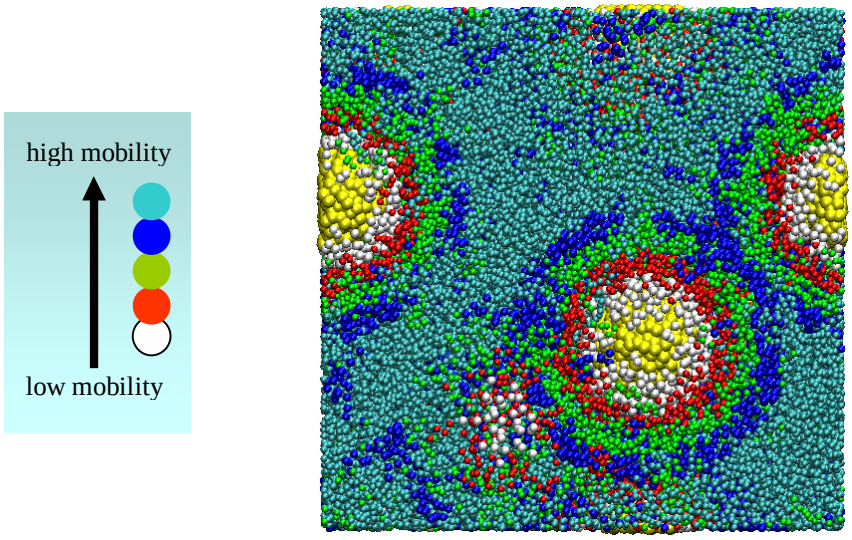

Abstract

Performing coarse-grained molecular dynamics simulations, the local dynamics of the free and grafted polystyrene chains surrounding a spherical silica nanoparticle has been investigated, where the silica nanoparticle was either bare or grafted with 80-monomer polystyrene chains. The effect of free (matrix) chain molecular weight and grafting density on the relaxation time of both the free and grafted polystyrene chains and also on the local mobility of the grafted chains at different separations from the nanoparticle surface, as well as on the mean square displacement of the nanoparticles has been investigated. Proximity to the surface, confinement by the surface, increased grafting density and increased matrix chain length were found to slow down the dynamics of the chain monomers and hence increase the corresponding relaxation times. “Drying” of the grafted network of the nanoparticle via increasing the free chain lengths, which is known to shrink the brush-height, was found to slow down the relaxation of the brush, too. The thickness of the

interphase, beyond which the polymers assumed bulk-like behavior, was ~ 1.5 nm for a bare nanoparticle, corresponding to four monomer layer, for all matrix chain lengths investigated. It increased to ~ 3 nm for grafted nanoparticles depending on the grafting density and the matrix chain molecular weight. We further determined the polymer-mediated effective interaction (potential of mean force) between two nanoparticles, examining the effect of the matrix-polymer molecular weight and grafting density. The matrix-induced interaction of *bare* nanoparticles promoted a strongly attractive potential at small separations, independent of matrix chain length, whereas a significant repulsion emerged farther out at ~ 1.2 nm because of the layered structure of the matrix around the particles. The grafted corona induced a strong repulsion between grafted particles, an effect which increased with higher grafting density and lower matrix molecular weight, the latter being in qualitative agreement with the experiments. Increasing the molecular weight of the grafted chains, surprisingly, led to less repulsion, due to the adsorption of the grafted chains of a given nanoparticle to the grafted corona of the second one.

4.1. Introduction

Nanocomposite materials (NCMs) exhibit novel properties which give them the potential for a variety of applications in industry, ranging from biomedical and electronic to automotive and aerospace aplications[1-3]. Such a high industrial potential, in turn, causes attention from the scientific community to understand and ultimately predict some of the features of the NCMs, which makes the development of new NCMs with desired properties easier. In our previous study, we investigated the structural properties of polystyrene (PS) chains around a spherical silica nanoparticle (NP), that was either bare or grafted with similar PS chains using coarse-grained (CG) molecular dynamics (MD) simulations[4]. They revealed a layered polymer structure around the particle, manifested as peaks of enhanced density. Moreover, the chain segments in the vicinity of the NP showed tangential orientation along the surface for all chain lengths. In the current study the same CG model is employed to investigate how the dynamical properties of the PS-silica NCM are affected near the filler particle.

On the level of an individual filler particle, matrix chains experience structural and dynamical perturbations by the surface of the particle[4-8]. The nature of these perturbations, at the qualitative level, and also their amplitude and spatial extent from the filler surface, at the quantitative level, depend on the nature of the polymer-nanoparticle interaction as well as quantitative aspects of the

filler (its shape, grafting state, particle/chain size ratio, …)[8-11]. The question of how deep into the polymer phase the chain structure and dynamics is affected by the presence of the nanoparticle, i.e. how thick this so-called *interphase* is, is not entirely academic. The interphase influences the properties of the entire composite, especially in nanocomposites, for which also the interstitial space can be of nanometer size and the polymer nowhere has the opportunity to show its bulk behavior. For example, changing the filler-matrix interaction type from strongly attractive to purely repulsive, in a CG model of a nanocomposite, Liu et. al[10] reported (respectively) tangential and perpendicular orientation of bonds, segments and whole chains with respect to the particle surface in the interfacial region. It has also been shown that the NP-induced changes in the conformation of whole chains depend on the ratio of the chains' radius of gyration to the nanoparticle size. Whereas short chains become more stretched close to the filler, longer chains tend to pack, compared to bulk chains, and wrap around the NP[4,7].

In order to predict and control the properties of NCMs, it is essential to characterize the structure and properties of the interfacial region around individual particles quantitatively. Whereas the changes in the local structural and dynamical properties of the matrix polymer confronting the NP surface have been investigated by experimental[12-14], theoretical[15-17], and computer simulation methods[5,6,9,18-21], a conclusive understanding about the interphase region has not been reached yet, and its dynamical properties have been a subject of an ongoing debate. For example, several independent experiments (including NMR, quasi-elastic neutron scattering, dielectric relaxation spectroscopy, differential scanning calorimetry and dynamical mechanical measurements)[22-28] have shown the existence of two distinct dynamic processes in NCMs, manifested by different relaxation times. One is characteristic for an immobile region (or at least of reduced mobility) caused by the adhesion of the polymer chains to the surface, which grows with the filler content[29]. The second refers to a free region which shows shorter relaxation times. It has been shown that functionalizing the filler surface by compatible polymer chains weakens the adhesion of matrix chains to the surface, whereas increasing the interfacial surface area and the polymer-surface attraction enhances it. There are also contradicting experimental studies (like dynamical mechanical spectroscopy, NMR, dielectric spectroscopy and calorimetry) which conclude that the local segmental dynamics of the chains in the vicinity of filler particles is basically the same as that of the unfilled system[30-33]. Despite some stiffening of the elastomer in the vicinity of fillers, there is no appreciable difference in the segmental dynamics[34]. There are even reports of increased mobility of the interfacial chains[35-38],

which, together with the above mentioned ones, shows the lasting complexity of the subject. Robertson et al.[39] have reviewed the literature dealing with the effects of proximity to the filler surface on the local segmental mobility of polymer chains. They mentioned that some of these discrepancies can be ascribed to ambiguous methods of data analysis; others likely reflect the variation in the filler-polymer interaction among different systems.

Interpretation of the empirical data can be difficult, as alternative methods/models of data analysis can lead to completely different results for the same experimental observation. In fact some alternative interpretations of the measurements on interfacial chain mobility have been proposed[39,40], showing that care must be taken in this issue. On the other hand, there is the additional complication by the necessary distinction between different regions of a sample (under study) contributing to the experimental measurements. For the interracial dynamics of polymer chains, Robertson et al.[39] have emphasized that, it is not always clear from experimental studies that a distinction is made between chain segments immobilized by their spatial proximity to filler particles versus specific chemical units adsorbed at specific sites on the filler surface. Such a precise distinction, being very difficult (if not impossible) in experiment, is rather straightforward in computer simulation.

Computer simulation methods have been employed to study the interfacial region in NCMs, where structural[5,7,41,42] and dynamical[6,8,10,43-45] properties of the interphase region have been investigated. For example, employing a bead-spring polymer model, Star et al.[43] showed that the relaxation of the monomers closest to the nanoparticle surface is slowest when the monomers and the nanoparticle have an attractive interaction. Such a reduced mobility in the presence of an attractive filler-polymer interaction has been observed in other investigations[6,46-48], too. Conversely, Star et al. observed a significantly enhanced (compared to the bulk) relaxation of surface layer monomers when there was only repulsion between the monomers and the nanoparticle[8]. Borodin et al.[49] reported the same reduced local polymer mobility near the surface, accompanied by enhanced polymer density for attractive interactions between the surface and the polymer chains. Moreover, the dynamic behavior of matrix PS chains was found by Ndoro et al.[6] to be affected both by the grafting state of the silica nanoparticle (moderately) and its diameter or curvature (strongly), where a lower curvature radius leads to slower polymer dynamics and to an increased thickness of the “slow zone” around the particle. Investigating the effect of the grafting state, as well as the grafting density and matrix-chain length, on the dynamical properties of the interphase region, is one main aim of the present coarse-grained study of PS-Silica NCM.

The common result of all computer simulations is that the mere existence of the interface between the polymer and filler modifies the polymer structure. Even though these perturbations can reach beyond the first molecular layer, they persist only for a few nanometers from the filler surface[4-8,49,50]. Beyond such a distance all structural and dynamical properties show bulk-like behavior. This indicates that all the alteration of properties of a NCM compared to an unfilled bulk polymer can be attributed to the altered behavior of polymer in the interphase. Since each filler particle contributes to this enormous interface region, the interface area is most efficient when nano-sized particles are uniformly dispersed in the matrix polymer.

Dispersability of nano-fillers in the polymer matrix, depends on the appropriate selection of the polymer-particle combination in the first place. Introduction of nano-fillers, however, may also lead to immiscibility of particles with the polymer matrix, which manifests itself by particle aggregation. This happens either due to strong van der Waals interactions between the filler particles or due to polymer-mediated inter-particle attractions[11,51-55]. Ultimately, particle aggregation is detrimental to the NCMs, since most of their properties arise from the significant interfacial area of filler and matrix, as mentioned above. Aggregation of the particles obviously results in a reduced surface area accessible for the matrix polymer. So the dispersion of nano-sized filler particles within the polymer matrix is a vital control parameter in NCM engineering and development, and hence also from a theoretical point of view[56]. On the other hand, while dispersion of the filler particles is believed to critically affect properties of the NCMs, it is not clear how the optimization of one (for example mechanical) property can affect other properties (like electrical or thermal) of the given NCM, depending on whether or not cross-property bounds exist[57].

Experimentally, the functionalization of NPs by attachment (grafting) of polymer chains to the surface is well established to enhance the miscibility of particles with the matrix[51,52,58,59]. In this way, the favorable interaction of the grafted and matrix polymers is exploited to stabilize the dispersion of the particles. The type and strength of nanoparticle-polymer interactions not only influences the structure and dynamics of the matrix chains around the particle as mentioned above, but also the dispersion of nanoparticles[60-65]. For example, Smith et al.[66] have reported a polymer-matrix promoted aggregation of (bare) nanoparticles. It is enlarged with the polymer molecular weight, if the nanoparticle-polymer interaction is relatively weak. Increasing the attractiveness of nanoparticle–polymer interactions, they further reported strong adsorption of the polymer chains on the surface of the nanoparticles which promoted dispersion of the nanoparticles. Although a large

number of empirical and theoretical investigations have recently been carried out in the field, a comprehensive theory capable of quantitatively describing the NPs organization in the polymer matrix is still missing. In the present coarse-grained MD study we examine the polymer-induced interactions between bare and grafted silica NPs in a dense matrix of atactic polystyrene. The polymer-mediated effective interaction potential of the NPs, or the potential of mean force, is measured for different grafting densities, as well as for different molecular weights of the matrix and the grafted polymers, to correlate effects of polymer matrix and grafting state on the dispersion of nanoparticles in a PS-silica nanocomposite model.

4.2. Systems and Methods

4.2.1. Mapping Scheme and Coarse-Grained Potentials

In the present study we have employed the coarse-graining scheme proposed by Qian et al.[67] for PS matrix, where each repeat unit of PS is represented by one CG bead whose interaction center is located at the repeat unit's center-of-mass. The same mapping scheme is used for both free and grafted PS chains. Two different beads (R and S) are used to account for the chirality of atactic PS. The grafted chains are attached to the NP via a linker unit (-$[H_2C(H(C_2H_3)C)]_3(CH_3)_2Si$-) as used in experiments (see Supporting Information of ref 5 for its structure). The linker has been divided into four CG beads of two kinds having approximately the same mass. The first corresponds to -$CH_2CHCHCH_2$- and the second to -$(CH_3)_2Si$. For both, the CG interaction centers are located at the center of mass of the group of atoms. The spherical silica NP has a diameter of ~ 4 nm and is filled with 873 CG beads of SiO_2 which their centers of mass are located at the position of the Si atoms. The NP beads have been distinguished as either surface or core beads which have different interactions with the polymer, the surface beads contributing more.

The CG interaction potentials for PS, which contain nonbonded pairwise intermolecular interactions, bond interactions between neighbors, and angle potentials between three subsequent beads, are prepared using iterative Boltzmann inversion (IBI). The aim of this method is a CG structure which reproduces as much as possible the atomistic structure defined by radial distribution functions between different bead types, as well as bond-length and angle distributions. In our previous study we have shown that the agreement between the CG and the atomistic structures was very satisfactory[4]. Furthermore, the reliability of the CG potentials was confirmed by back-mapping the

equilibrated CG structure to an atomistic resolution via a new back-mapping scheme[68]. For more details of the potential development and the adopted mapping scheme the reader is referred to our previous study[4]. In the current study, no nonbonded interactions between NPs have been considered, since the NPs are well dispersed and far from one another.

4.2.2. Initial Configurations

To prepare the initial configuration of the model NCM, silica NPs of radius 2 nm were randomly distributed in the simulation box, and PS chains were added to the system afterwards. All of the initial configurations were generated by a method developed and described previously[4]. At first, the complete NPs with all their superatoms were copied to their random (non-overlapping) positions in the simulation box. Then the linker beads (connecting the grafted chains, if any, to the NP) were placed next to the NP beads which they are supposed to be bound to. These linkers constitute the first beads of each grafted chain. At the next step a new bead was added to each grafted chain, simultaneously, using a self-avoiding random walk (SARW), such that its distance from the previous bead is equal to b (the average bond length of polymer beads). This step was repeated, taking care of any overlap between beads of different grafted chains or with NP beads, until all the grafted chains possessed their desired length. To add N_f free chains to the system, we placed N_f random seeds (first monomers) in the simulation box first and then grew them simultaneously in the same way as for grafted chains. To circumvent the possible overlap of the free and grafted chains during the SARW process, we checked the overlap of each newly added free bead to the beads of those chains whose seed were less than $2R$ from the current chain's seed. Upon an overlap between beads, the position of the newly added bead was randomly sampled again. Here R is the theoretically expected value of the end-to-end distance of a freely-jointed chain of N_f beads, each at distance b from each other: $\sqrt{N_f}\,b$. This way of checking possible overlaps circumvents the heavy load of checking each new bead against all existing beads, which is computationally expensive for large systems or long polymers.

In order to calculate the potential of mean force we have used two identical silica NPs of 2 nm radius. A different initial configuration was created for each inter-particle separation. We have inserted the center-of-mass of two NPs at the given positions. The size of the simulation box is chosen such that the NPs do not interact with the image of each other, limiting their interactions to

the direct interaction at the given inter-particle separation. Then grafted and free chains, respectively, were added by the same method as mentioned above.

4.2.3. Systems and Simulation Details

We have performed simulations for different grafting states of the nanoparticle (bare, low grafted and high grafted density NPs). In the first part of the study, in which dynamical properties of the interfacial chains have been investigated, we have put 6 NPs in the simulation box of a volume ~ $(24.5\ nm)^3$, the NP volume fraction initially being ~ 1.4%. For comparison, we have also included a pure unfilled PS system. Details of the systems studied in this part are provided in Table 1.

Grafting density (chains/nm^2)	Number of grafted chains per NP	Grafted chain length (monomers)	Number of free chains	Free chain length (monomers)	Diffusion coefficient of free chains ($\times 10^{-6}\ \frac{nm^2}{ps}$)
0	0	-	2706	20	2.44 ± 0.09
0	0	-	1353	40	1.03 ± 0.07
0	0	-	679	80	0.38 ± 0.04
0	0	-	270	200	-
0.5	25	80	2106	20	2.25 ± 0.11
0.5	25	80	1053	40	1.01 ± 0.07
0.5	25	80	526	80	0.42 ± 0.11
0.5	25	80	211	200	-
1	50	80	1507	20	1.87 ± 0.08
1	50	80	753	40	0.82 ± 0.07
1	50	80	376	80	0.43 ± 0.03
1	50	80	151	200	-

Table 1. *Nanocomposite systems with a fixed nanoparticle radius of 2 nm studied for dynamic properties (T = 590 K, P = 101.3 kPa). There are 6 nanoparticles in a simulation box of $(22\ nm)^3$, the nanoparticle volume fraction is 2%. The diffusion coefficients of free chains are given in last column where the corresponding value for 200-mer chains are not reported, because they did not reach the diffusion limit within 40 ns of production run.*

The prepared initial configurations of the systems are far below the equilibrium density (~ 660-680 kg/m^3 at the beginning) and still have some overlaps, and hence need to be relaxed. In order to equilibrate the initial configuration, the systems were simulated in the NPT ensemble for 12-20 ns, depending on the chain length, to reach the desired density (~ 940-970 kg/m^3), at which point the simulation box has the a volume ~ (22 nm)^3 and a NP volume fraction is 2%. The systems were then simulated for 40 ns for analysis using a time step of 4 fs. All MD runs were carried out at a pressure of 101.3 kPa and a temperature of 590 K. Berendsen's thermostat (with a coupling time of 0.2 ps) and barostat (with a coupling time of 5 ps and isothermal compressibility of 1.0×10^{-6} kPa) were used to control temperature and pressure. The cutoff for the nonbonded interactions was 1.5 nm, and the neighbor list cutoff was 1.6 nm. Configurations were sampled every 1000 time steps (4 ps). All CG simulation were performed with the IBIsCo code which has been developed in our group[69].

In the second part of the study, the potential of mean force between NPs is investigated. The same simulation parameters and process were used to relax the initial configurations. The only difference was that the positions of the NPs were fixed at the given inter-particle distance. After relaxation time, systems were run for another 4 ns, for the force calculation. Fixing the position of a NP was done by choosing the bead closest to its center, and removing it from the beads whose positions were updated at each time step. Obviously, in this way NPs still can rotate around their centers of mass. The systems calculated are summarized in Table 2. All have the same NP volume fraction (~ 1.6 %). The force experienced by the center bead through its interaction with all the other beads within the cut-off range, was measured at each time step and was averaged over 4 ns. As the center of mass of each NP is fixed, the net force experienced by it must be equal (in magnitude) to the sum of those experienced by all the other beads of the NP; otherwise the NP would translate in space. Recall that the direct nonbonded interaction between different NP beads was turned off, keeping all the other interactions (as described elsewhere[4]) untouched. As there is no direct interaction between the two NPs, any force experienced by each NP is mediated by the polymer (both free and grafted chains) and hence is called "polymer-mediated" mean force. For a given NCM system (with its free and grafted chain length as well as grafting density) the mean force is averaged at different separations of the two NPs together with its standard deviation (error bar). The resulting "mean force versus distance" can easily be converted into the potential of mean force versus center-to-center distance *r*,

via integration $V(r) = -\int_{r_{max}}^{r} F(x).dx$, where r_{max} = 3.0 nm is the maximum inter-particle separation of the NPs considered for the potential calculation, i.e. the practical infinity. For easier comparison, the center-to-center distances have been converted to surface-to-surface distances in the following.

Grafting density (chains/nm^2)	Number of grafted chains per NP	Grafted chain length	Number of free chain	Free chain length
0	0	-	1044	20
0	0	-	104	200
0.5	25	80	854	20
1	50	80	644	20
1	50	20	944	20
1	50	80	129	100

Table 2. *Nanocomposite systems for polymer-mediated potential of mean force calculated between two nanoparticles with a fixed nanoparticle radius of 2 nm (T = 590 K, P = 101.3 kPa)*

4.3. Polymer Dynamics in the Interphase

4.3.1. Monomer Dynamics of Free Chains

The effect of addition of filler particles on the matrix chain dynamics is investigated. Table 1 shows the center-of-mass diffusion coefficient of the PS chains in the presence of nanoparticles for different grafting densities and matrix chain lengths. Even though the volume fraction of filler particles is low (2 %), introduction of the NPs always leads to a lower diffusion coefficient, and hence higher viscosity, of the polymer chains in the NCM. The diffusion of the polymer chains, however, provides only a global view of changes in their dynamics by NPs. In order to elucidate the local dynamics of monomers around the NP in the presence of free chains of different length, we have used the self scattering function, S(q,t). It shows the correlation of monomer positions at time *t* with their initial position at *t = 0*. The self scattering function is defined as $S(q,t) = \frac{1}{N}\left\langle \sum_{j=1}^{N} e^{-i\vec{q}.\left[\vec{r}_j(t) - \vec{r}_j(0)\right]} \right\rangle$ where $\vec{q}$ is the wave vector, N is total number of monomers,

$\vec{r}_j(t)$ is a vector pointing to the position of monomer j at time *t*, and <...> denotes the ensemble average for all PS monomers in the system. The monomer dynamics can also be monitored by the mean square displacement (MSD). The main advantage of the self scattering function over MSD, however, is being experimentally measurable. Moreover, S(q,t) makes the quantitative comparison of dynamics in different shells and systems easier, as it varies between 1 (highly correlated) an 0 (totally uncorrelated), unlike MSD. In the definition of S(q,t), which has been given above, the wave vector q determines the range of displacement beyond which a monomer can be considered out-of-phase or losing spatial correlation with its original position (at t=0). Choosing an appropriate value for q, regarding the length scales which we have in the system, gives us an additional degree of freedom, compared to MSD, to define and measure the degree of auto-correlation of the monomer position. We have chosen $q = 0.78\ nm^{-1} = \frac{\pi}{4nm}$, such that it leads to a phase difference of π when a monomer is displaced from its position by a distance equal to the NP diameter. S(q,t) calculated in this way provides the spatial correlation of monomers with their initial position.

We have considered concentric spherical shells of equal thickness of 1 nm around each nanoparticle. This has enabled us to study how and to which extent the mobility of the monomers at different distances from surface (i.e. in the chosen shells) is affected by the presence of the NP. By definition, a monomer belongs to that NP around which it has spent most (at least 50%) of its time around. Among the multiple layers around that NP, the monomer belongs to a particular shell in which it has spent most of its time. The self scattering function of monomers of a given (*nth*) shell is defined as $S^n(q,t) = \left\langle \frac{1}{N_{n,p}} \sum_{j=1}^{N_{n,p}} e^{-i\vec{q}.\left[\vec{r}_j(t) - \vec{r}_j(0)\right]} \right\rangle$ where $N_{n,p}$ is total number of the monomers in the shell n around *NP* p and <...> denotes ensemble average over PS monomers belonging to that particular shell and over *nth* shells of all NPs in the system.

The way of assignment of monomers to the NPs and their surrounding shells, as described above, excludes those monomers which have passed from one NP to the other and stayed more than 50% of their residence time around neither of them. If a monomer has regularly visited different shells of a given NP and has stayed most of its time in one of the shells (even not persistently), it is assigned to that particular shell.

The influence of the grafting density on the dynamics of monomers of the matrix chains of different length in the grafted corona is investigated. In Figure 1, S(q,t) is shown for monomers of free chains in the second shell around the NP (1 to 2 nm from its surface) for different grafting densities. It is also compared with that of bulk PS (black curve). Different panels show different free chain lengths. Independent of grafting state and matrix chain length, the presence of NP slows the dynamics of the free polymer compared to the bulk, albeit to different extent. Increasing the free-chain length leads to decrease in the dynamics, as expected, for both bulk polymer and the free polymer in the NCM (Figure 1A -D). The overall effect of grafting density on the dynamics of matrix chains is: the larger the grafting density, the slower is the dynamics of free monomers at a given distance.

Figure 1A shows that when the radius of gyration R_g of matrix chains (1.03 nm) is less than the average distance of the in shell from the surface (1.5 nm), the monomer dynamics of the matrix chains does not deviate considerably from that of bulk polymer, independent of particle's grafting state. It happens despite the dominant presence of the grafted corona manifested by radius of gyration and brush height of the grafted chains of 2.44 nm and 3.23 nm for high grafting density and 2.38 nm and 2.96 nm for low grafting density. The brush height is defined as the average radial distance of the grafted chain monomers from the surface. When R_g of matrix chains is 1.51 nm (Figure 1B), the monomer dynamics of the matrix chains slows down at least for grafted NPs, indicating that the thickness of the region with reduced mobility, called the interphase, depends on the radius of gyration of the matrix chains. The dynamics of the matrix chains around a bare NP is still not affected, which shows that the interphase thickness depends on the grafting density, too. Further increasing the radius of gyration of the matrix chains to 2.20 nm and 3.4 nm (Figures 1C and 1D, respectively) results in further slowing-down, though small, around bare NP. Moreover, the dynamics of the matrix chains for high grafting density shows a qualitatively different trend when chains with $R_g > 1$ nm are used, manifested as slower dynamics accompanied by a plateau at long times. Considering our preceding study on the structural properties of the same NCM[4], this can be attributed to the “drying effect” of the grafted corona. Grafted chains contract from further (mainly beyond 3 nm the surface) to closer distances, which leads to ~ 25% increase in the density of grafted monomers, together with ~ 50% decrease in the density of matrix chains, at 1.5 nm from the surface (middle of the current shell). The ultimate effect of such a change in the composition of the monomers at this distance is suppressed dynamics of the remaining free chains because of their increased involvement with grafted ones. The fact that the same magnitude of slowing-down does

not happen in low grafting density case is in line with the observation that wet-to-dry transition in the grafted corona was much weaker in this case[4]. When the matrix chain R_g becomes > 2 nm (i.e. about twice their distances from the surface) the difference between matrix monomer dynamics around bare and low grafting density NPs disappears.

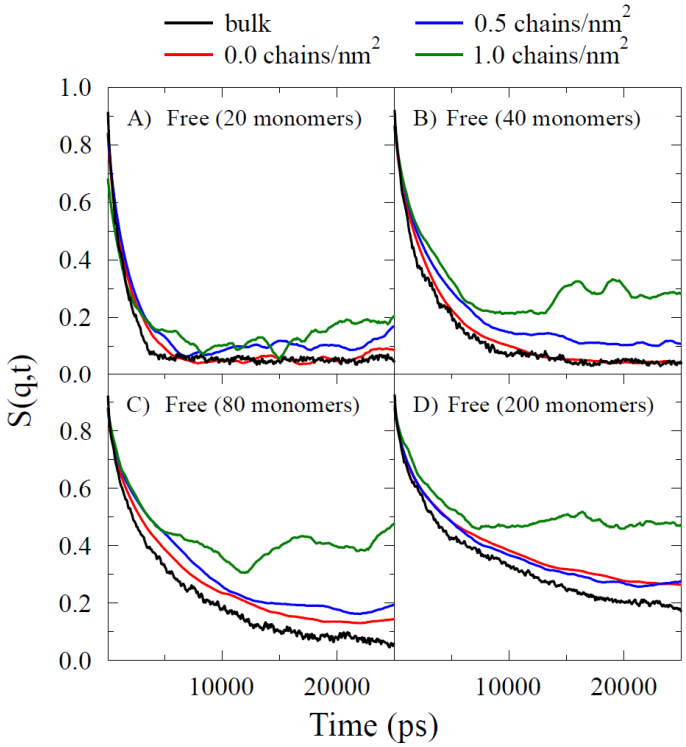

Figure 1. *Self-scattering-function of free-chain monomers in the second shell (1-2 nm from surface), $S^{n=2}(q,t)$, around the nanoparticle as a function of the density of grafted chains (length 80 monomers) on the nanoparticle surface and of the length of the free chains (20, 40, 80, 200 monomers in panels A-D, respectively) for a constant q = 0.78 nm^{-1}. The scattering function for an unfilled polymer bulk with the same chain lengths is shown for comparison.*

In the next shell, which is 2-3 nm from surface (Supporting Information, Figure SI-1), the dynamics around a bare and low grafted NPs is bulk-like for all free-chain lengths. This means that the NP, whether bare or low-grafted, barely affects the matrix chains mobility beyond 2 nm from its surface. Should the changes in the dynamics of the free chains be interpreted as a manifestation of an interphase, its thickness would be ~ 2 nm in this case. Such a length scale is in agreement with the interphase thickness defined by the extent to which the *structure* of the chains is altered by the NP[4].

In the presence of a high grafting density NPs, on the other hand, the dynamics is still perceptibly slower than for bulk polymers, showing that the interphase thickness for the same NP can be extended to ~ 3 nm by increasing the grafting density. Such a behavior is again in line with the grafting-density dependence of the interphase thickness when measured using structural properties (radius-of-gyration) of the chains[4]. This further shows that the monomers dynamics is perturbed to the same distance as the chain structure. Beyond 3 nm, the chain dynamics is bulk-like independent of grafting density and length of the free chains (data not shown here).

4.3.2. Monomer Dynamics of Grafted Chains

The influence of the lengths of the free chains and grafting density on the mobility of the *grafted* chains has been also investigated. To this end, the appropriate S(q,t) are calculated in different shells. An example (low grafting density) is given in Figure SI-2 (Supporting Information). It shows a clear attenuation of the dynamics of grafted chains in the presence of longer free chains. The dynamics can, however, be condensed into a more compact form by using the relaxation time τ of the scattering function $S(q,\tau)$, Figure 2. The τ parameter is the time where $S(q,\tau) = 0.5$. Alternative definitions of τ probably would not change the result qualitatively. Figure 2 shows relaxation times of grafted monomers in 4 different shells around the NP of high grafting density, for different free chain lengths. Grafted monomers in the first layer (0-1 nm) are mainly linker units and undergo very limited displacements being attached to the NP surface. Their S(q,t) do not meet the required criterion (for relaxation time) as they do not decrease below 0.6 in most cases (see Figure SI-2 in the Supporting Information). So we show relaxation times only for shells 2-5 around the NP, which cover distances of 1-5 nm from the surface.

Figure 2A shows, for all free chain lengths, the expected faster relaxation of grafted chains as the distance the NP surface increases. The same trend is observed as well for low grafting density (Figure 2B). Moreover, the concentration of the grafted monomers decreases with distance from the NP, considering its spherical geometry, which leads to a higher contribution of the more mobile free chains. In each shell, the relaxation of grafted monomers is faster when the free chains are shorter. This behavior is observed for all shells at both grafting densities, except for the 1-2 nm shell of highly grafted NP where relaxation times are typically very large and not that much different. The large relaxation times in the first few shells around NP occur because of the attachment to the surface together with high grafting density which strongly restricts the dynamics of the grafted

chains in those shells. Very slowly decaying S(q,t) together with statistical variations led to this reversal of the order in the monomers dynamics. The general decrease of relaxation speed with chain can be understood noting the faster dynamics and lower viscosity of the shorter matrix chains on the one hand, and more infiltration of the shorter free chains into the grafted corona on the other hand. The latter, leading to so called wetting of the grafted corona, has been reported for the same NCM[4]. It is also clearly visible in Table 3, as the brush height of the grafted chains (defined as the average radial distance of their monomers from the surface) decreases for an increase of the length of the free chains. This corresponds to a deswelling of the corona chains in large matrix length. Whereas the dependence of the dynamics of the grafted monomers on the length of the free chains is stronger at closer distances from the NP, it becomes less pronounced at farther distances, for both grafting densities. Moreover, for a given free chain length, grafted monomers relax faster as grafting density decreases (Figure 2, compare panels A and B). This can be attributed to the larger infiltration of the free chains in the low density corona, reflected by their higher contribution in density profile[4], which have generally faster dynamics by being "free".

At larger distances from the NP (Figure 2, 4-5 nm from surface), relaxation times converge to ~ 2500 ps for both grafting densities. This shows that the grafting density plays no significant role in the determination of the dynamics of grafted monomers at large distances. This is possibly an effect of the convex geometry of the nanoparticle which necessarily leads to a decrease of grafted-chain density with distance.

At high grafting densities a closer look at the S(q,t), shown in Figure SI-3, reveals a difference in the relaxation process of grafted chains in the presence of short and long matrix chains, moving from inner (panels A and B) to outer shells (panels C and D). While the S(q,t) of grafted monomers in the presence of different free chain lengths are ordered as 20-mer = 40-mer < 80-mer < 200-mer in the inner shells (0-2 nm from surface), they follow 20-mer = 40-mer < 80-mer = 200-mer in the outer shells (2-4 nm from surface), showing that short and long matrix chains induce a qualitatively different dynamics in the grafted corona. Again the explanation is provided by the wet-to-dry transition of the grafted corona when the matrix chain length varies from shorter to longer than that of grafted chains (Table 3). Similarity of the corona relaxation in the presence of short and long free chains is accompanied by the same similarity in its monomer composition at 2-4 nm form surface, according to the density profile (see Figure 9 of ref 4). Such a difference, however, is not assured at low grafting densities, in line with a much weaker wet-to-dry transition effect in this case.

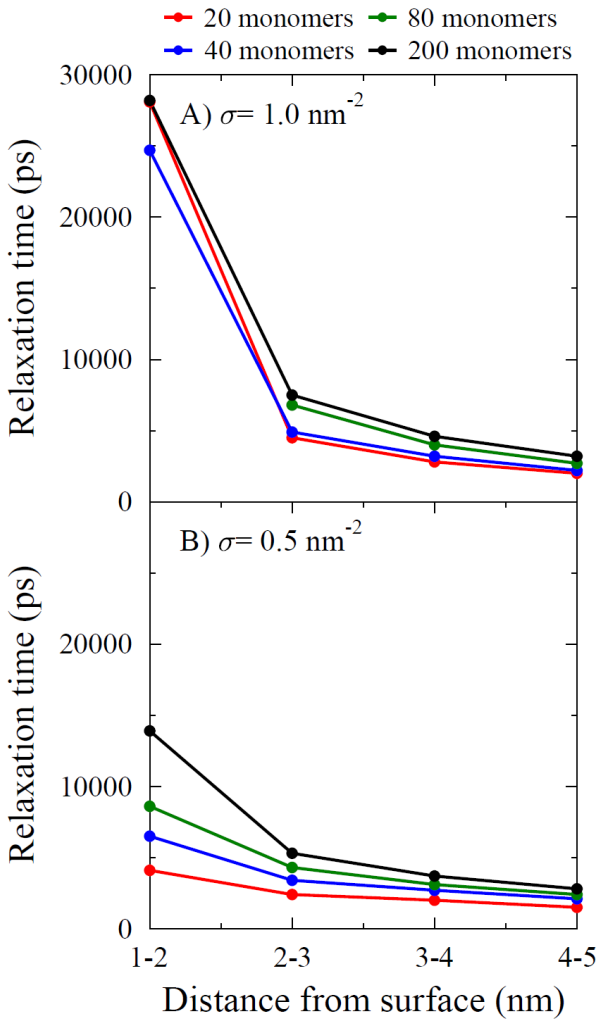

Figure 2. *Relaxation time τ of S(q, t), q = 0.78 nm^{-1}, of grafted monomers at different distances, for high (σ = 1.0 chains/nm^2) and low (σ = 0.5 chains/nm^2) grafting densities are shown in panels A and B, respectively. Free chains have 20, 40, 80 and 200 monomers, respectively, and grafted chains 80 monomers. Data for the first shell (0-1 nm) is not shown, as they are mainly caused by linker molecules which relax too slow to estimate their relaxation time.*

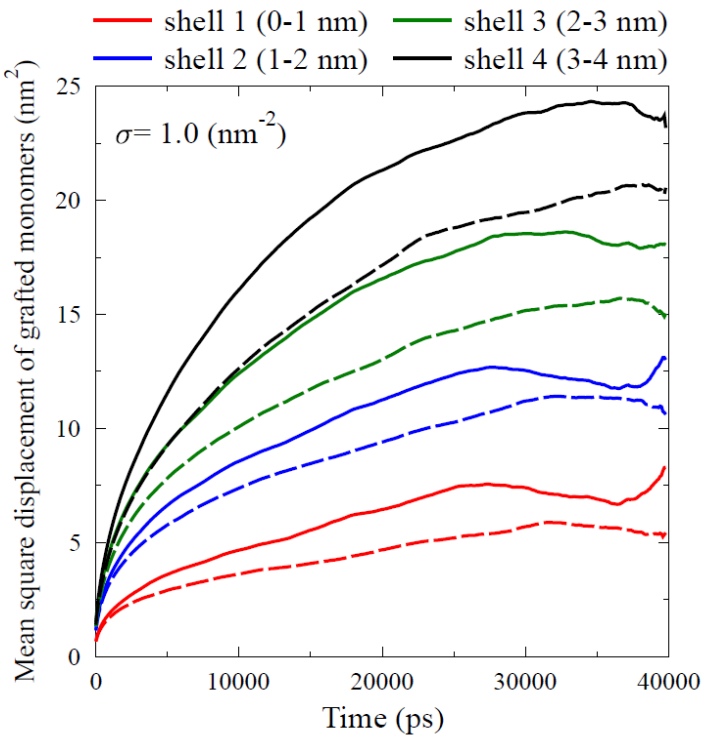

Figure 3. *Mean square displacement (MSD) of monomers of grafted chains at different distances from a high-grafting-density (σ =1.0 chains/nm^2) nanoparticle, measured in the coordinate frame of the nanoparticle center-of-mass. MSD in different shells (each with 1 nm thickness, where the first one surveys 0-1 nm from surface) are shown by different colors, during 40 ns. Solid and dashed lines show the MSD in the presence of short (20 monomers) and long (200 monomers) free chains.*

As grafted chains are restricted by being attached to the NP, grafted monomers will experience a restricted motion depending on their distance from the surface. Their mobility can also be further reduced by grafting density and free chain length as shown above using the self scattering function concept (Figure 2). Although the S(q,t) is more convenient to study the monomer dynamics, as mentioned above, still the restricted motion of the grafted monomers can be better monitored using the mean square displacement (MSD). The MSD of grafted monomers, defined by $MSD(t) = \left\langle \left(\vec{R}(0) - \vec{R}(t) \right)^2 \right\rangle$, is calculated for different shells. $\vec{R}(0)$ and $\vec{R}(t)$ are position vectors of the monomers in a particular shell at time 0 and t, respectively, in the coordinate frame of the center-of-mass of their parent NP. <…> denotes the ensemble average in that particular shell, as

well as an average over all NPs. Assignment of the monomers to different shells has been done by a criterion of minimum 50% residence time in a given shell, as described above. Figure 3 shows the MSD of grafted monomers in different shells versus time, in the presence of free chains of 20 and 200 monomers length. As expected, the mobility of grafted monomers increases with distance from the NP; it decreases with the length of the matrix chains according to their increased viscosity; all MSDs saturate, since the chains are tethered to the NPs.

	σ =1.0 chains/nm^2	σ = 0.5 chains/nm^2
Free chain length (monomers)	Brush height (nm)	Brush height (nm)
20	3.29 ± 0.99	2.85 ± 1.01
40	3.16 ± 0.96	2.83 ± 1.04
80	3.07 ± 0.96	2.67 ± 0.95
200	3.03 ± 0.96	2.64 ± 0.97

Table 3. *Calculated brush height of nanoparticles for high (σ = 1 chains/nm^2) and low grafted (σ = 0.5 chains/nm^2) density cases, with different free chain lengths; the grafted chain length is constant (80 monomers).*

4.3.3. Dynamics of Nanoparticles

To investigate the mobility of the nanoparticles, their center-of-mass mean square displacements are shown in Figure 4, averaged over the 6 NPs. Free chains of different lengths (from 20 to 200 monomers) are examined for each grafting density. Increasing the grafting density from 0 to 0.5 and 1 chains/nm^2 has an overall effect of decreasing the MSD of the NP. Grafting a bare NP with low grafting density results in 3-10 times smaller MSD (depending on free-chain length), whereas it is only ~ 2 times smaller for high grafting density compared to low grafting density. This shows that motion of a bare nanoparticle is much easier than of grafted ones, due to its lower mass and hydrodynamic radius.

For each grafting density, shorter matrix chains lead to larger values of the MSD of the NP in comparison to the longer chains. This shows that the mobility of the NP in the polymer matrix depends not only on the grafting density, but also on the length of the free chains. In the case of bare

NP, there is a difference of more than one order of magnitude in the MSD of NP after 40 ns between free chain length of 20 and of 200 monomers. Whereas the MSD decreases substantially between the free chain lengths of 20 and 80 monomers, the change between 80 to 200 monomers is much smaller. Note that only for bare NP in the shortest free chains the regime of anomalous diffusion is left and Einstein diffusion is observed (Figure 4A) at the simulation time considered here. The MSD of grafted NPs shows a quantitatively weaker dependency on the free-chain length, compared to the bare NPs. In particular, the MSD is almost equal for free chains of 80 and 200 monomers.

One can tentatively try to rationalize the nanoparticle diffusion coefficients D_{NP} in relation to their hydrodynamic radii R_{NP} using the Stokes-Einstein approximation $D_{NP} = \frac{k_B T}{6\pi\eta R_{NP}}$, where k_B is Boltzmann's constant, T the temperature, and η the viscosity of the matrix. The viscosity can be taken as approximately inversely proportional to the diffusion coefficient of the matrix polymer D_P. The hydrodynamic radius of the NP is obtained as the sum of its geometrical radius and the mean brush height if grafted, cf. Table 3. If the Stokes-Einstein relation were the governing law for the NP diffusion, the ratio $Z = \frac{D_{NP} R_{NP}}{D_P}$ should be a constant for all systems of a given temperature. We have analysed Z for nanoparticles of all grafting states in matrices of chain length 20, 40 and 80 (data not shown). Note, however, that only for the 20-monomer matrix, both NPs and matrix chains have reached the diffusion limit after 40 ns. Thus, the D_{NP} and D_P extracted from the MSDs represent only upper bounds to the real diffusion coefficients for the 40 and 80 monomer systems. With this caveat we note the following features: (i) Z is not a constant but varies by a factor of 6 between different matrix chain lengths and particle grafting states. This indicates that other factors than hydrodynamic radius and matrix viscosity are important, too. (ii) For bare nanoparticles, Z is reduced by 40% from 1.8 nm to 1.1 nm when the matrix chain length is increased from 20 to 80 monomers (corresponding to size ratios between polymer and nanoparticle of $0.5 < \frac{R_g}{R_{NP}} < 1.1$). This means that the nanoparticle mobility is reduced more than expected from the Stokes-Einstein relation. (iii) In contrast, for the high-grafted nanoparticles, Z doubles from 0.3 nm to 0.69 nm for

the same change of polymer length (which now corresponds to size ratios of $0.17 < \frac{R_g}{R_{NP}} < 0.43$, due to the particle radius being incremented by the brush).

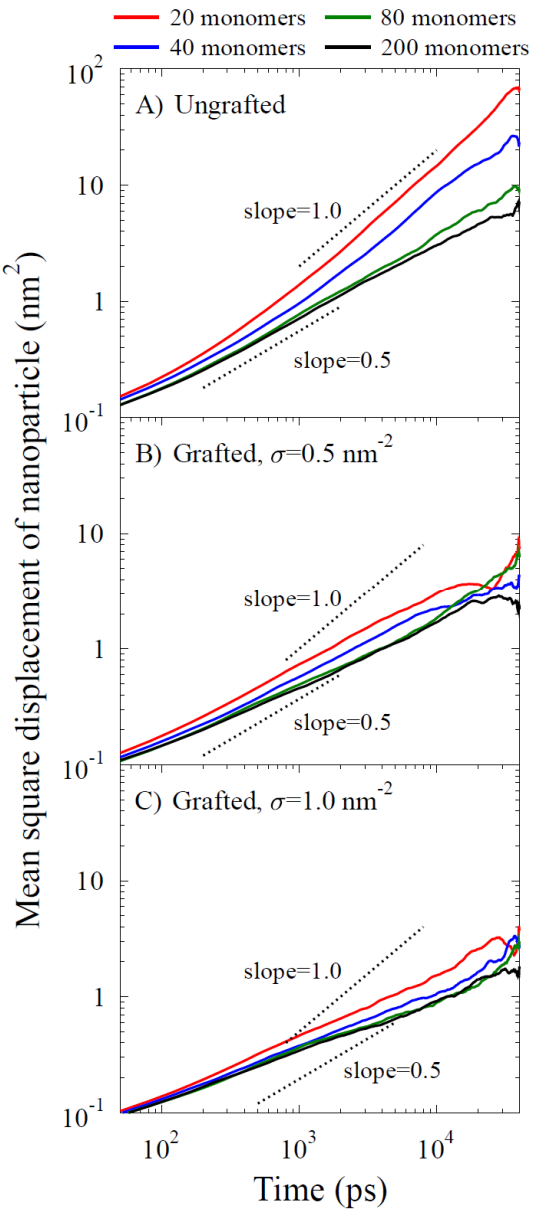

Figure 4. *Mean square displacement of (A)bare and (B) low-grafted (σ =0.5 chains/nm^2) and (C)high-grafted (σ =1.0 chains/nm^2) nanoparticles in the presence of free chains length of 20 monomers (red), 40 monomers (blue), 80 monomers (green) and 200 monomers (black) are shown. The grafted chains have 80 monomers. The slopes 1 and 0.5 (dotted lines) have been shown here for better comparison with Einstein diffusion limit.*

This indicates that the dynamics of grafted nanoparticles is affected less than predicted by the simple concept of Stokes-Einstein. One can only speculate about possible reasons for these findings, but it is clear that more complex effects such as an interplay of the dynamics of matrix polymer and grafted corona or a particular interphase contribution to the transport must be important.

In Table 3 the measured brush height is shown, as a function of matrix chain lengths, at low and high grafting densities. The small angle neutron scattering (SANS) observations as reported by Chevigny et al.[13], however, showed that the shrinking of the grafted corona induced by longer matrix chains further affects the spatial organization of the NPs. The mobility of the NPs in our NCM simulation is slow, such that a NP in high grafting density system in the presence of 80-mer matrix chains needs ~ 200 ns production run to reach the diffusion regime. Moreover, several simulations of the similar NCMs with different initial configurations must be run to achieve a good statistics about diffusion of NPs and their dispersion throughout the NCM. This makes the investigation of the interaction and dispersion of the NPs in different NCMs computationally very expensive. As mentioned in the following section, however, a more straightforward and easier way is taken to study the dependency of NPs interaction on the surrounding matrix, ratio of matrix to grafted chain length and grafting density.

4.4. Polymer-Mediated Interaction of nanoparticles

In this section, the polymer-induced interaction (potential of mean force) between two either bare or grafted NPs is investigated, as a function of free and grafted chains of different length, as well as different grafting densities. The potential of mean force is shown versus surface-to-surface distance of two NPs along the axis connecting their centers of mass, called inter-surface distance.

4.4.1. Bare Nanoparticle

The potential of mean force V(r) as a function of inter-particle separation r of two bare particles is shown in Figure 5A. The overall shape of V(r) for short (20 monomers) free chains is very similar to that of long (200 monomers) chains, suggesting that the length of the free chains plays no significant role in the polymer-mediated interaction of bare NPs. This is in agreement with results of a CG study carried out by Smith et al. who reported a molecular-weight independent potential of mean force for systems with strong polymer-NP interactions[66].

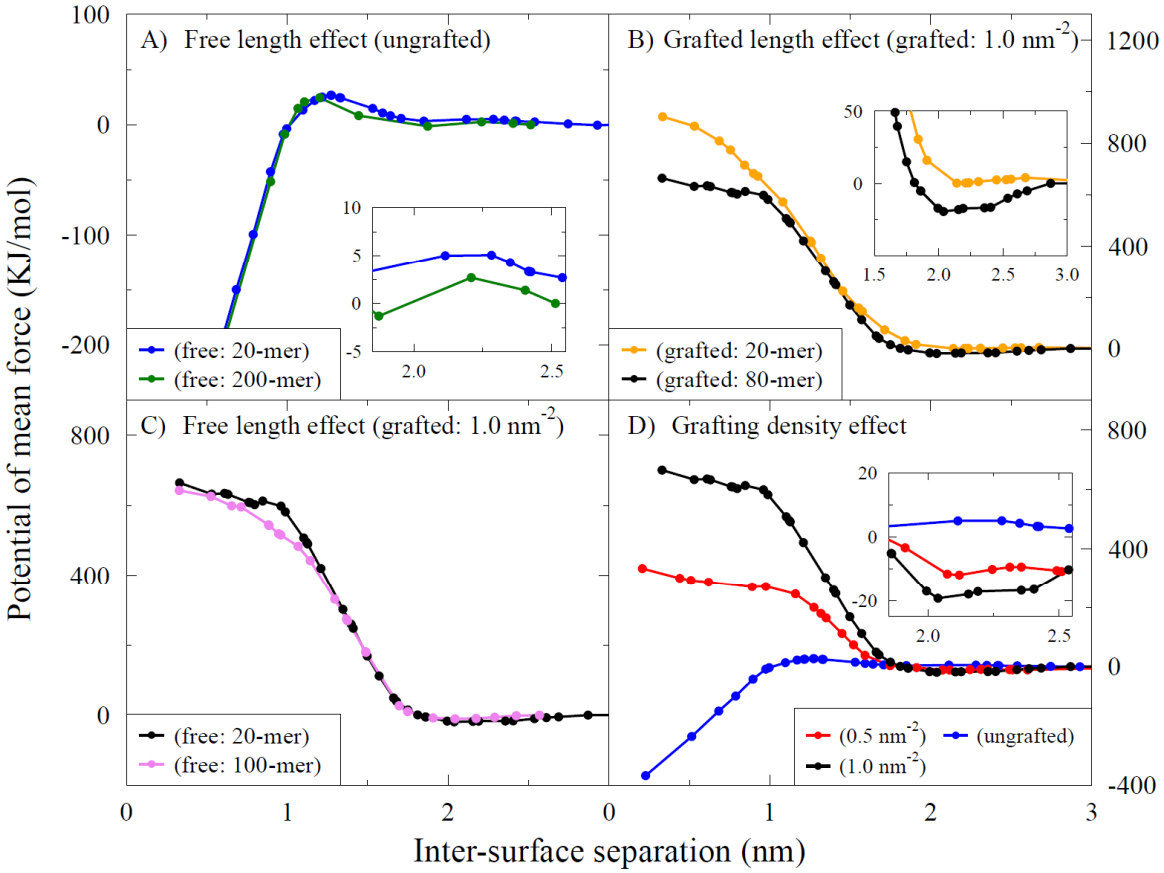

Figure 5. *Polymer-induced potential of mean force between two nanoparticles, as a function of inter-particle separation. A) Two ungrafted nanoparticles, free-chain lengths of 20 (blue) and 200 monomers (green). The inset shows a magnification of the second peak around 2.2 nm. B) Grafted-chain length effect is shown for nanoparticles grafted with 20-monomer (orange) and 80-monomer chains length (black), and free chains of 20 monomers (σ = 1 chains/nm^2).The attractive region at ~ 2 nm is magnified in the inset. C) Effect of the length of free chains on the interaction potential of grafted nanoparticles (σ = 1 chains/nm^2, grafted chain length 80 monomers). The free chains have 20 monomers (black) or 100 monomers (violet). D) Grafting density effect on the potential of mean force. Ungrafted (blue) and low (σ = 0.5 chains/nm^2, red) and high (σ = 1 chains/nm^2, black) grafted nanoparticles are shown for free chains of 20 monomers whereas and grafted of 80 monomer. Note that the black and the blue curves denote the same systems in all panels.*

For small inter-surface separations (less than 1 nm) there is a strong attractive part in V(r), as shown in Figure 5A. As there is no interaction potential between particles, however, the bare NPs can coalesce to reduce the volume, and hence V(r) can not be trusted below 1 nm. While it is uniform at large inter-surface separations, V(r) shows an appreciable maximum (27 kJ/mol) at the inter-surface distance of ~ 1.2 nm, right before the strong attractive part starts.

Since there is no explicit interaction between the two NPs, any repulsion in V(r) must be a result of free chain beads occupying the contact region between the particles. The position of this peak in V(r) suggests that the monomers causing the polymer-induced repulsion between them are located at an average distance of ~ 0.6 nm from the surface of each particle. This distance, on the other hand, corresponds perfectly to the distance at which the first peak appears in the density profile of free chains around the same NP, as shown in our previous studies[4,5] on the same NCM (see Figure 2A of ref 4). The origin of the peak in the potential V(r) can thus be attributed to the layer structure of the polymer around the NP. As the bead diameter is approximately 0.6 nm, there are two layers of free polymer, which must make way for the NPs to approach each other. Since there are more than one polymer layers around a bare NP[4], further (though weaker) maxima in the V(r) are expected to appear at longer inter-particle distances. In fact, a much weaker (3-5 kJ/mol) second bump is found at an inter-surface distance of approximately 2.2 nm, corresponding to an average distance of ~ 1.1 nm from the surface (see inset of Figure 5A). This is again in agreement with the second density peak at ~ 1 nm from NP surface.

The stronger first peak in the V(r) profile provides a free-energy barrier to particle aggregation. It can be explained energetically. When surfaces are as close as ~ 1.2 nm NPs interact mainly via polymer beads located in the overlap region of their first polymer shells, which experience the highest attraction from both particles. As NPs approach one another, the inter-particle region becomes narrower and polymer beads are forced to leave this space, as there is not enough room for them. Polymer beads will not easily leave this space, as they are attracted strongly by both particles. The density of matrix polymers between two NPs separated by a surface-to-surface distance of 1.2 nm is 12.07 nm^{-3} for 20-mer (and 12.46 nm^{-3} for 200-mer) matrix chains. In agreement with the bead-spring model of Smith et al.[66], this density is higher than amplitude of the first density peak around a single NP (11 nm^{-3})[4] .

Figure 6 shows an snapshot of two NPs at inter-surface distance of 1.2 nm, in the presence of 200-mer matrix chains. While the red chain is mediating the interaction between particles by only being

in the inter-particle region, the blue chain touches both NPs from the sides, too. Such an additional interaction between NPs can explain the slightly higher repulsion in the case of long matrix chains compared to the shorter ones, in Figure 5A.

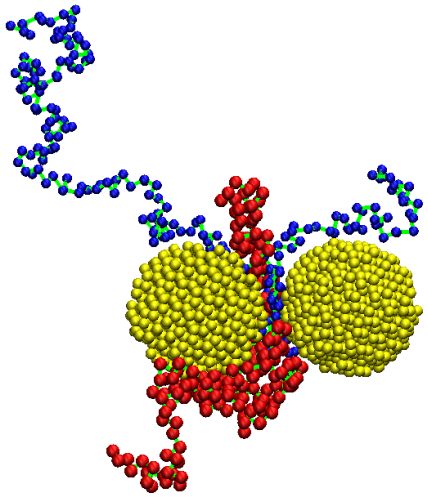

Figure 6. *Free chains of 200 monomers touching both bare nanoparticles (yellow) at the same time. The red chain mediates the interaction of the NPs via being mainly in the inter-surface region, the scenario which is possible also for short free chains of 20 monomers length. The blue free chain, on the other hand, is extended such that it touches both NPs at regions outside the inter-surface region as well.*

4.4.2 Grafted Nanoparticle

4.4.2.1. Effect of the Length of Grafted Chains

Figure 5B shows the potential of mean force of two NPs grafted with 50 chains of 20 or 80 monomers (grafting density of 1.0 chains/nm^2) surrounded by free chains of 20 monomers. For the longer chains a small attractive part is present at inter-surface separations of 2.1 nm (well depth: -20 kJ/mol), whereas a steep repulsion is observed for distances below 1.8 nm for both chain lengths.

When the NPs are close, their grafted chains can penetrate the grafted corona of the other particle. This can be studied by observing the density of monomers grafted to particle 2 as a function of distance from particle 1, which we denote as non-self-grafted monomers. Figure 7 shows the

density of those non-self-grafted monomers which are geometrically closer to particle 1 than particle 2 for different inter-particle separations, different lengths of free chains, and different grafting densities. Mutual infiltration is found for all compositions. At inter-surface separations of 2 nm and less, there is a qualitative change: above this distance, the density maximum of non-self-grafted polymer falls somewhere between the particles away from the surface. Below 2 nm, the surface-adsorbed non-self-grafted monomers dominate, and a surface-adsorbed layer is clearly visible. This adsorption on the other particle's surface is caused by the attractive PS-silica potential.

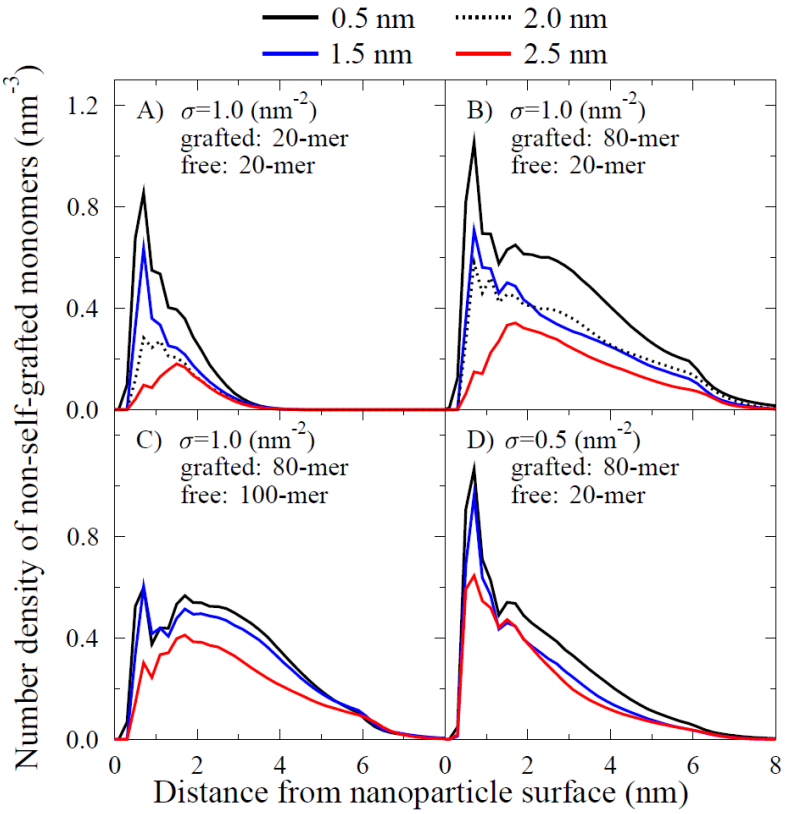

Figure 7. *Number density profiles of non-self grafted monomers (monomers grafted to the other nanoparticle) for different inter-surface separations: 0.5 nm (black), 1.5 nm (blue), 2 nm (dotted line, only in panels A and B) and 2.5 nm (red). A) High grafting density (σ = 1.0 chains/nm^2), free and grafted chains contain 20 monomers. B) High grafting density, free chains of 20 monomers and grafted chains of 80 monomers. C) High grafting density, free chains of 100 monomers and grafted chains of 80 monomers. D) Same as panel B, but low grafting density (σ = 0.5 chains/nm^2).*

It is promoted by longer grafted chains, which have a longer range, lower grafting density, which leaves more space to attach for chains from the opposite NP, and shorter matrix chains which are a better solvent and support swollen "wet" brushes (Table 3, see also ref 4). This explains the deeper minimum in the potential of mean force near inter-surface separation of 2 nm for longer grafted chains in Figure 5B.

There is also a change in the lateral distribution of monomers form chains grafted to the other NP. Figure 8 shows the angular distribution of the non-self grafted beads for the same cases as in Figure 7. The angle is defined between the vector from particle 1 to particle 2 and the vector from the center of particle 1 to the monomer in question, which is grafted to particle 2. An angle of 0 degrees corresponds to a monomer occupying the inter-particle axis, the angular distributions are averaged over all radial distances. The most conspicuous trend is that, for all systems, the average angle increases, as the particles approach each other. This is not surprising as monomers are squeezed out of the inter-particle region, when it becomes smaller. The shift of the maximum is strongest for short grafted chains (20 monomers, Figure 8A). This finding might be a structural explanation for the differences in the potential of mean force for different grafted-chain lengths (Figure 5B): Between the attractive minimum around 2 nm and 1 nm, both systems generate the same repulsion, due to the reduction of available space. At lower inter-surface separations (< 1 nm) the 20-monomer grafted chains cause more repulsion than the 80-monomer grafted chains. Both experience the same confinement, but the longer chains can compensate some of it by attractive surface contacts. The tendency for chains to spread on the surface of the other nanoparticle is corroborated by the second observation, which concerns the difference between high and low grafting densities. For 0.5 chains/nm^2 (Figure 8D), there is a significantly larger proportion of angles above 90 degrees at an inter-surface separation of 0.5 nm than for 1.0 chains/nm^2. This is a result of surface adsorption, for which there is more space for low-grafted particles (cf. the red chain in Figure 6).

4.4.2.2. Effect of the Length of Free Chains

For a given grafting density (1 chains/nm^2) and grafted-chain length (80 monomers), the lengths of the free chains has only a small effect. The potentials of mean force for free chains of 20 and 100 monomers (Figure 5C) are basically indistinguishable, except between 0.5 and 1.2 nm inter-surface separations. In this region, the longer free chains lead to a slightly weaker interaction potential. Again the better solvent quality of the short free chains provides the explanation. It expands the

grafted coils, so they feel the repulsion from brush of the other nanoparticle more strongly. This explanation is borne out by structural features. For example, Figure 7 shows that more non-self-grafted monomer density reaches the opposite nanoparticle, when the free chains are 20 monomers long (Figure 7B) than when have 100 monomers (Figure 7C).

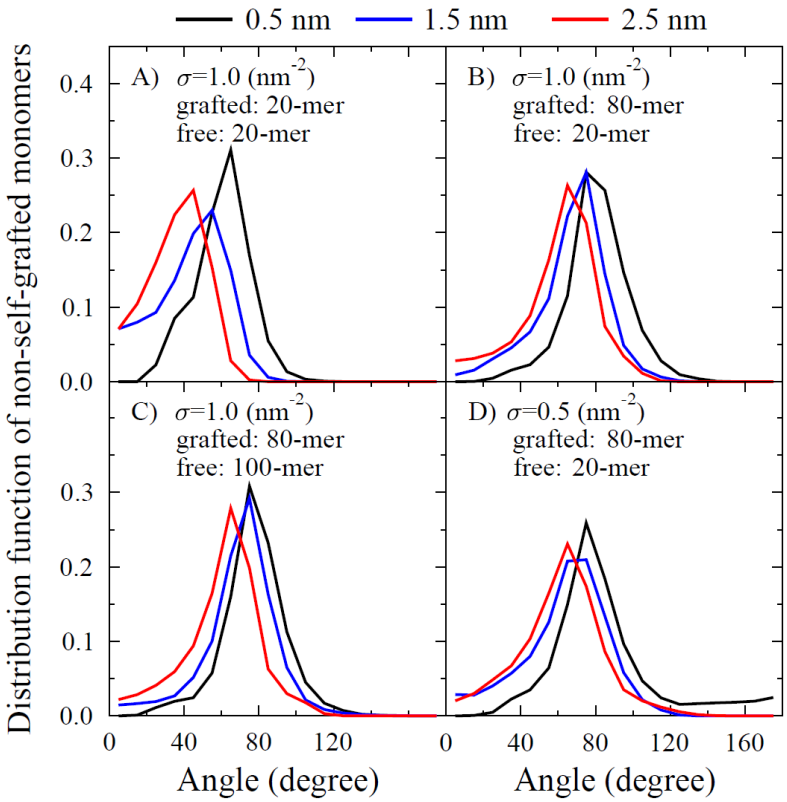

Figure 8. *Distribution of non-self-grafted monomers as a function of the angle between the inter-particle axis and the vector from the particle center to the monomer. Systems and line types are as in Figure 7.*

The better solvent quality of short free chains is also reflected in the radius of gyration of grafted chain (Figure 9), which is always larger for short free chains. The R_g has also been shown for different attachment positions of the grafted chains; in Figure 9 it is reported for different values of the "latitude", i.e. the angle between the inter-particle axis and the vector from the NP center to the grafting point of the chain, represented by the first atom of the linker unit. At the shorter inter-surface separation of 0.5 nm, the grafted chains have a higher R_g at lower latitude. This is explained by the chains near the "pole" being stretched in the direction of the opposite NP via surface

adsorption there. At the larger separation of 2.5 nm - just above one unperturbed R_g - the distribution of R_g is flat for short free chains, i.e. there is no directionality in the influence of the NP on the polymer structure. Changing the matrix to long chains, shorter radii of gyration are observed for those grafted chains located at a position in the direction toward the opposite particle. A possible explanation is that the compression of grafted chains by long matrix chains ("dry brush", ref 4) is synergistic with confinement. However, further analysis of this side aspect has not been carried out. The difference of the particle-particle potential of mean force induced by different chain length of the polymer matrix is in agreement with the experimental observation that for a fixed grafting density short free chains lead to individual nanoparticle dispersion, whereas longer free chains can result in particle aggregation[13].

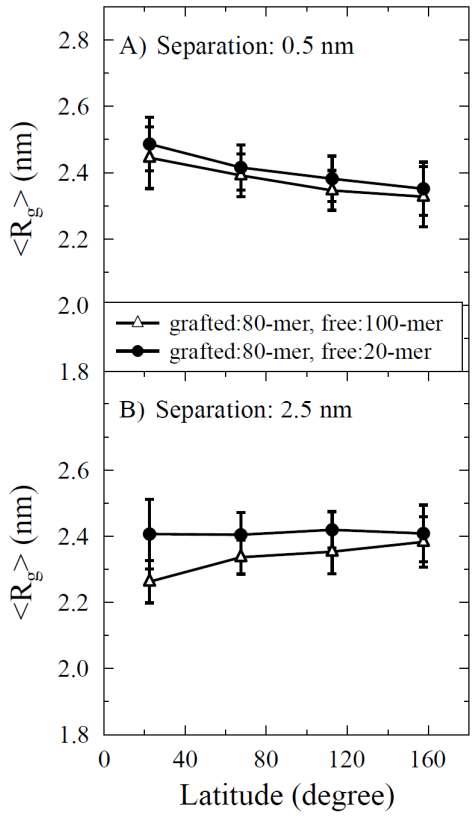

Figure 9. *Average radius-of-gyration of grafted chains attached to different locations of the nanoparticle, specified as angle between the inter-particle axis and the vector from the particle center to the position of the linker unit. Grafting density is 1 chains/nm^2, grafted chains have 80 monomers. Radius-of-gyration of grafted chains in the presence of short (20-monomer) and long (100-monomer) free chains are shown for inter-surface separations of (A) 0.5 and (B) 2.5 nm.*

4.4.2.3. Grafting Density Effect

Comparing ungrafted, low-grafted and high-grafted nanoparticles (Figure 5D, grafted chains: 80 monomers, free chains: 20 monomers), the expected effects are found. Increasing the grafting density increases the repulsion at short distances (< 1.7 nm). One reason is the entropic repulsion of the grafted chains of opposite nanoparticle, which becomes stronger when there are more chains and which disappears altogether when there are no grafted chains. The latter behavior has already been discussed above. A second reason is again the adsorption of grafted chains of particle 1 onto the surface of particle 2, which can offset part of the entropic repulsion. There is more space for adsorption of foreign chains at lower grafting density, as becomes evident by comparing Figures 7B and 7C. The engulfing of one nanoparticle by grafted chains from the other at short inter-particle distances (cf. Figures 8B and 8D) has already been discussed above. However, the inset of Figure 5D clearly shows that grafting also increases the depth of the attractive well in the region of 2 nm. This indicates that the mechanism of particle-particle attraction by grafted chains bridging the inter-particle gap is operative at longer distances, too.

4.4.3 Polymer Conformation in the Inter-Particle Region

In addition to the structural changes upon particle-particle approach discussed in Section 4.2 (Figures 6-9), more structural characteristics have been obtained to further elucidate the particularities of the interphase region between the particles. The monomer density and its components have been monitored for systems with grafted chains of 80 and free chains of 20 monomers in the inter-particle region (Figure 10). This region is defined as a cylinder which has the same radius as the NPs (2 nm) and which covers the surface-to-surface distance of two particles, along the inter-particle axis. Note, that this definition includes some volume in very close proximity of nanoparticle surface, which is of course not available for the polymer. Thus the “densities” reported in Figure 10 contain in their denominators a too large polymer volume fraction. Still, they can be usefully compared. Figure 10A shows a general decrease of the total polymer density with decreasing inter-particle distance for both grafting densities. At inter-surface distances > 2.5 nm, the monomer density assumes its known value for the environment of a single nanoparticle[4]. The overall decrease is larger for higher grafting densities. In both cases, the free polymer is ejected first from the inter-particle region (Figure 10B). This process is, however much stronger and uniform for high-

grafted chains, where all free monomers are gone at an inter-surface distance of 1 nm. For low grafted particles, the loss of free chains is more oscillatory. The density of grafted chains, on the other hand, is nearly constant at weak confinement (inter-surface distance > 1nm), before also some of the grafted monomers are displaced from the region. Again the decrease is less steep and more oscillatory for low grafting densities.

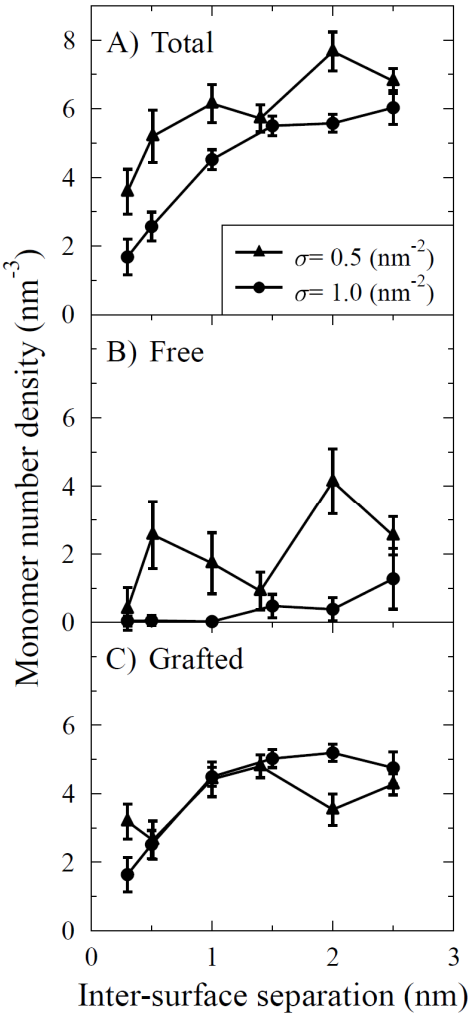

Figure 10. *Monomer number density in a cylinder of 2 nm radius between two nanoparticle surfaces as a function of inter-surface separation for high (σ = 1.0 chains/nm^2, circle) and low (σ = 0.5 chains/nm^2, triangle) grafting density. The grafted chain length is 80 monomers and the free chain length is 20 monomers in both systems. Panels A, B and C show the number densities of all monomers, of free and of grafted monomers, respectively.*

The observed density changes are in line with conformational changes of the grafted chains in the inter-particle region. To highlight these, the radii of gyration of grafted chains oriented toward the other nanoparticle are shown in Figure 11. Only those grafted chains have been included in the average, whose attachment points are within a cone of 90 degrees opening around the inter-particle axis ("latitude" < 45 degrees). For both grafting densities, the R_g converges to that of grafted chains on a single nanoparticle (2.4 nm, ref 4), at large inter-particle separations. This value is again reached at short distance, when the particles almost touch. In between, high and low grafting densities lead to qualitatively different behavior: There is a R_g maximum for high grafting densities and a minimum for low grafting densities. At high grafting density, the chains escape sideways and need to elongate, as soon as the brushes touch (< 2 nm). When the particles are close enough (< 1 nm), monomers are concentrated onto the particle surfaces by adsorption and the R_g shrinks again. For low grafting densities, adsorption onto the opposite particle sets in much earlier (compare Figures 7B and 7D), which has the effect of contracting grafted polymers toward the inter-particle axis, thereby decreasing their R_g. At even closer particle separation (< 1.5 nm), grafted polymers follow the surface of the other NP, which increases their R_g again.

Monomer dynamics of the grafted chains also becomes slower in the inter-particle region, as investigated by S(q,t) (data not shown here), probably because of the confinement effect. For example at high grafting densities when NPs are inter-surface distance of 2.5 nm, relaxation time of the grafted monomers which belong to the inter-particle region increased by a factor of ~ 2.1 above the average relaxation time of grafted chains. This ratio becomes 2.9 and 5.7 when NPs are at inter-surface distances of 1.5 and 0.5 nm, respectively.

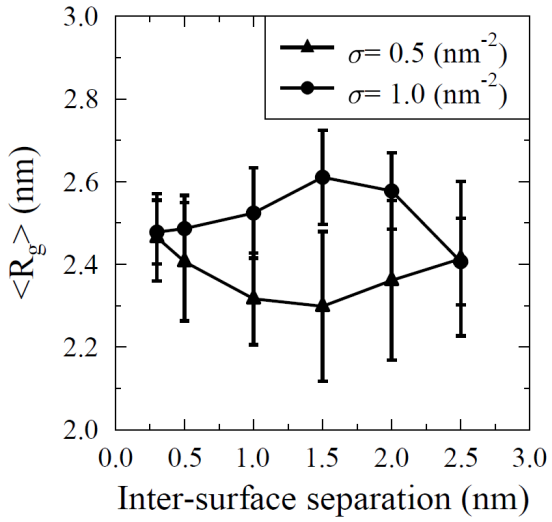

Figure 11. *Average radius of gyration of the grafted chains located in the inter-surface region (grafting points in a 90-degree cone around inter-particle axis) as a function of inter-surface separation. Grafted chain length is 80 monomers while free chain length is 20 monomers in both systems, the grafting densities are σ = 0.5 (triangle) and σ = 1.0 (circle) chains/nm^2, respectively.*

4.5. Summary and Conclusions

We have investigated the effect of matrix chain length and grafting density on the dynamics of the matrix and grafted chains in the interfacial region, and also, together with grafted chain length, on the potential of mean force of two bare and grafted silica NPs of radius 2nm imbedded in atactic polystyrene, using coarse-grained MD simulations. Our results indicate that the presence of filler particle attenuates the polymer dynamics in the interfacial region. This effect smoothly decreases with distance from the surface, as shown by the color code in the Table of Content figure (the mobility of the monomers measured by their average velocity (magnitude) in each shell: white = 0.5 nm from surface, red = 1 nm, green =1.5 nm, dark blue = 2nm, cyan = matrix monomers, yellow = nanoparticles). At any given distance from the surface, the dynamics is further influenced by matrix chain length and grafting density. The matrix chain length controls the dynamics in the grafted corona as well as the diffusion of the nanoparticle. Shorter matrix chains are not only able to swell the grafted corona (known as wet grafted corona), but also induce faster relaxation of the grafted chains compared to the longer matrix chains. This effect is stronger for lower grafting densities. For a given matrix chain length, high grafting density slows the polymer dynamics and expands the

interphase thickness, in addition to decreasing the nanoparticles' mobility. Whereas the interphase region, measured by local dynamics, persists only up to ~ 2 nm (corresponding to four monomer layers) from the surface of a bare particle, surface grafting increases the interphase thickness up to ~ 3 nm.

The layer structure of the matrix chains around a filler particle, which was studied in detail around a single nanoparticle in ref 4, also appears around and between two approaching nanoparticles, though perturbed by the additional confinement. The overlap of the first observed monomer layers of the two particles in the inter-particle region induces a repulsive region in the polymer-mediated potential of mean force of the two bare nanoparticles. The matrix chain length seems to play no significant role in the dispersion of bare nanoparticles as it has a negligible effect on the potential of mean force of bare particles. The increased matrix chain length leads to a synergistically enhanced “drying” of the grafted corona and to contraction of the grafted chains in the inter-particle region, compared to a single nanoparticle [ref 4]. Moreover, for a given grafting density, the interaction of nanoparticles becomes a bit less repulsive at close inter-surface distances for longer matrix chains, in qualitative agreement with the experimental observation[13] that particle aggregation is associated with collapse of the grafted chains in the presence of long-chains matrix. Increasing the grafted chain length was surprisingly found to weaken the repulsiveness of the potential of mean force, because of grafted monomers adsorbed to the surface of the other NP, a feature which grows with grafted chain length. This bridging is due to the attractive nanoparticle-polystyrene interaction characteristic of the silica-polystyrene composite. It energetically offsets part of the entropic repulsion of the grafted corona of the two particles. Without violating the positive effect of surface grafting on dispersibility of the particles, this means that short grafted chains make the interaction of the nanoparticles repulsive enough, whereas longer ones increase the chance of particle aggregation by bridging.

4.6. References

(1) Green, P. F. *Soft Matter* **2011**, *7*, 7914-7926.
(2) Sanchez, C.; Julian, B.; Belleville, P.; Popall, M. *Journal of Materials Chemistry* **2005**, *15*, 3559-3592.
(3) Hule, R. A.; Pochan, D. J. *MRS Bull.* **2007**, *32*, 354-358.
(4) Ghanbari, A.; Ndoro, T.; Leroy, F.; Rahimi, M.; Böhm, M. C.; Müller-Plathe, F. *Macromolecules* **2012**, *45*, 572-584.
(5) Ndoro, T. V. M.; Voyiatzis, E.; Ghanbari, A.; Theodorou, D. N.; Böhm, M. C.; Müller-Plathe, F. *Macromolecules* **2011**, *44*, 2316-2327.
(6) Ndoro, T. V. M.; Böhm, M. C.; Müller-Plathe, F. *Macromolecules* **2012**, *45*, 171-179.
(7) Vogiatzis, G. G.; Voyiatzis, E.; Theodorou, D. N. *European Polymer Journal* **2011**, *47*, 699-712.
(8) Starr, F. W.; Glotzer, S. C. *Soft Mater.* **2004**, 107-124.
(9) Frischknecht, A. L.; McGarrity, E. S.; Mackay, M. E. *J. Chem. Phys.* **2010**, *132*, 204901-204906.
(10) Liu, J.; Wu, Y.; Shen, J.; Gao, Y.; Zhang, L.; Cao, D. *Physical chemistry chemical physics : PCCP* **2011**, *13*, 13058-13069.
(11) Ganesan, V.; Ellison, C. J.; Pryamitsyn, V. *Soft Matter* **2010**, *6*, 4010-4025.
(12) Chevigny, C.; Jestin, J.; Gigmes, D.; Schweins, R.; Di-Cola, E.; Dalmas, F. *Macromolecules* **2010**, *43*, 48833-44837.
(13) Chevigny, C.; Dalmas, F.; Di Cola, E.; Gigmes, D.; Bertin, D.; Boue, F.; Jestin, J. *Macromolecules* **2010**, *44*, 122-133.
(14) Harton, S. E.; Kumar, S. K.; Yang, H. C.; Koga, T.; Hicks, K.; Lee, E.; Mijovic, J.; Liu, M.; Vallery, R. S.; Gidley, D. W. *Macromolecules* **2010**, *43*, 3415-3421.
(15) Borukhov, I.; Leibler, L. *Macromolecules* **2002**, *35*, 5171-5182.
(16) Hooper, J. B.; Schweizer, K. S. *Macromolecules* **2006**, *39*, 5133-5142.
(17) Trombly, D. M.; Ganesan, V. *J. Chem. Phys.* **2010**, *133*, 154904-154907.
(18) Adnan, A.; Sun, C. T.; Mahfuz, H. *Composites Science and Technology* **2007**, *67*, 348-356.
(19) Brown, D.; Mele, P.; Marceau, S.; Alberola, N. D. *Macromolecules* **2003**, *36*, 1395-1406.
(20) Milano, G.; Santangelo, G.; Ragone, F.; Cavallo, L.; Di Matteo, A. *Macromolecules* **2011**, *115*, 15154–15163.
(21) Barbier, D.; Brown, D.; Grillet, A. C.; Neyertz, S. *Macromolecules* **2004**, *37*, 4695-4710.
(22) Kaufman, S.; Slichter, W. P.; Davis, D. D. *Journal of Polymer Science Part a-2-Polymer Physics* **1971**, *9*, 829-839.
(23) Arrighi, V.; Higgins, J. S.; Burgess, A. H.; Floudas, G. *Polymer* **1998**, *39*, 6369-6376.
(24) Gagliardi, S.; Arrighi, V.; Ferguson, R.; Telling, M. T. F. *Physica B* **2001**, *301*, 110-114.
(25) Fragiadakis, D.; Pissis, P.; Bokobza, L. *J. Non-Cryst. Solids* **2006**, *352*, 4969-4972.
(26) Fragiadakis, D.; Pissis, P. *J. Non-Cryst. Solids* **2007**, *353*, 4344-4352.
(27) Fragiadakis, D.; Pissis, P.; Bokobza, L. *Polymer* **2005**, *46*, 6001-6008.
(28) Tsagaropoulos, G.; Eisenberg, A. *Macromolecules* **1995**, *28*, 396-398.
(29) Arrighi, V.; McEwen, I. J.; Qian, H.; Prieto, M. B. S. *Polymer* **2003**, *44*, 6259-6266.
(30) Bogoslovov, R. B.; Roland, C. M.; Ellis, A. R.; Randall, A. M.; Robertson, C. G. *Macromolecules* **2008**, *41*, 1289-1296.
(31) Leisen, J.; Breidt, J.; Kelm, J. *Rubber Chem. Technol.* **1999**, *72*, 1-14.
(32) Hu, W. G.; Ellul, M. D.; Tsou, A. H.; Datta, S. *Rubber Chem. Technol.* **2007**, *80*, 1-13.

(33) Waldrop, M. A.; Kraus, G. *Rubber Age* **1969**, *101*, 70-&.
(34) Robertson, C. G.; Lin, C. J.; Rackaitis, M.; Roland, C. M. *Macromolecules* **2008**, *41*, 2727-2731.
(35) Nakatani, A. I.; Ivkov, R.; Papanek, P.; Yang, H.; Gerspacher, M. *Rubber Chem. Technol.* **2000**, *73*, 847-863.
(36) Litvinov, V. M.; Steeman, P. A. M. *Macromolecules* **1999**, *32*, 8476-8490.
(37) Zhaohui, Y.; Fujii, Y.; Fuk Kay, L.; Chi-Hang, L.; Tsui, O. K. C. *Science* **2010**, *328*, 1676-1679.
(38) Oh, H.; Green, P. F. *Nat. Mater.* **2009**, *8*, 139-143.
(39) Robertson, C. G.; Roland, C. M. *Rubber Chem. Technol.* **2008**, *81*, 506-522.
(40) Robertson, C. G.; Rackaitis, M. *Macromolecules* **2011**, *44*, 1177-1181.
(41) Eslami, H.; Karimi-Varzaneh, H. A.; Müller-Plathe, F. *Macromolecules* **2011**, *44*, 3117-3128.
(42) Vacatello, M. *Macromolecules* **2001**, *34*, 1946-1952.
(43) Starr, F. W.; Schroder, T. B.; Glotzer, S. C. *Macromolecules* **2002**, *35*, 4481-4492.
(44) Starr, F. W.; Schroder, T. B.; Glotzer, S. C. *Phys. Rev. E* **2001**, *64*, 021802-021805.
(45) Smith, G. D.; Bedrov, D.; Li, L. W.; Byutner, O. *J. Chem. Phys.* **2002**, *117*, 9478-9489.
(46) Binder, K.; Milchev, A.; Baschnagel, J. *Annu. Rev. Mater. Sci.* **1996**, *26*, 107-134.
(47) Torres, J. A.; Nealey, P. F.; de Pablo, J. J. *Phys. Rev. Lett.* **2000**, *85*, 3221-3224.
(48) Egorov, S. A. *J. Chem. Phys.* **2011**, *134*, 084903-084906.
(49) Borodin, O.; Smith, G. D.; Bandyopadhyaya, R.; Byutner, E. *Macromolecules* **2003**, *36*, 7873-7883.
(50) Brown, D.; Marcadon, V.; Mélé, P.; Albérola, N. D. *Macromolecules* **2008**, *41*, 1499-1511.
(51) Giannelis, E. P.; Krishnamoorti, R.; Manias, E. *Polymers in Confined Environments* **1999**, *138*, 107-147.
(52) Moniruzzaman, M.; Winey, K. I. *Macromolecules* **2006**, *39*, 5194-5205.
(53) Oberdisse, J. *Soft Matter* **2006**, *2*, 29-36.
(54) Grossiord, N.; Loos, J.; Regev, O.; Koning, C. E. *Chem. Mat.* **2006**, *18*, 1089-1099.
(55) Kropka, J. M.; Putz, K. W.; Pryamitsyn, V.; Ganesan, V.; Green, P. F. *Macromolecules* **2007**, *40*, 5424-5432.
(56) Janes, D. W.; Moll, J. F.; Harton, S. E.; Durning, C. J. *Macromolecules*, *44*, 4920-4927.
(57) Kumar, S. K.; Krishnamoorti, R. In *Annual Review of Chemical and Biomolecular Engineering, Vol 1*; ANNUAL REVIEWS: Palo Alto, 2010; Vol. 1, pp 37-58.
(58) Fornes, T. D.; Hunter, D. L.; Paul, D. R. *Macromolecules* **2004**, *37*, 1793-1798.
(59) Rong, M. Z.; Zhang, M. Q.; Zheng, Y. X.; Zeng, H. M.; Walter, R.; Friedrich, K. *Polymer* **2001**, *42*, 167-183.
(60) Ginzburg, V. V.; Balazs, A. C. *Adv. Mater.* **2000**, *12*, 1805-1809.
(61) Ginzburg, V. V.; Gibbons, C.; Qiu, F.; Peng, G. W.; Balazs, A. C. *Macromolecules* **2000**, *33*, 6140-6147.
(62) Balazs, A. C.; Ginzburg, V. V.; Qiu, F.; Peng, G. W.; Jasnow, D. *J. Phys. Chem. B* **2000**, *104*, 3411-3422.
(63) Ginzburg, V. V.; Qiu, F.; Balazs, A. C. *Polymer* **2002**, *43*, 461-466.
(64) Thompson, R. B.; Ginzburg, V. V.; Matsen, M. W.; Balazs, A. C. *Macromolecules* **2002**, *35*, 1060-1071.
(65) Shen, J. X.; Liu, J.; Gao, Y. Y.; Cao, D. P.; Zhang, L. Q. *Langmuir*, *27*, 15213-15222.

(66) Smith, J. S.; Bedrov, D.; Smith, G. D. *Composites Science and Technology* **2003**, *63*, 1599-1605.
(67) Qian, H. J.; Carbone, P.; Chen, X. Y.; Karimi-Varzaneh, H. A.; Liew, C. C.; Müller-Plathet, F. *Macromolecules* **2008**, *41*, 9919-9929.
(68) Ghanbari, A.; Böhm, M. C.; Müller-Plathe, F. *Macromolecules* **2011**, *44*, 5520-5526.
(69) Karimi-Varzaneh, H. A.; Qian, H. J.; Chen, X. Y.; Carbone, P.; Müller-Plathe, F. *J. Comput. Chem.* **2011**, *32*, 1475-1487.

4.7. Appendix

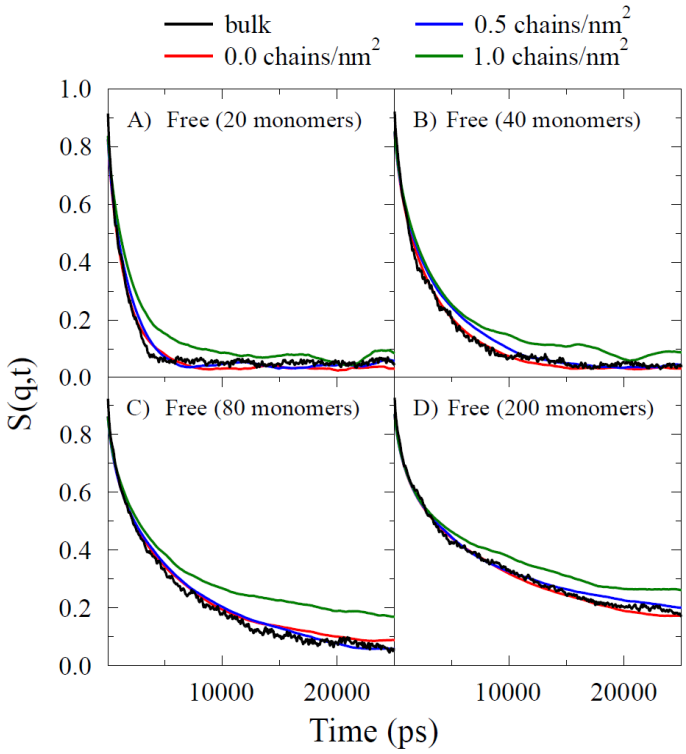

Figure SI-1. *Self scattering function of free-chain monomers in third shell (2-3 nm from surface), $S^{n=3}(q,t)$, around the nanoparticle as a function of the density of grafted chains (length 80 monomers) on the nanoparticle surface and of the length of the free chains (20, 40, 80 and 200 monomers in panels A-D, respectively) for a constant q=0.78 nm^{-1}. The scattering function for an unfilled polymer bulk with the same chain lengths is shown for comparison.* *Figure SI-1. Self scattering function of free-chain monomers in third shell (2-3 nm from surface), $S^{n=3}(q,t)$, around the nanoparticle as a function of the density of grafted chains (length 80 monomers) on the nanoparticle surface and of the length of the free chains (20, 40, 80 and 200 monomers in panels A-D, respectively) for a constant q=0.78 nm^{-1}. The scattering function for an unfilled polymer bulk with the same chain lengths is shown for comparison.*

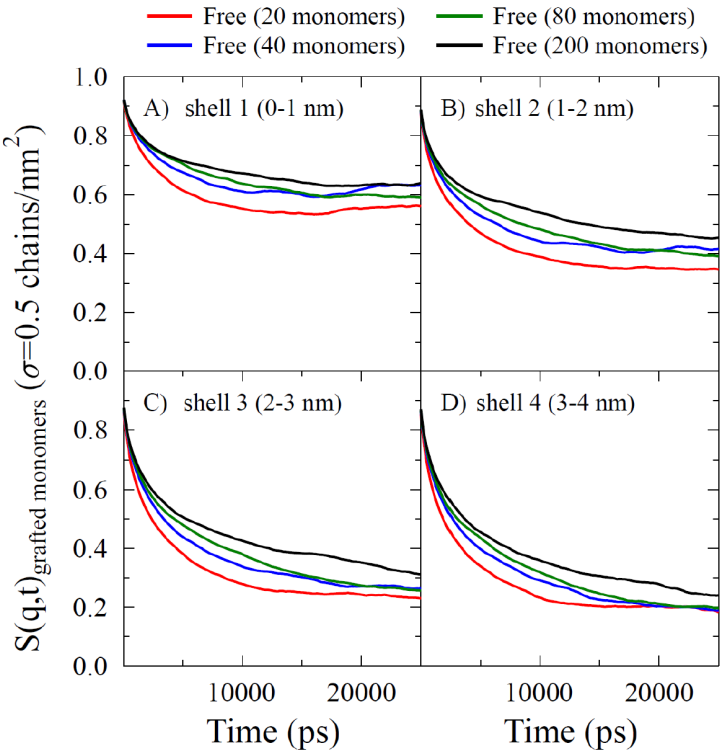

Figure SI-2. *Self scattering function, for a constant q=0.78 nm^{-1}, versus time in different shells around grafted NP of σ = 0.5 chains/nm^2 is shown during 25 ns. Shells of 1 nm thickness are considered around NP, and shown in panels A to D, where the first shell surveys 0-1 nm from surface. At each given shell dependency of monomers dynamics of grafted chains on the length of free chains (20, 40, 80 and 200-mer) is shown by different colors (red, blue, green and black, respectively).*

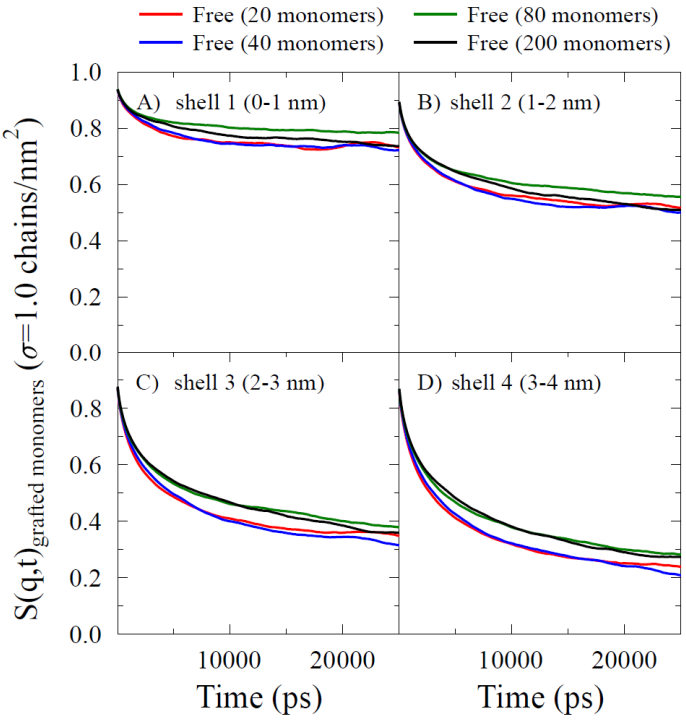

Figure SI-3. Self scattering function, for a constant q=0.78 nm^{-1}, versus time at different shells around grafted NP of σ = 1.0 chains/nm^2 is shown during 25 ns. Shells of 1 nm thickness are considered around NP, and shown in panels A to D, where the first shell surveys 0-1 nm from surface. At each given shell dependency of monomers dynamics of grafted chains on the free chains length (20, 40, 80 and 200-mer) is shown by different colors (red, blue, green and black, respectively).

5. Conclusion and Outlook

The present PhD thesis has been focused on investigating the structural and dynamical properties of the polymer chains in the interface of atactic polystyrene near bare and grafted spherical silica nanoparticle using coarse-grained Molecular Dynamics simulation tool, IBIsCO. One aim of the current study was to optimize the material-specific coarse-grained potentials via iterative Boltzmann inversion method in order to reproduce the correct structure near surface. The polymer structure was successfully predicted by the coarse-grained model and compared with the preceding atomistic simulations of the same system as well as neutron scattering experiments, using a back-mapping method developed in the second chapter. Moreover, the transferability of the coarse-grained potentials, which were originally developed for a bare system, to the grafted nanoparticle systems, by augmenting them with the additional terms involving the linker units, was ascertained. The advantage of studying specific composites, like Silica-polystyrene here, is that the ultimate results can be directly compared to the real experiment data. Such a feature is not always the case for generic models. The results of the specific model can in turn be directly applied and tested, on the corresponding composite, in the industry. For example our findings about Silica-polystyrene nanocomposite show no immobilized region near the filler surface, and, as will be discussed below, short and dense grafted chains can be more effective than the longer ones in dispersing the filler particles.

The mere presence of the nanoparticle led to monomer layering and tangential orientation of the chain segments for any grafting state and chain length. Particle was further found to attenuate the polymer dynamics in the interfacial region. This is in agreement with those experimental observations of slower dynamics, and hence higher glass transition temperature, induced by the introduction of filler particles. The advantage here, however, is further resolving the contributing regions to the observed slowed dynamics, which is not achievable experimentally, as this effect smoothly decreases with distance from the surface. Moreover, at any given distance from the surface, the dynamics is farther influenced by matrix chain length and grafting density, as discussed below. The interphase extends to a few nanometers away from particle surface. Hence, the argument that the experimentally detected slower relaxation is due to some surface-adsorbed chain segments, as brought up for NMR studies, is ruled out. The fact that monomer density and segment orientation profiles, as two local structural properties, did not change significantly by grafting state and chain

length, shows that modifications happened in the interphase area is rather controlled by whole chain properties. In the following the effect of three main parameters, namely the matrix and grafted chain length and grafting density, on the interphase properties and nanoparticle dispersion is provided.

5.1. Chain Length Effect

The matrix chain length was found to influence the whole chain rather than local structural properties of the interphase polymer chains. Whereas monomer density and segment orientation profiles near the surface did not change by increasing the chain length, the entire chain properties (like radius of gyration and chain orientation angle profile) were strongly chain length dependent. While the short matrix chains (R_g less than filler size) became stretched in the interface of a bare nanoparticle, the longer ones wrapped around particle leading to relatively smaller R_g, thicker interphase and slower monomer dynamics. Only at distances beyond one coil radius away form a grafted surface, the bulk like (structural and dynamical) behavior can be observed which consequently varies the extension of the interphase thickness up to 3 nm form surface in the range of the chain lengths studied in this work. Matrix chain length was further found to modify both structure and dynamics of the grafted corona, by brush wetting and drying. Matrix chains shorter than grafted ones penetrated into the grafted corona, swelling the brush much like a solvent, whereas longer matrix chains were expelled from the NP's vicinity by the grafted brush. Moreover, shorter matrix chains induced faster monomer dynamics in the grafted chains compared to the longer ones. This is more enhanced for low grafting densities due to the presence of relatively more free chains. On the level of polymer mediated interaction of nanoparticles, however, the brush drying induced by longer free chains led to small reduction in their repulsive potential of mean-force. Consequently it can be concluded that a good dispersion of the grafted nanoparticles is possible by matrix chains shorter than grafted ones, which on the other hand causes an enhancements of the NCM properties by increasing the interphase region. The matrix chain length had no significant role in the dispersion of bare nanoparticles, in correlation with no effect on the local structural properties around bare nanoparticles.

The structure and dynamics of the grafted chains is found deeply dependent on the grafting density and matrix chain length. Increasing the grafted chain length was found to weaken the repulsiveness of the potential of mean force, because of the grafted monomers adsorbed to the surface of the other NP, a feature which grows with grafted chain length. This bridging is due to the attractive

nanoparticle-polystyrene interaction characteristic of the silica-polystyrene composite. This means that the shorter grafted chains make interaction between nanoparticles repulsive enough whereas in the longer case, due to mixing of the grafted halos, the separation between nanoparticles is not achieved easily. Based on this, a dense grafted corona with short grafted chains is recommended to manufacture NCMs with well dispersed filler particles, to reduce the chance of particles aggregation because of long grafted chains.

5.2. Grafting Density Effect

The repulsiveness of the polymer-mediated interaction potential of two nanoparticles increased with grafting density, which shows that surface functionalization of the filler particles with grafted chains can avoid their aggregation, in agreement with the experimental observations. Grafting density increased the interphase thickness, measured by modifications in either structural or dynamical properties of the polymer chains, besides slowing down the nanoparticle dynamics as well as matrix and grafted monomer dynamics up to 3 nm from surface. The point at which the contribution of the matrix and grafted chains in the monomer population is equal becomes farther from the surface as grafting density increases. The better infiltration of free and grafted chains, in low grafting densities, would be favorable for the propagation of mechanical stress from the bulk polymer and also useful in reducing adhesive failure.

5.3. Outlook

Following the investigations done in this work, many new challenges still await to be tackled. For instance, it is shown in the experiment[1] that the bound rubber content of the rubber-filler composite increases, though slowly, with the storage time. This is considered to be due to the slow desorption of the short chains, which have been initially adsorbed to the surface, and their replacement with the longer chains. For better understanding this mechanism of preferential replacements of long chains by short ones more simulations with matrix polymers of different chain lengths are requested. The basic difference between short and long matrix chains facing a NP, which were considered separately in this study, was that the longer ones could wrap around the particle. If and how the adsorption / desorption rate of the chains depends on their length needs to be examined via longer time runs.

The mechanical properties of the same silica-polystyrene NCM can be investigated, compared to the bulk PS, and related to the structural properties of the interfacial polymer chains, using the CG model developed here. Deformations of the layer structure and orientation preference of the chains and segments under mechanical stress can be monitored at different distances from surface. Curvature (or NP size) dependence of these mechanical properties will be very interesting to study, considering the fact that nano-size nature of the fillers makes NCMs much different from conventional composites. To study the mechanical properties larger CG scale systems are needed because the filler reinforcement of the polymeric material happens by co-existence of two effects: the filler-polymer matrix effect and the filler network contribution. Without the latter single filler induced modifications would disappear beyond the interphase and the bulk polymer properties would dominate. Moreover, the bigger model systems will enable us to compare the larger scale structural properties of the model with the experimental data of SANS and SAXS experiments.

Characterizing the relative stability of nanoparticles (dispersion) in different matrix conditions is another challenge. It would be interesting to test the effect of anisotropic particle shape on the nanocomposite properties. For example, an ellipsoidal nanoparticle will introduce even more surface area to the nanocomposite material, than a spherical one, with the same volume fraction. Additionally, calculating the dependency of the surface free energy to the grafted or matrix chain molecular weight in the interfacial region and separating the enthalpic and entropic contribution in the systems will lead to better understanding of current results like wet-to-dry transition. Such knowledge will give both the modeler and experimentalist significant control in tailoring polymer nanocomposites for specific purposes.

5.4. References

(1) Leblanc, J. L. *Journal of Applied Polymer Science* **1997**, *66*, 2257-2268.

Simulation Packages and Super-Computers

The molecular dynamics simulation package YASP developed by Prof. Dr. Florian Müller-Plathe has been used to perform all the required atomistic simulations. All equilibrium coarse-graining simulations have been performed with the IBIsCO package developed in the group of Prof. Dr. Florian Müller-Plathe by Dr. Hossein Ali Karimi-Varzaneh.

Publications

1) Ndoro, T., Voyiatzis, E., Ghanbari, A., Theodorou, D. N., Böhm, M. C., & Müller-Plathe, F. (2011). Interface of Grafted and Ungrafted Silica Nanoparticles with a Polystyrene Matrix: Atomistic Molecular Dynamics Simulations. *Macromolecules 2011, 44, 2316*-2327.

2) Ghanbari, A., Böhm, M. C., and Müller-Plathe, F. A Simple Reverse Mapping Procedure for Coarse-Grained Polymer Models with Rigid Side Groups. *Macromolecules 2011, 44, 5*520-5526.

3) Ghanbari, A., Ndoro, T., Leroy, F., Rahimi, M., Böhm, M. C., and Müller-Plathe, F. Interphase Structure in Silica-Polystyrene Nanocomposites: A Coarse-Grained Molecular Dynamics Study, *Macromolecules 2012, 45, 572-584*

4) Ghanbari, A., Rahimi, M., Böhm, M. C., and Müller-Plathe, F. A Coarse-Grained Molecular Dynamics Simulation of Polystyrene-Silica Nanocomposite: Dynamics in the Interphase and Polymer-Mediated Interactions of Nanoparticles (submitted to *The Journal of Physical Chemistry*)

5) Mohammad Rahimi, Irene Iriarte-Carretero, Azadeh Ghanbari, Michael C. Böhm, Florian Müller-Plathe. Mechanical Behavior and Interphase Structure in a Silica-Polystyrene Nanocomposite under Uniaxial Deformation (submitted to editorial office)

Financial Support

This work has been funded by the EU project NanoModel (211778) as well as by the Deutsche Forschungsgemeinschaft through the Priority Programme 1369 “Polymer-Solid Contacts: Interfaces and Interphases”.

Acknowledgments

I am very grateful to my supervisor Prof. Florian Müller-Plathe who gave me the chance to join his group as a PhD student. His impressive knowledge and guidelines were crucial during my PhD work. His hints and punctual advice was a great treasure during theses three years and for this I will always be indebted to him.

I would like thank Prof. Michael C. Böhm for his support, encouragement and daily attention to my work which forced me to be more productive. I also, greatly appreciated the help and suggestions of Dr. Hans-Jürgen Bär who helped me to develop an ability to conduct exercise courses and learn to deal with students.

Many thanks to Dr. Frédéric Leroy who had a positive effect in my self-confidence and inner progress, as well as my scientific work. I would like to thank him for times he spent listening to my problems and helping me to find a good solution for each of them. His efforts provide me with a warm and friendly atmosphere as an officemate was admirable. Many thanks to Mohammad Rahimi for his technical support, and to Dr. Enrico Riccardi for maintaining an active and friendly atmosphere in our group that had a positive effect on my work. I wish to offer my deep gratitude to Jessica Alhuwalia and Kristin Adolph for their kindness and patience in helping me in my administrating “stuff”. Beside this, they had unforgettable role in my work and life with their friendly and warm-hearted behavior. I am also very appreciative to Michael Langeloth and Kristin Adolph for helping me to translate my thesis into German and for time and effort he spent helping me at the end of my PhD work. I would like acknowledge all my colleagues, who left or who are still in the group, for the moments we spent together during the past 3 years. I have learned many things from each of them.

A person who had a positive impression at the beginning of my PhD was my English teacher and my kind friend, Stephen Giguere, who convinced me to believe in myself. I will never forget his effort and his suggestions which were very effective in helping me during my PhD work.

I would especially like to acknowledge my parents for their greatly appreciated encouragement and of for compelling me to continuing my education. There is no doubt that without their support none of my achievements would have been possible. I hope with this dissertation I can compensate a

small part of their tireless and selfless efforts in raising me into the woman I am today. And I would like to thank my father and mother–in-law who are supporting me with their kind prayers and good wishes for success.

Finally, I want to dedicate my deep thanks to my beloved and kind husband, Jaber Dehghany for his support and encouragement from the start to the finish of my PhD. There are no words to express my gratitude to him for the moments he devoted to discussing and assisting me. He sacrificed a lot for me and traveled to and from his job in Brunswick to spend more time with me and help me when I needed it most. His presence and patience during my moments of frustration and stress moments were invaluable and I will also treasure his help and support. I want to say how much I love him and how much his presence left a lasting impression in my PhD work and in my personal spiritual development.

Curriculum Vita

Name: Azadeh

Last Name: Ghanbari

Place of Birth: Tehran (Iran)

Date of Birth: 16/9/1983

Nationality: Iranian

Education

2003-2006: Zanjan University (Iran), (BSc of Physics)

2006-2008: Zanjan University (Iran), (MSc of physics)

2009-2012: PhD student in theoretical physical chemistry, Technical University of Darmstadt, Germany.

(Azadeh Ghanbari)

Azadeh Ghanbari
Holzhofallee 22
64295 Darmstadt
Germany

Darmstadt, 30 of March, 2012

Erklärung

Ich erkläre hiermit, noch keinen Promotionsversuch unternommen zu haben.

_____
(Azadeh Ghanbari)

Azadeh Ghanbari
Holzhofallee 22
64295 Darmstadt
Germany

Darmstadt, 30 of March, 2012

Eidesstattliche Erklärung

Ich erkläre hiermit an Eides Statt, dass ich meine Dissertation selbständig und nur mit den angegebenen Hilfsmitteln angefertigt habe.

_____

(Azadeh Ghanbari)